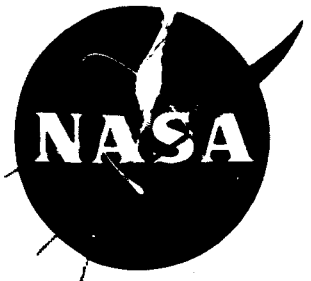

TECHNICAL MEMORANDUM

X-661

LONGITUDINAL AERODYNAMIC CHARACTERISTICS AT TRANSONIC SPEEDS OF A V/STOL AIRPLANE CONFIGURATION WITH A FIXED DELTA WING HAVING AUXILIARY VARIABLE-SWEEP OUTBOARD PANELS

By Arvo A. Luoma

Langley Research Center
Langley Air Force Base, Va.

NATIONAL AERONAUTICS AND SPACE ADMINISTRATION
WASHINGTON

December 1961

[redacted]

NATIONAL AERONAUTICS AND SPACE ADMINISTRATION

TECHNICAL MEMORANDUM X-661

LONGITUDINAL AERODYNAMIC CHARACTERISTICS AT TRANSONIC SPEEDS OF A V/STOL AIRPLANE CONFIGURATION WITH A FIXED DELTA WING HAVING AUXILIARY VARIABLE-SWEEP OUTBOARD PANELS*

By Arvo A. Luoma

SUMMARY

29466

An investigation of the longitudinal aerodynamic characteristics of several versions of a V/STOL airplane configuration which employed a fixed delta wing of low aspect ratio with auxiliary variable-sweep outboard panels was made in the Langley 8-foot transonic pressure tunnel at Mach numbers from 0.60 to 1.20. Retracted-wing and extended-wing configurations were tested. The models included internal flow.

Unsatisfactory subsonic minimum drag characteristics exhibited by the original version of the V/STOL airplane configuration and which appeared to be associated with interference effects from the ducting were eliminated by configuration revisions. The longitudinal stability of the retracted-wing configurations was stable and that of the extended-wing configurations was essentially neutral. The change in longitudinal stability from that for the extended-wing configuration at a Mach number of 0.60 to that for the retracted-wing configuration at a Mach number of 1.20 corresponded to a rearward movement of the aerodynamic center of 13 percent of the reference length for the original version of the V/STOL airplane configuration and 8.5 percent of the reference length for the revised version.

INTRODUCTION

Extensive studies made by the National Aeronautics and Space Administration of airplane configurations employing variable-sweep wings have indicated that configurations of this type appear to be a satisfactory means of realizing the efficient subsonic and supersonic flight

*Title, Unclassified.

characteristics required in a multimission airplane. A further mission recently considered for variable-sweep configurations is that of V/STOL capability based on a vectored lift-thrust engine with rotatable jet-exit nozzles. Included in the study of such V/STOL airplane configurations is a configuration which employed a fixed delta wing of low aspect ratio with auxiliary variable-sweep outboard panels. The configuration had two air inlets and four exit nozzles. The results of an investigation of the longitudinal and lateral aerodynamic characteristics of this V/STOL configuration in the Langley 4- by 4-foot supersonic pressure tunnel at a Mach number of 2.01 are presented in reference 1.

An investigation of the longitudinal aerodynamic characteristics at transonic speeds of this V/STOL configuration was made in the Langley 8-foot transonic pressure tunnel, and the results are presented herein. These results include information on the effect on the longitudinal aerodynamic characteristics of a change in the leading-edge sweep of the fixed delta wing, of sweeping the variable-sweep outboard panels of the fixed delta wing from the extended position to the retracted position, and of various modifications made in an attempt to improve the performance of the airplane. The tests were made at Mach numbers from 0.60 to 1.20 for the configurations in the retracted-wing position and at Mach numbers from 0.60 to 0.95 for the configurations in the extended-wing position.

SYMBOLS

The aerodynamic force and moment data are referred to the wind axes, with the origin for all models at body station 429.0 inches (full scale) and at water line 6.240 inches (full scale).

A_b base area of body (includes area of sting hole)

$A_{e,1}$ area (total) of forward exit of duct

$A_{e,2}$ area (total) of rearward exit of duct

A_1 projected area (total) of inlet of duct on plane perpendicular to reference line of model

C_D external drag coefficient, $\frac{\text{External drag}}{q_\infty S}$

$C_{D,i}$ internal drag coefficient,

$$\frac{w_1}{q_\infty S}(V_\infty - V_{e,1}\cos\alpha) - C_{p,e,1}\frac{A_{e,1}}{S}\cos\alpha$$

$$+ \frac{w_2}{q_\infty S}(V_\infty - V_{e,2}\cos\alpha) - C_{p,e,2}\frac{A_{e,2}}{S}\cos\alpha$$

$C_{D,min}$ minimum value of external drag coefficient

C_L lift coefficient, $\frac{\text{Lift}}{q_\infty S}$

$C_{L,(L/D)_{max}}$ lift coefficient at maximum lift-drag ratio

C_m pitching-moment coefficient, $\frac{\text{Pitching moment}}{q_\infty Sc}$

$C_{p,e,1}$ pressure coefficient of flow in duct at forward exit, $\frac{p_{e,1} - p_\infty}{q_\infty}$

$C_{p,e,2}$ pressure coefficient of flow in duct at rearward exit, $\frac{p_{e,2} - p_\infty}{q_\infty}$

c reference length used for computing pitching-moment coefficient (see tables I to V)

L/D lift-drag ratio, C_L/C_D

$(L/D)_{max}$ maximum value of lift-drag ratio

M Mach number of undisturbed stream

$p_{e,1}$ static pressure of flow in duct at forward exit

$p_{e,2}$ static pressure of flow in duct at rearward exit

$p_{t,\infty}$ total pressure of undisturbed stream

p_∞ static pressure of undisturbed stream

q_∞ dynamic pressure of undisturbed stream, $\frac{1}{2}\rho_\infty V_\infty^2$

R Reynolds number, based on a reference length of 1 foot

S reference area used for computations (see tables I to V)

$t_{t,\infty}$ stagnation temperature of undisturbed stream

$V_{e,1}$ velocity of flow in duct at forward exit

$V_{e,2}$ velocity of flow in duct at rearward exit

V_∞ velocity of undisturbed stream

w total mass flow into inlet of duct, $w_1 + w_2$

w_1 mass flow in duct at forward exit, $\rho_{e,1} V_{e,1} A_{e,1}$

w_2 mass flow in duct at rearward exit, $\rho_{e,2} V_{e,2} A_{e,2}$

w/w_∞ mass-flow ratio based on inlet area, $\frac{w}{\rho_\infty V_\infty A_1}$

Λ leading-edge sweep of auxiliary outboard panels of fixed delta wing

α angle of attack, based on reference line of model

δ_h horizontal-tail deflection

$\rho_{e,1}$ mass density of flow in duct at forward exit

$\rho_{e,2}$ mass density of flow in duct at rearward exit

ρ_∞ mass density of undisturbed stream

$C_{L_\alpha} = \frac{dC_L}{d\alpha}$ per deg

$C_{m_{C_L}} = \frac{dC_m}{dC_L}$

Components of model:

B	body (including canopy, engine air ducts, and fixed delta wing)
H	horizontal tail (at rear of fixed delta wing)
V	vertical tail
W	auxiliary variable-sweep outboard panels of fixed delta wing

APPARATUS

Tunnel

The investigation was made in the Langley 8-foot transonic pressure tunnel. The test section of this tunnel has a square cross section, the upper and lower walls being axially slotted to permit continuous testing through the transonic speed range. The total pressure of the tunnel air can be varied from a minimum value of about 0.25 atmosphere at all test Mach numbers to a maximum value of about 2.0 atmospheres at Mach numbers of 0.4 and less and about 1.5 atmospheres at transonic Mach numbers. The tunnel air is dried sufficiently to avoid condensation effects.

Model

Three sting-supported models were used in the present investigation: one 1/20-scale model and two 1/30-scale models. The 1/20-scale model represented configurations of a possible V/STOL airplane configuration employing a fixed delta wing of low aspect ratio with auxiliary variable-sweep outboard panels. The airplane would obtain V/STOL capability with a vectored lift-thrust engine with two air inlets and four swivelling nozzles. All models were designed for internal flow. The ducting consisted of two side inlets and four side exits (two forward exits and two rearward exits). Each of the inlets was ducted separately to a forward exit and a rearward exit.

Several versions of the 1/20-scale model of the V/STOL airplane configuration were tested; the original versions designated herein as models 1a and 1b and the revised versions, models 2a and 2b. Drawings of these various versions are given in figures 1 and 2 and the geometric characteristics, in tables I, II, and III. The two 1/30-scale models, designated herein as models 3, 4a, and 4b, were simplified research

representations of the V/STOL airplane configuration and were tested in an attempt to reduce a subsonic drag-coefficient rise with an increase in Mach number which in earlier tests had been found to occur for models 1a and 1b but not for model 1b with the ducts removed. Drawings and geometric characteristics of model 3 are given in figure 3 and table IV, respectively, and of models 4a and 4b in figure 4 and table V.

The main differences between models 1a and 1b were in the leading-edge sweep of the fixed delta wing (81° for model 1a and 73° for model 1b) and in the overall span of the horizontal tail (11.14 inches for model 1a and 13.75 inches for model 1b); otherwise, the horizontal tails were the same. Models 2a and 2b differed in several respects from models 1a and 1b: the leading-edge sweep of the fixed delta wing was 71.75°, the leading-edge sweep of the outboard panel of the horizontal tail was the same as that of the fixed delta wing, the dihedral of the outboard panel of the horizontal tail was changed from -25° to the uncanted position, the body in the region of and ahead of the engine air inlets had been modified (a larger nose and, to maintain pilot vision, a higher canopy) in an attempt to improve the air flow to the engine air inlets, and the ramps rearward of the duct exits had been changed so that they were parallel to the body center line in an attempt to improve the air flow in this region. Models 1a and 1b are designated as the "original configuration" and model 2a as the "revised configuration" in reference 1.

The only difference between models 2a and 2b was in the external contours of the duct: those on model 2b had been modified into an NACA 1-series nose inlet profile as one attempt to reduce the subsonic drag-coefficient rise which occurred for models 1a and 1b.

The 1/30-scale models (models 3, 4a, and 4b) had simplified body cross sections, a simplified delta wing (flat lower surface and a wedge (spanwise) on the upper surface), no tail surfaces, and the duct exits were parallel to the model reference line. Model 4 had the engine air inlets 25° below the horizontal plane instead of 35° below as on models 1, 2, and 3. Model 4 had a longer nose than model 3, had a flattened body shape ahead of the air inlets, and had the canopy moved forward relative to the air inlets. Model 4a was modified into model 4b by extending the forward duct exits rearward (somewhat beyond the rearward exits) so that there was only a single duct exit on each side of the body.

The longitudinal distribution of cross-sectional area (full-scale dimensions) for model 1a is shown in figure 5.

Instrumentation

A six-component strain-gage balance, which was housed in the model body, was used for determining the overall forces and moments on the model. A static-pressure orifice located within the chamber surrounding the strain-gage balance was connected to a pressure transducer; this static pressure was used in the base-pressure correction. Rakes consisting of total-pressure and static-pressure tubes were used at the duct exits for mass-flow and internal-drag measurements.

The overall forces and moments on the model, the no-load angle of attack, and the static pressure in the chamber surrounding the strain-gage balance were recorded electronically on punch cards. During the mass-flow tests the total and static pressures at the duct exits were measured by use of a multiple-tube manometer containing tetrabromoethane. All manometer tubes were photographed simultaneously.

TESTS, CORRECTIONS, AND ACCURACY

Tests

All the tests were made with the transition fixed on the model by 1/16-inch-wide strips of No. 120 carborundum grains on the 1/20-scale models and No. 180 carborundum grains on the 1/30-scale models. The strips were shellacked 1/2 inch back from the body nose and the leading edge of the inlets on all models and on the 1/20-scale models 1/2 inch back from the leading edge of the vertical tail and 1/4 inch back from the leading edge of the horizontal tail. One test (model 2a) was also made with strips of No. 80 carborundum grains.

The investigation included tests to determine the effects of a change in the leading-edge sweep of the fixed delta wing, of a change in the sweep of the auxiliary variable-sweep outboard panels of the fixed delta wing from the extended position to the retracted position, and of model modifications. Model 1b was also tested with the ducts removed.

All the tests were made at an angle of sideslip of 0°. The configurations with the variable-sweep outboard panels of the fixed delta wing in the extended position were tested at Mach numbers from 0.60 to 0.95; the configurations in the retracted-wing position were tested at Mach numbers from 0.60 to 1.20. The configurations were generally tested at a total pressure of 1,060 pounds per square foot or 2,120 pounds per square foot; some configurations were tested at both values of total pressure.

The Reynolds number of the investigation is shown as a function of Mach number at several values of total pressure in figure 6. The stagnation temperature of the investigation was 121° F.

All the configurations were investigated with internal flow. Mass-flow measurements were made for all models except model 1a. The static pressure in the chamber surrounding the strain-gage balance was measured for all configurations.

Corrections

The external drag coefficient C_D was corrected by adjusting the static pressure in the balance chamber and at the body base to the free-stream value. The external drag coefficient also includes the correction for the internal drag coefficient $C_{D,i}$. The internal-drag results obtained for model 1b were used in correcting the drag data of model 1a. The internal-drag and mass-flow results are presented in figure 7.

Data presented herein at supersonic Mach numbers consist of minimum drag results at Mach numbers of 1.02, 1.03, and 1.10 (1/30-scale models only), and of force and moment results for the angle-of-attack range at Mach numbers of 1.15 (1/30-scale models only) and 1.20. At Mach numbers of 1.02 and 1.03 the flow over the model was subject to influence by wall-reflected compression and expansion disturbances originating at the model; the effect on drag was probably small. The configurations were clear of wall-reflected disturbances at the other test Mach numbers. The angle of attack has been corrected for the flexibility under aerodynamic load of the balance, model sting, and sting extension.

Accuracy

The accuracy of the data, based primarily on the static calibrations and the repeatability of the data, is estimated to be as follows:

C_L	±0.005
C_D	±0.001
C_m	±0.0008
α, deg	±0.1
M	±0.003

PRESENTATION OF RESULTS

The basic longitudinal aerodynamic characteristics of the various models are presented in figures 8 to 13, and summary data on performance and longitudinal-stability derivatives are shown in figures 14 to 23. The slopes C_{L_α} and $C_{m_{C_L}}$ were taken at an angle of attack of approximately 0°. During the tests of model 2a in the extended-wing position ($\Lambda = 15°$), some filler used at the root of the variable-sweep outer panels came loose; therefore, the results obtained for this configuration, more likely the drag results, may have been affected. The results of this investigation are presented as follows:

SUMMARY OF RESULTS

A detailed discussion of the longitudinal aerodynamic results obtained in the investigation at transonic speeds of a V/STOL airplane configuration with a fixed delta wing having auxiliary variable-sweep outboard panels has been omitted in order to expedite publication of the data. A few observations are made, however, in order to point out some of the more important results obtained.

Changing the leading-edge sweep of the fixed delta wing from 81° (model 1a, $\Lambda = 81°$) to 73° (model 1b, $\Lambda = 73°$) increased the minimum

drag coefficient by 0.0010 to 0.0020 over the Mach number range. (See fig. 14(a).) Both models 1a and 1b (the original versions of the V/STOL airplane configuration) exhibited an undesirable increase in minimum drag coefficient with increase in Mach number at the lower subsonic Mach number. This increase in drag coefficient with increase in Mach number appeared to be associated with interference effects between the ducting and the other parts of the model since removal of the ducts from model 1b resulted in a zero variation of minimum drag coefficient with Mach number at the lower Mach numbers. (See fig. 16(a).) Accordingly, various design changes were incorporated in model 2 (the revised version of the V/STOL airplane configuration) and in the simplified research models 3 and 4 to reduce the interference effects associated with the ducting. The results of figures 21 and 22 show that the design changes eliminated the unsatisfactory minimum drag characteristics at the lower Mach numbers. Also, model 2a had a lower minimum drag coefficient than that of model 1b, 0.0015 lower at a Mach number of 0.60 and 0.0025 lower at a Mach number of 1.20.

L 1 9 7 7

The change from model 2a to model 2b resulted in a substantial increase in minimum drag coefficient at a Mach number of 1.20 (fig. 20(a)); the subsonic drags were the same. The usual decrease in minimum drag coefficient generally observed with an increase in total pressure was indicated in the present tests. (See figs. 14(a), 15(a), and 19(a).) Changing the transition grit size from No. 120 grit to No. 80 grit resulted in a slight increase in minimum drag coefficient. (See fig. 18.)

The variation of pitching-moment coefficient with lift coefficient was stable and uniform for the retracted-wing configurations. The extended-wing configurations had essentially neutral stability at lift coefficients below 0.4; the stability increased at lift coefficient above 0.4. Changing the leading-edge sweep of the fixed delta wing from 81° (model 1a; $\Lambda = 81°$) to 73° (model 1b; $\Lambda = 73°$) increased the stability over the Mach number range by an amount which corresponded to a rearward movement of the aerodynamic center of 0.05c to 0.06c. (See fig. 14(b).) The change in longitudinal stability from that for the extended-wing configuration at a Mach number of 0.60 to that for the retracted-wing configuration at a Mach number of 1.20 corresponded to a rearward movement of the aerodynamic center of 0.13c for model 1b and 0.085c for model 2a. The reference length c is defined herein as the distance from the leading edge of the inlet to the trailing edge of the fixed delta wing.

Langley Research Center,
National Aeronautics and Space Administration,
Langley Air Force Base, Va., December 7, 1961.

REFERENCE

1. Spearman, M. Leroy, and Foster, Gerald V.: Static Longitudinal and Lateral Aerodynamic Characteristics at a Mach Number of 2.01 of a Tailless Delta V/STOL Configuration Having Variable-Sweep Wing Panels. NASA TM X-634, 1961.

TABLE I.- GEOMETRIC CHARACTERISTICS OF MODEL 1a

Model scale	1/20
Reference areas and dimensions used in computations:	
Area (planform area of body (without ducts) with fixed delta wing having 81° leading-edge sweep included between model stations 9.700 inches (leading edge of inlet) and 31.900 inches (intersection of projection of trailing edge of fixed delta wing and plane of symmetry of model)), S, sq ft	0.760
Length (distance between model stations 9.700 inches and 31.900 inches), c, in.	22.200
Span (maximum width of fixed delta wing with 81° leading-edge sweep body), in.	8.150
Location of moment reference point:	
Station (full scale), in.	429
Water line (full scale), in.	6.240
Body, B:	
Leading-edge sweep of fixed delta wing, deg	81
Model station of nose, in.	1.900
Length, in.	35.520
Maximum width (occurs from model station 29.807 inches to model station 32.257 inches), in.	8.150
Cross-sectional area (includes duct area), maximum, sq ft	0.0875
Base area, A_b, sq ft	0.0205
Auxiliary variable-sweep outboard panels W of fixed delta wing:	
Airfoil section (perpendicular to leading edge):	
Lower surface	Flat
Upper surface	Upper surface of NACA 65_1A012
Maximum thickness, percent chord	6
Span (projected; $\Lambda = 12°$ position), in.	19.80
Incidence of root chord with respect to model reference line, deg	1.5
Dihedral, deg	-6
Twist, deg	0

TABLE I.- GEOMETRIC CHARACTERISTICS OF MODEL 1a - Concluded

Horizontal tail, H:	
Dihedral of inboard panel, deg	-4.57
Dihedral of outboard panel, deg	-25
Leading-edge sweep of outboard panel (true), deg	50.5
Airfoil section of outboard panel	NACA 65A004
Area (true), two semispans:	
Outboard panels, sq ft	0.0349
Inboard panels, sq ft	0.0565
Total, sq ft	0.0914
Forward of hinge line, sq ft	0.0026
Span (projected), in.	11.140
Taper ratio of outboard panel	0.241
Mean aerodynamic chord of outboard panel, in.	1.710
Sweep of hinge line, deg	5
Vertical tail, V:	
Airfoil section	NACA 65A004
Root chord (at model reference line), in.	7.225
Tip chord, in.	1.285
Taper ratio	0.178
Span (from model reference line), in.	5.500
Area (from model reference line), sq ft	0.164
Aspect ratio	1.304
Mean aerodynamic chord, in.	4.940
Leading-edge sweep, deg	55
Duct areas:	
Projected inlet, A_i, sq ft	0.0264
Inlet throat (total), sq ft	0.0250
Exit:	
Forward, $A_{e,1}$, sq ft	0.0160
Rearward, $A_{e,2}$, sq ft	0.0146
$(A_{e,1} + A_{e,2})/A_i$	1.16

TABLE II.- GEOMETRIC CHARACTERISTICS OF MODEL 1b

Model scale	1/20
Reference areas and dimensions used in computations:	
Area (planform area of body (without ducts) with fixed delta wing having 81° leading-edge sweep included between model stations 9.700 inches (leading edge of inlet) and 31.900 inches (intersection of projection of trailing edge of fixed delta wing and plane of symmetry of model)), S, sq ft	0.760
Length (distance between model stations 9.700 inches and 31.900 inches), c, in.	22.200
Span (maximum width of fixed delta wing with 81° leading-edge sweep body), in.	8.150
Location of moment reference point:	
Station (full scale), in.	429
Water line (full scale), in.	6.240
Body, B:	
Leading-edge sweep of fixed delta wing, deg	73
Model station of nose, in.	1.900
Length, in.	35.520
Maximum width, in.	10.520
Base area, A_b, sq ft	0.0205
Auxiliary variable-sweep outboard panels W of fixed delta wing:	
Airfoil section (perpendicular to leading edge):	
Lower surface	Flat
Upper surface	Upper surface of NACA 65_1A012
Maximum thickness, percent chord	6
Span (projected; Λ = 12° position), in.	19.80
Incidence of root chord with respect to model reference line, deg	1.5
Dihedral, deg	-6
Twist, deg	0

TABLE II.- GEOMETRIC CHARACTERISTICS OF MODEL 1b - Concluded

Horizontal tail, H:	
Dihedral of inboard panel, deg	-4.57
Dihedral of outboard panel, deg	-25
Leading-edge sweep of outboard panel (true), deg	50.5
Airfoil section of outboard panel	NACA 65A004
Area (true), two semispans:	
Outboard panels, sq ft	0.0349
Inboard panels, sq ft	0.0565
Total, sq ft	0.0914
Forward of hinge line, sq ft	0.0026
Span (projected), in.	13.750
Taper ratio of outboard panel	0.241
Mean aerodynamic chord of outboard panel, in.	1.710
Sweep of hinge line, deg	5
Vertical tail, V:	
Airfoil section	NACA 65A004
Root chord (at model reference line), in.	7.225
Tip chord, in.	1.285
Taper ratio	0.178
Span (from model reference line), in.	5.500
Area (from model reference line), sq ft	0.164
Aspect ratio	1.304
Mean aerodynamic chord, in.	4.940
Leading-edge sweep, deg	55
Duct areas:	
Projected inlet, A_i, sq ft	0.0264
Inlet throat (total), sq ft	0.0250
Exit:	
Forward, $A_{e,1}$, sq ft	0.0160
Rearward, $A_{e,2}$, sq ft	0.0146
$(A_{e,1} + A_{e,2})/A_i$	1.16

[redacted]

TABLE III.- GEOMETRIC CHARACTERISTICS OF MODELS 2a AND 2b

Model scale	1/20
Reference areas and dimensions used in computations:	
Area (planform area of body (without ducts) with fixed delta wing having 81° leading-edge sweep included between model stations 9.700 inches (leading edge of inlet) and 31.900 inches (intersection of projection of trailing edge of fixed delta wing and plane of symmetry of model)), S, sq ft	0.760
Length (distance between model stations 9.700 inches and 31.900 inches), c, in.	22.200
Span (maximum width of fixed delta wing with 81° leading-edge sweep body), in.	8.150
Location of moment reference point:	
Station (full scale), in.	429
Water line (full scale), in.	6.240
Body, B:	
Leading-edge sweep of fixed delta wing, deg	71.75
Model station of nose, in.	-0.425
Length, in.	37.845
Maximum width (occurs from model station 28.650 inches to model station 31.282 inches), in.	10.650
Base area, A_b, sq ft	0.0205
Auxiliary variable-sweep outboard panels W of fixed delta wing:	
Airfoil section (perpendicular to leading edge):	
$\Lambda = 71.75°$ configurations:	
Lower surface	Flat
Upper surface	Upper surface of NACA 65_1A012
Maximum thickness, percent chord	6
$\Lambda = 15°$ configuration	NACA 65A006
Span (projected; $\Lambda = 15°$ position), in.	20.30
Incidence of root chord with respect to model reference line, deg	1
Dihedral, deg	-7.57
Twist, deg	0

[redacted]

TABLE III.- GEOMETRIC CHARACTERISTICS OF MODELS 2a AND 2b - Concluded

Horizontal tail, H:	
Leading-edge sweep of outboard panel, deg	71.75
Airfoil section of outboard panel	NACA 65A004
Area, two semispans:	
Outboard panels, sq ft	0.0156
Inboard panels, sq ft	0.0559
Total, sq ft	0.0715
Forward of hinge line, sq ft	0.0033
Span (projected), in.	12.358
Taper ratio of outboard panel	0
Mean aerodynamic chord of outboard panel, in.	1.755
Sweep of hinge line, deg	0
Vertical tail, V:	
Airfoil section	NACA 65A004
Root chord (at model reference line), in.	7.225
Tip chord, in.	1.285
Taper ratio	0.178
Span (from model reference line), in.	5.500
Area (from model reference line), sq ft	0.164
Aspect ratio	1.304
Mean aerodynamic chord, in.	4.940
Leading-edge sweep, deg	55
Duct areas:	
Projected inlet, A_i, sq ft	0.0250
Exit:	
Forward, $A_{e,1}$, sq ft	0.0123
Rearward, $A_{e,2}$, sq ft	0.0126
$(A_{e,1} + A_{e,2})/A_i$	1.00

[redacted]

TABLE IV.- GEOMETRIC CHARACTERISTICS OF MODEL 3

Model scale	1/30
Reference areas and dimensions used in computations:	
Area (planform area of fixed delta wing with 71.75° leading-edge sweep), S, sq ft	0.3694
Length (mean aerodynamic chord of fixed delta wing with 71.75° leading-edge sweep), c, in.	8.466
Span (span of fixed delta wing with 71.75° leading-edge sweep), in.	8.376
Location of moment reference point:	
Station (full scale), in.	429
Water line (full scale), in.	6.240
Body, B:	
Leading-edge sweep of fixed delta wing, deg	71.75
Model station of nose, in.	1.267
Length, in.	20.400
Base area, A_b, sq ft	0.0079
Fixed delta wing:	
Airfoil section (spanwise):	
Lower surface	Flat
Upper surface	Wedge
Maximum thickness at root chord, percent root chord	1.5
Mean aerodynamic chord, in.	8.466
Span, in.	8.376
Incidence of root chord with respect to model reference line, deg	1
Dihedral, deg	0
Twist, deg	0
Model station of leading edge of root chord, in.	8.333
Auxiliary variable-sweep outboard panels W of fixed delta wing	None on model
Duct areas:	
Projected inlet, A_i, sq ft	0.0109
Exit:	
Forward, $A_{e,1}$, sq ft	0.0068
Rearward, $A_{e,2}$, sq ft	0.0069
$(A_{e,1} + A_{e,2})/A_i$	1.26

[redacted]

TABLE V.- GEOMETRIC CHARACTERISTICS OF MODELS 4a AND 4b

Model scale	1/30
Reference areas and dimensions used in computations:	
Area (planform area of fixed delta wing with 71.75° leading-edge sweep), S, sq ft	0.3694
Length (mean aerodynamic chord of fixed delta wing with 71.75° leading-edge sweep), c, in.	8.466
Span (span of fixed delta wing with 71.75° leading-edge sweep), in.	8.376
Location of moment reference point:	
Station (full scale), in.	429
Water line (full scale), in.	6.240
Body, B:	
Leading-edge sweep of fixed delta wing, deg	71.75
Model station of nose, in.	-0.283
Length, in.	21.950
Base area, A_b, sq ft	0.0079
Fixed delta wing:	
Airfoil section (spanwise):	
Lower surface	Flat
Upper surface	Wedge
Maximum thickness at root chord, percent root chord	1.5
Mean aerodynamic chord, in.	8.466
Span, in.	8.376
Incidence of root chord with respect to model reference line, deg	1
Dihedral, deg	0
Twist, deg	0
Model station of leading edge of root chord, in.	8.333
Auxiliary variable-sweep outboard panels W of fixed delta wing	None on model
Duct areas:	
Model 4a:	
Projected inlet, A_i, sq ft	0.0107
Exit:	
Forward, $A_{e,1}$, sq ft	0.0061
Rearward, $A_{e,2}$, sq ft	0.0070
$(A_{e,1} + A_{e,2})/A_i$	1.22
Model 4b:	
Projected inlet, A_i, sq ft	0.0107
Exit:	
Forward, $A_{e,1}$, sq ft	0
Rearward, $A_{e,2}$, sq ft	0.0138
$A_{e,2}/A_i$	1.29

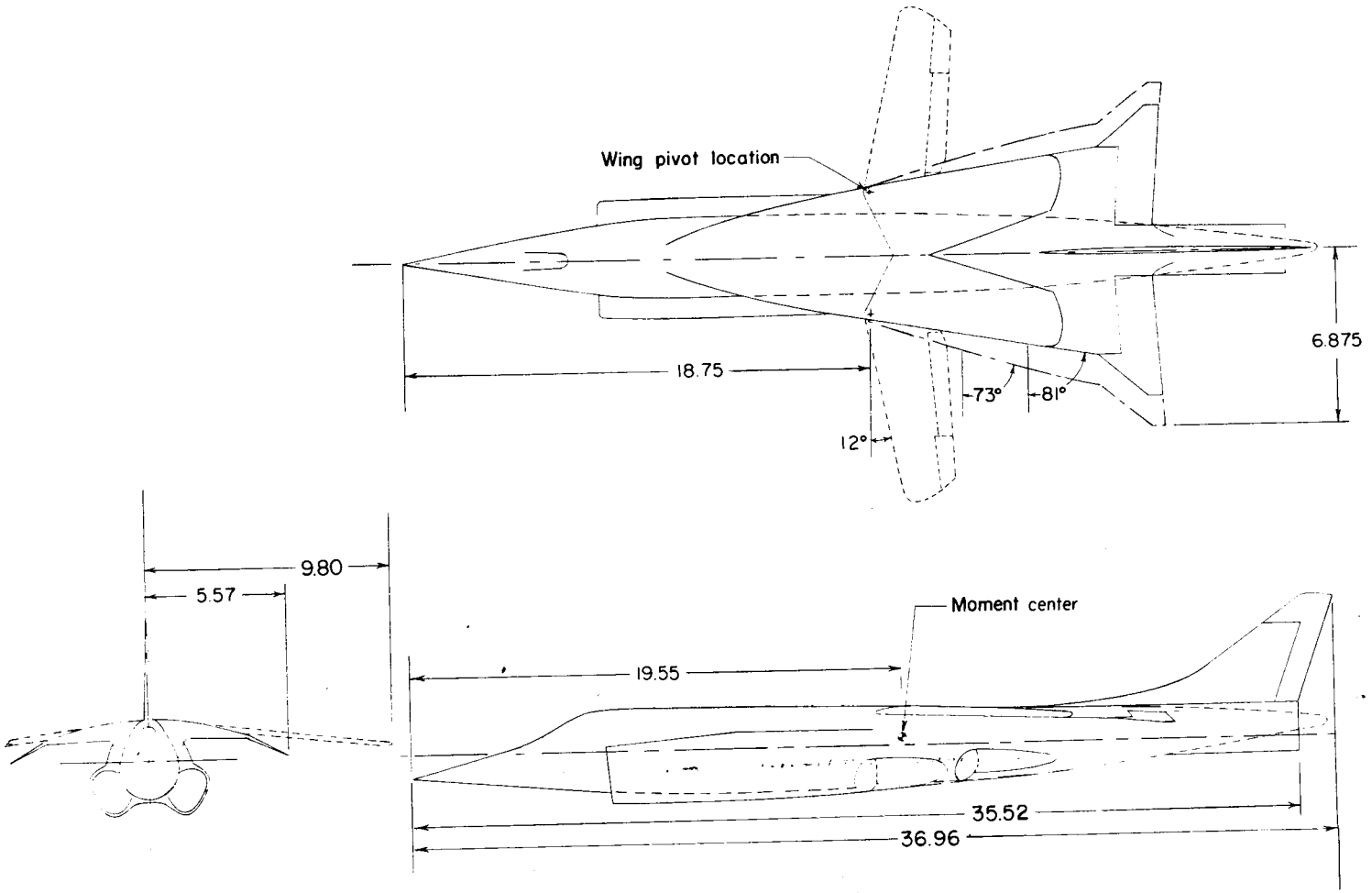

Figure 1.- General arrangement of 1/20-scale models 1a and 1b. All dimensions are in inches except as noted.

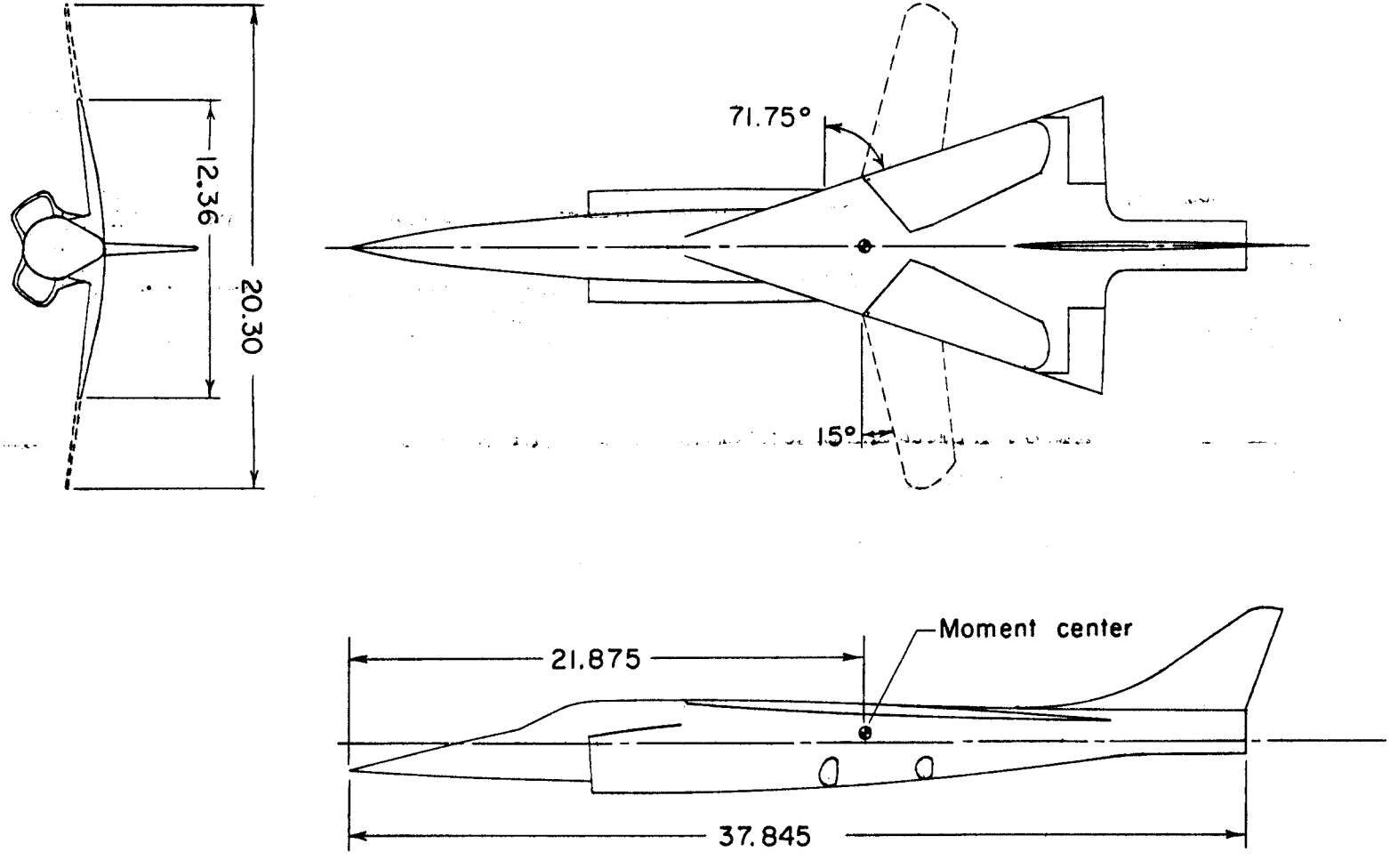

Figure 2.- General arrangement of 1/20-scale models 2a and 2b. All dimensions are in inches except as noted.

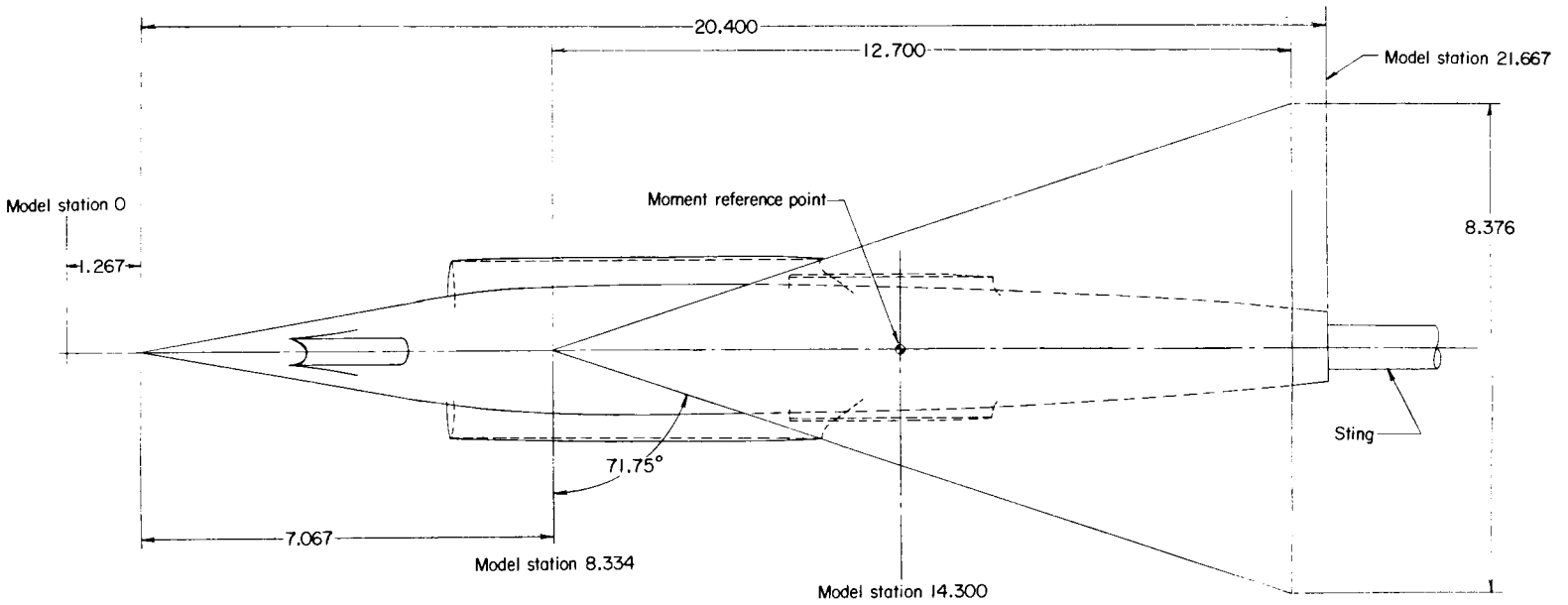

(a) Planform view.

Figure 3.- General arrangement of 1/30-scale model 3. All dimensions are in inches except as noted.

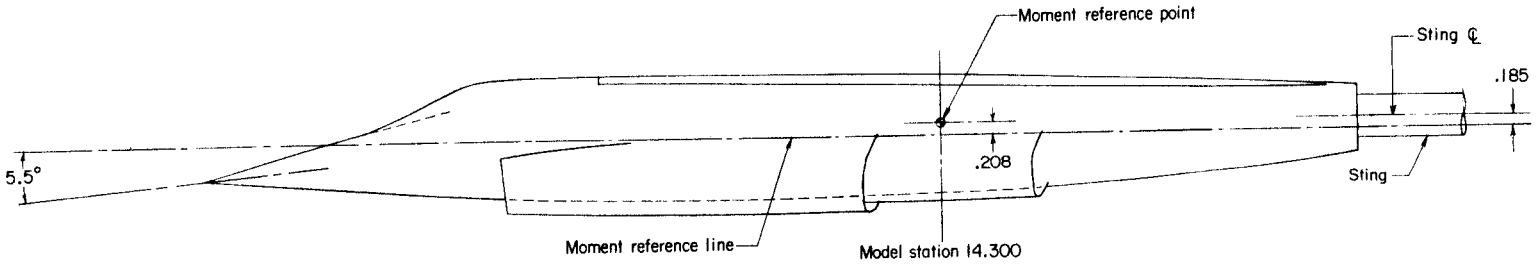

(b) Side view.

Figure 3.- Continued.

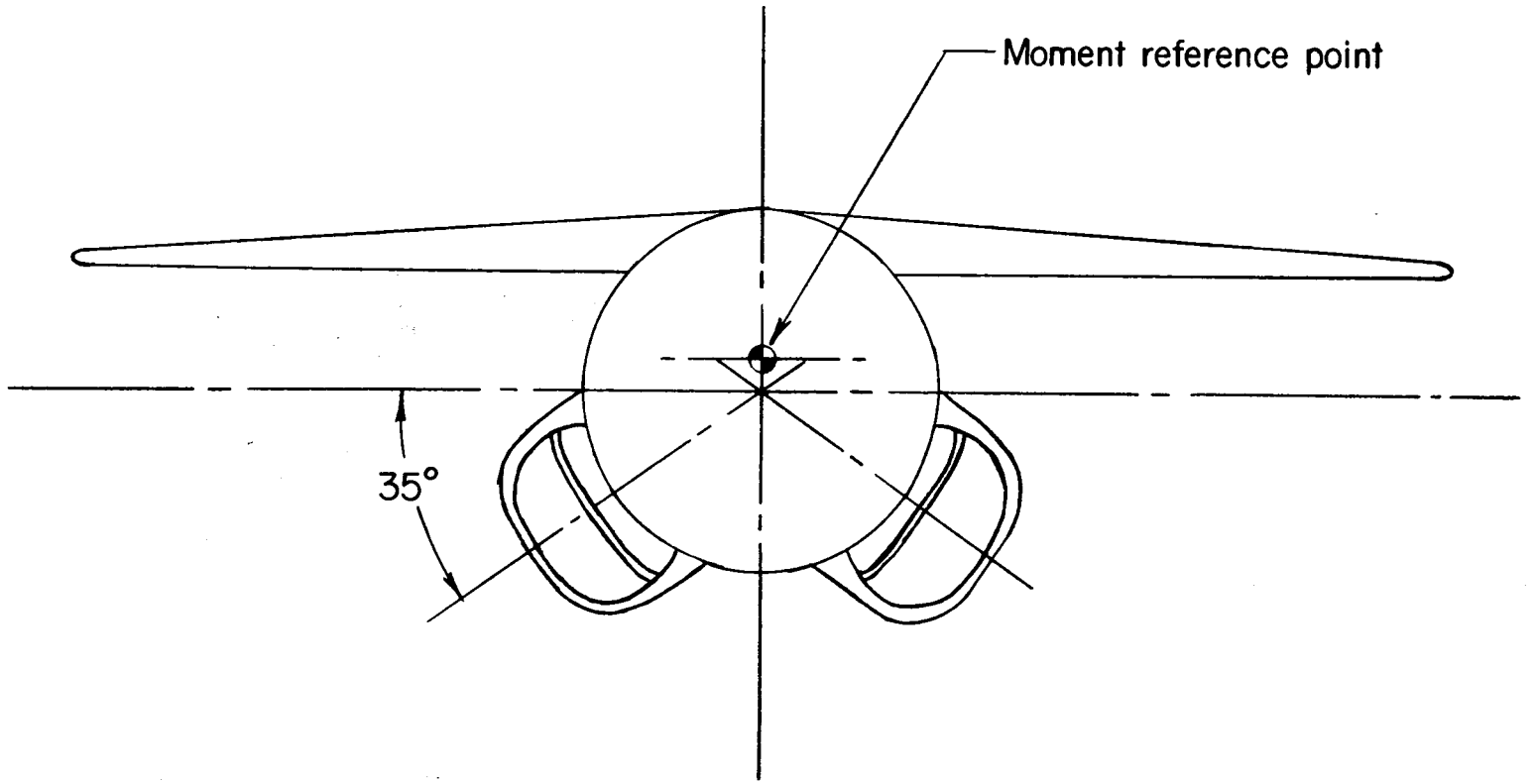

(c) Front view.

Figure 3.- Concluded.

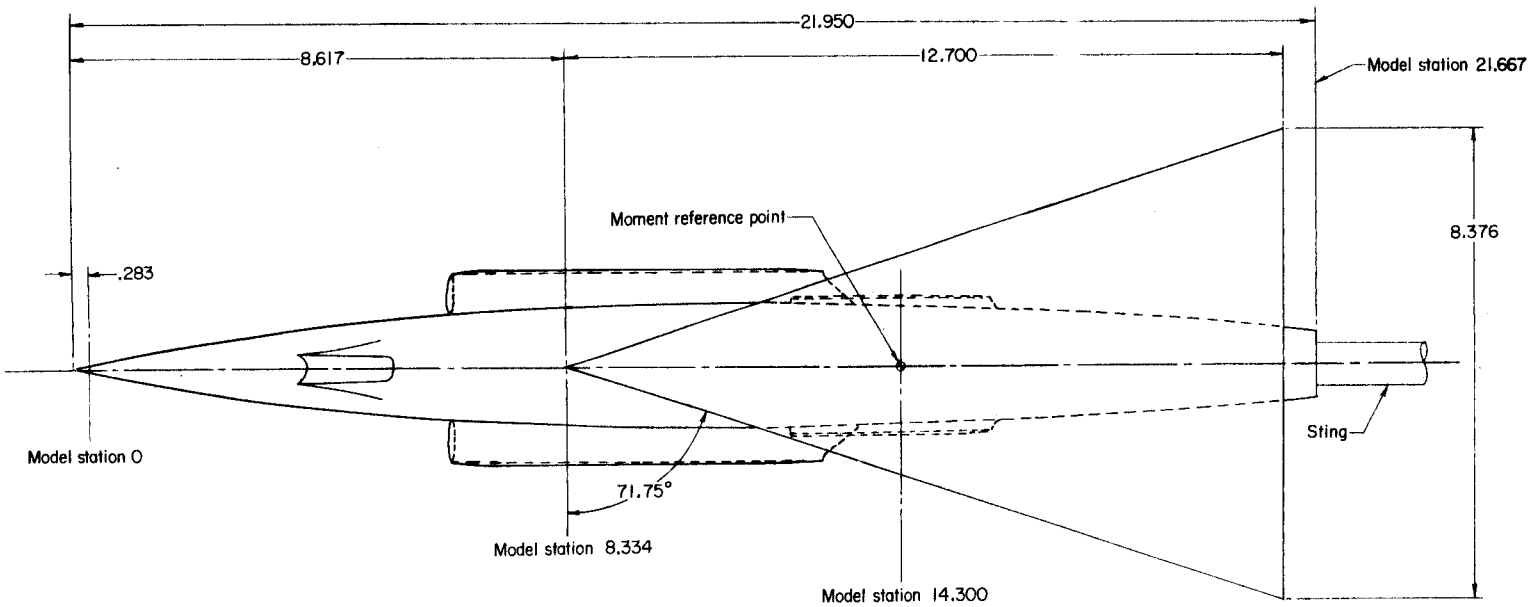

(a) Planform view.

Figure 4.- General arrangement of 1/30-scale models 4a and 4b. All dimensions are in inches except as noted.

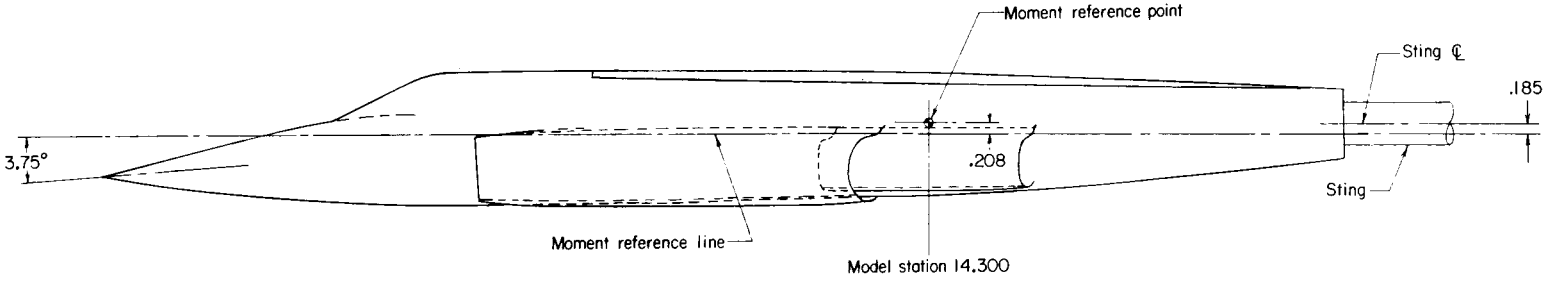

(b) Side view.

Figure 4.- Continued.

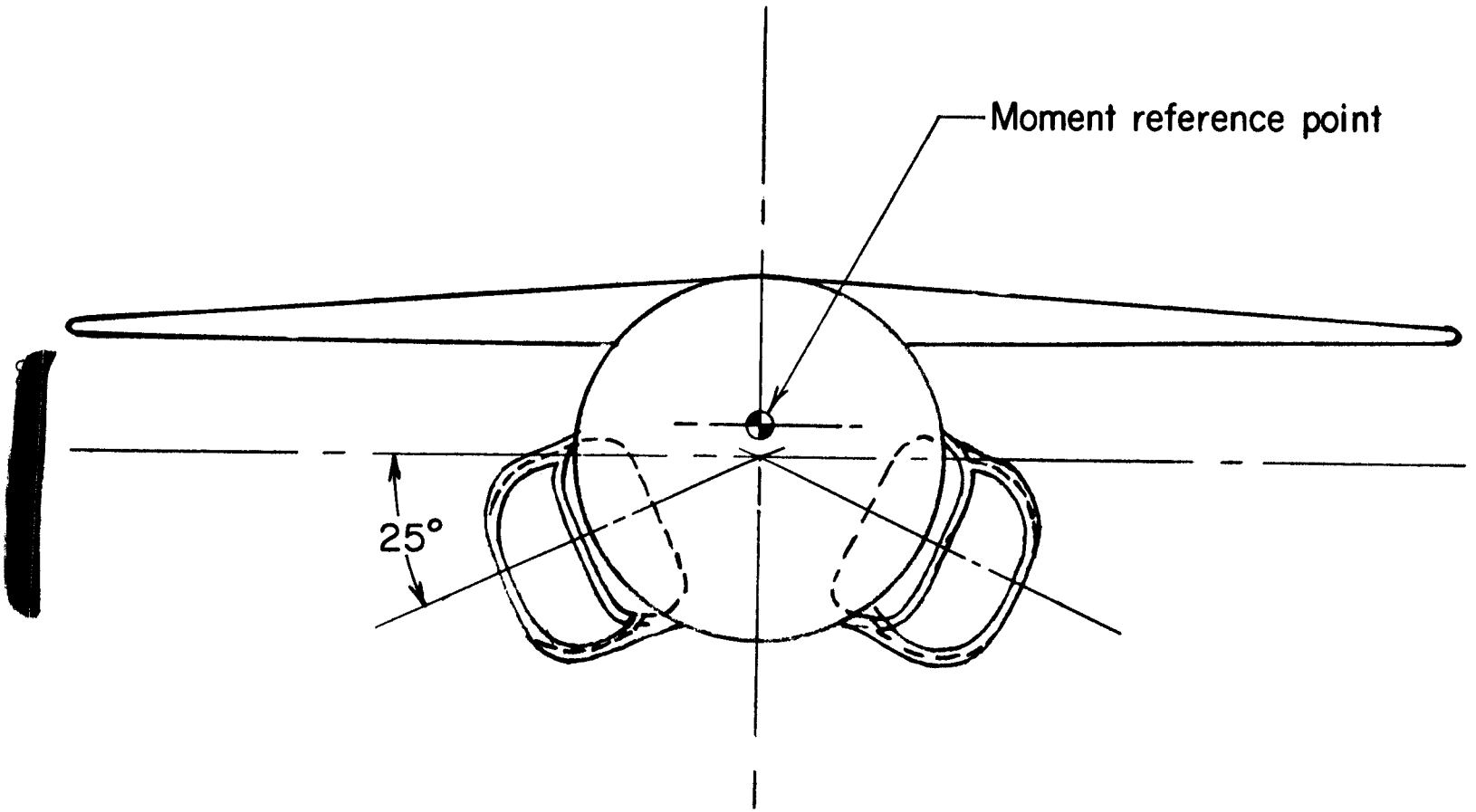

(c) Front view.

Figure 4.- Concluded.

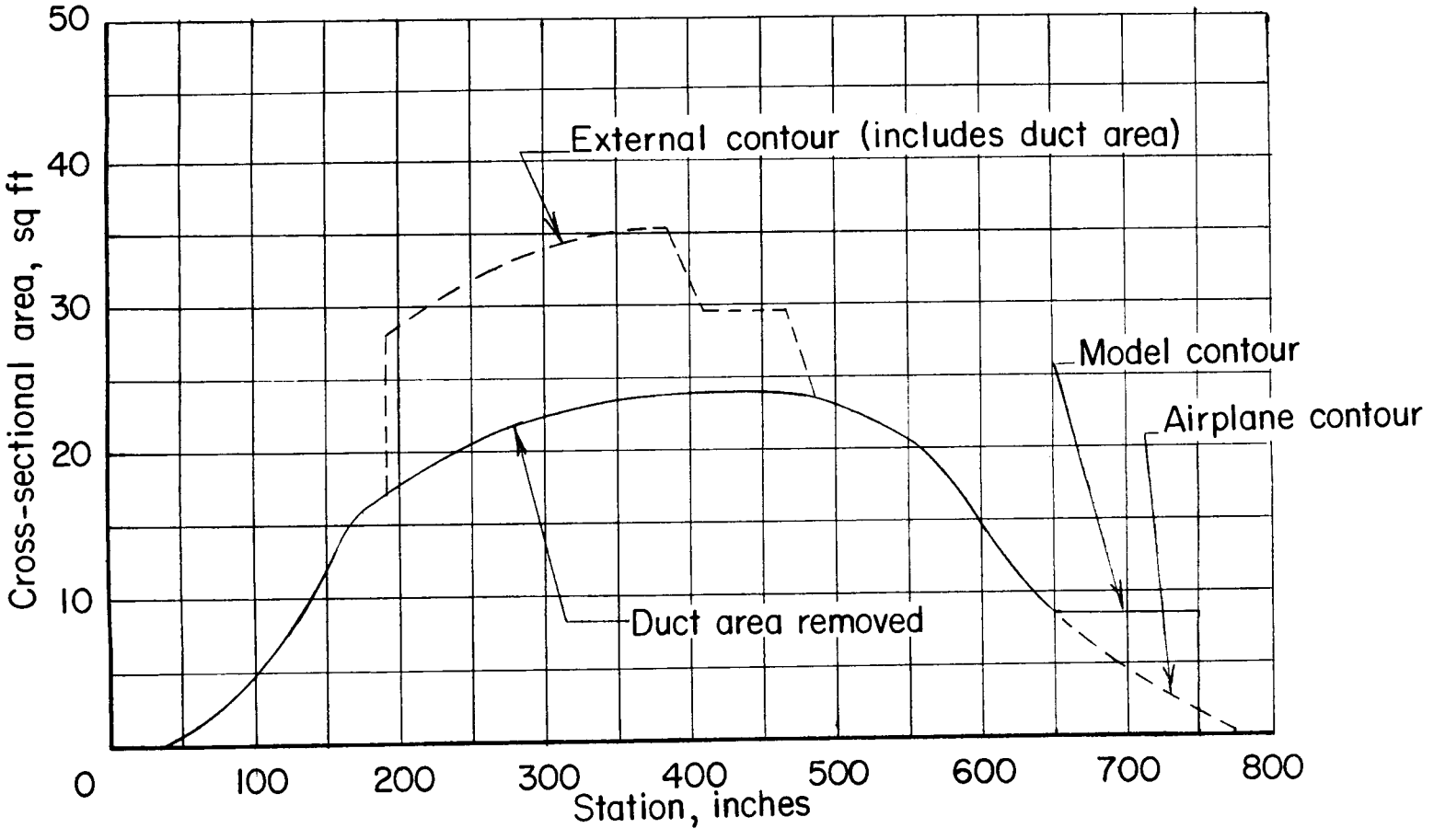

Figure 5.- Longitudinal distribution of normal cross-sectional area of model 1a (full-scale dimensions used). $\Lambda = 81^{\circ}$.

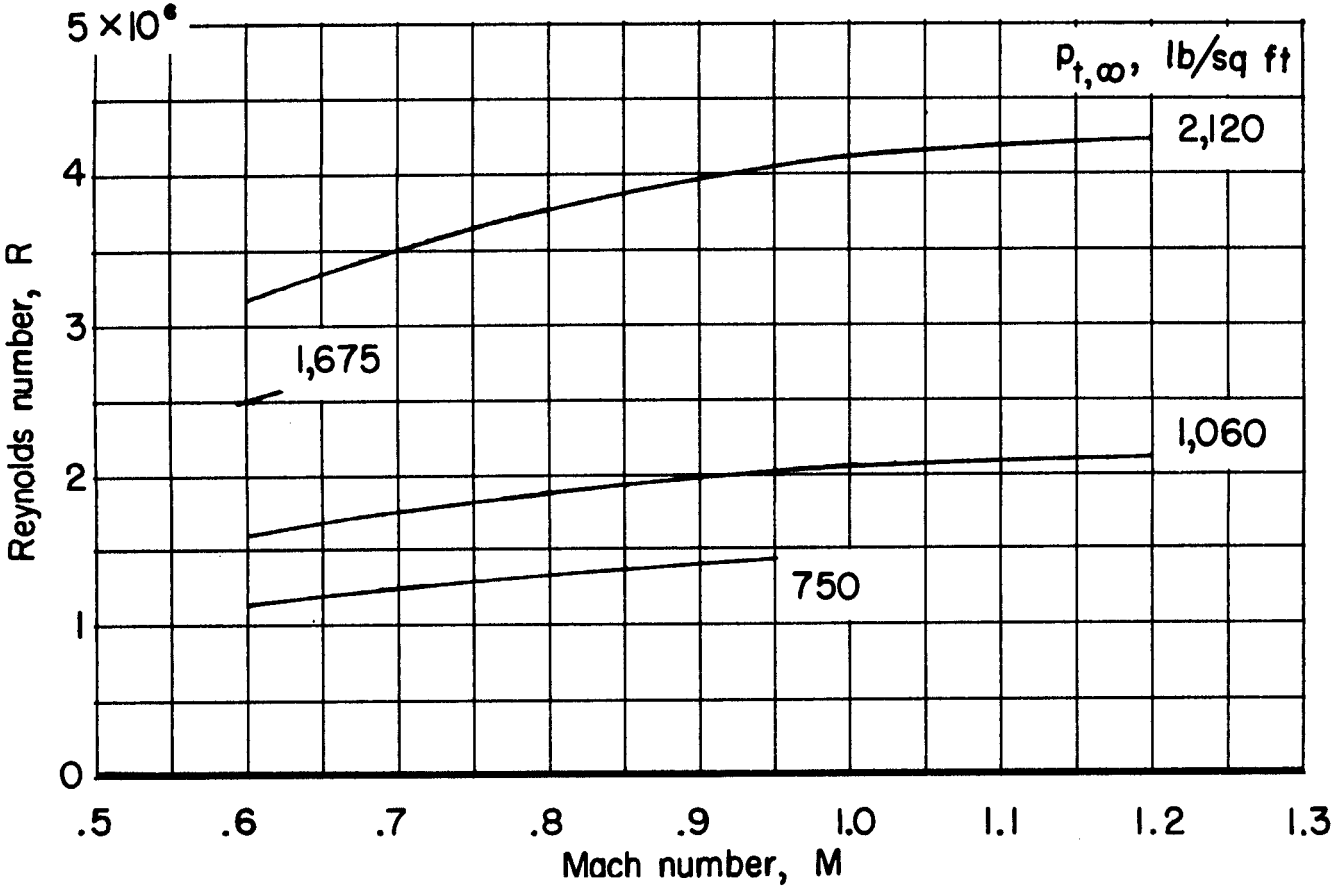

Figure 6.- Variation of Reynolds number (based on a reference length of 1 foot) with Mach number in present investigation. $t_{t,\infty} = 121^{\circ}$ F.

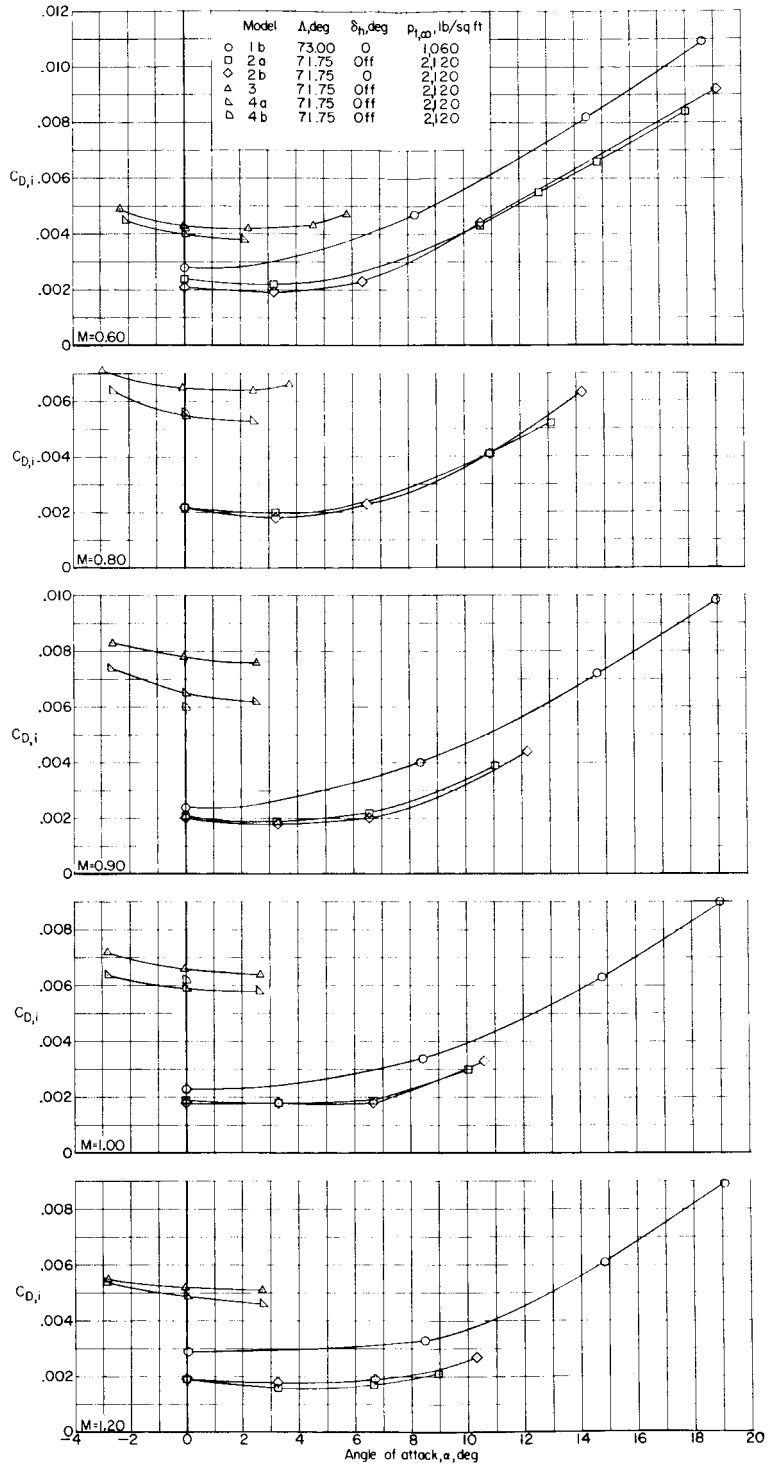

(a) Variation of $C_{D,i}$ with α.

Figure 7.- Internal drag coefficient and mass-flow ratio for various models.

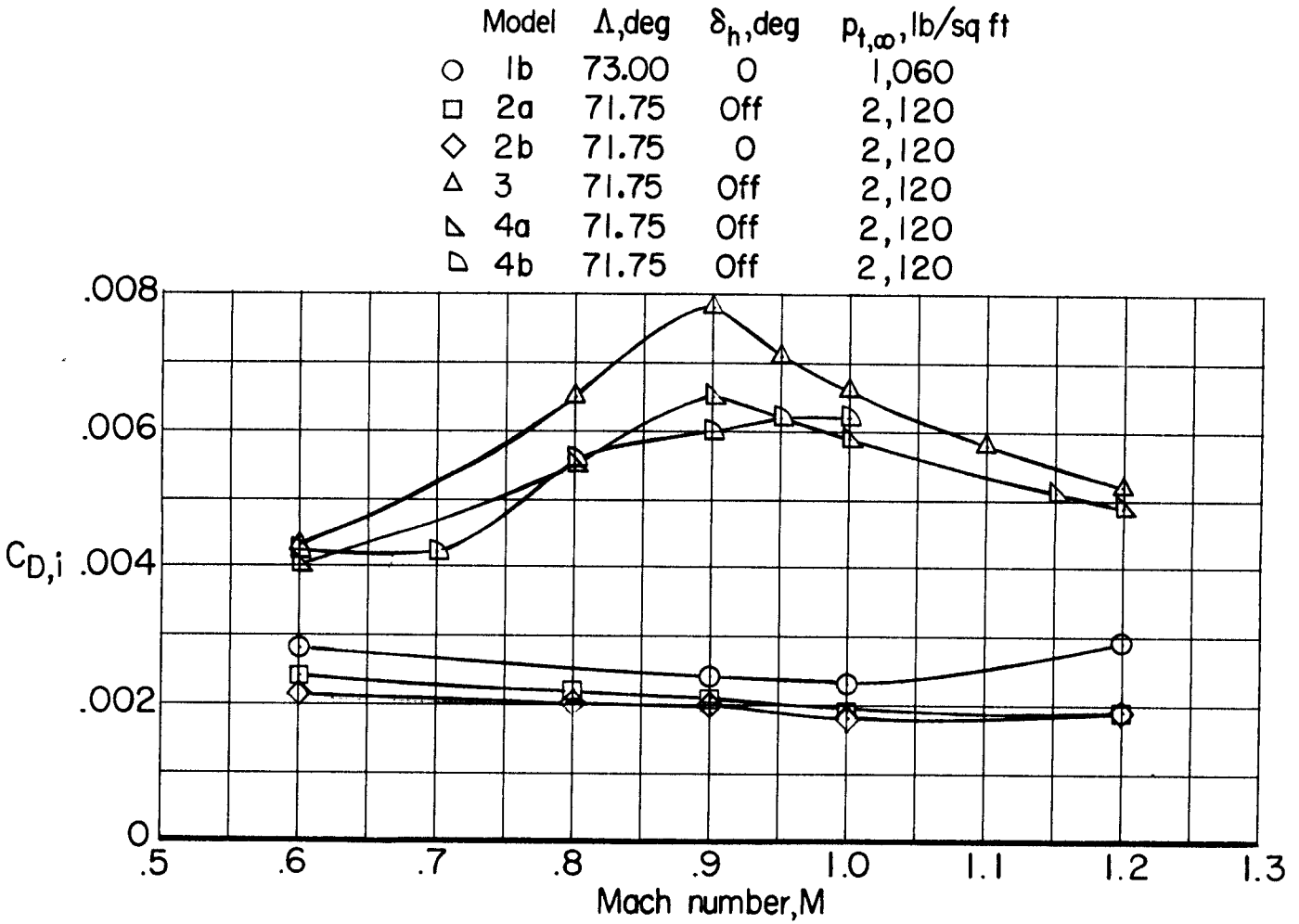

(b) Variation of $C_{D,i}$ with M. $\alpha = 0^\circ$.

Figure 7.- Continued.

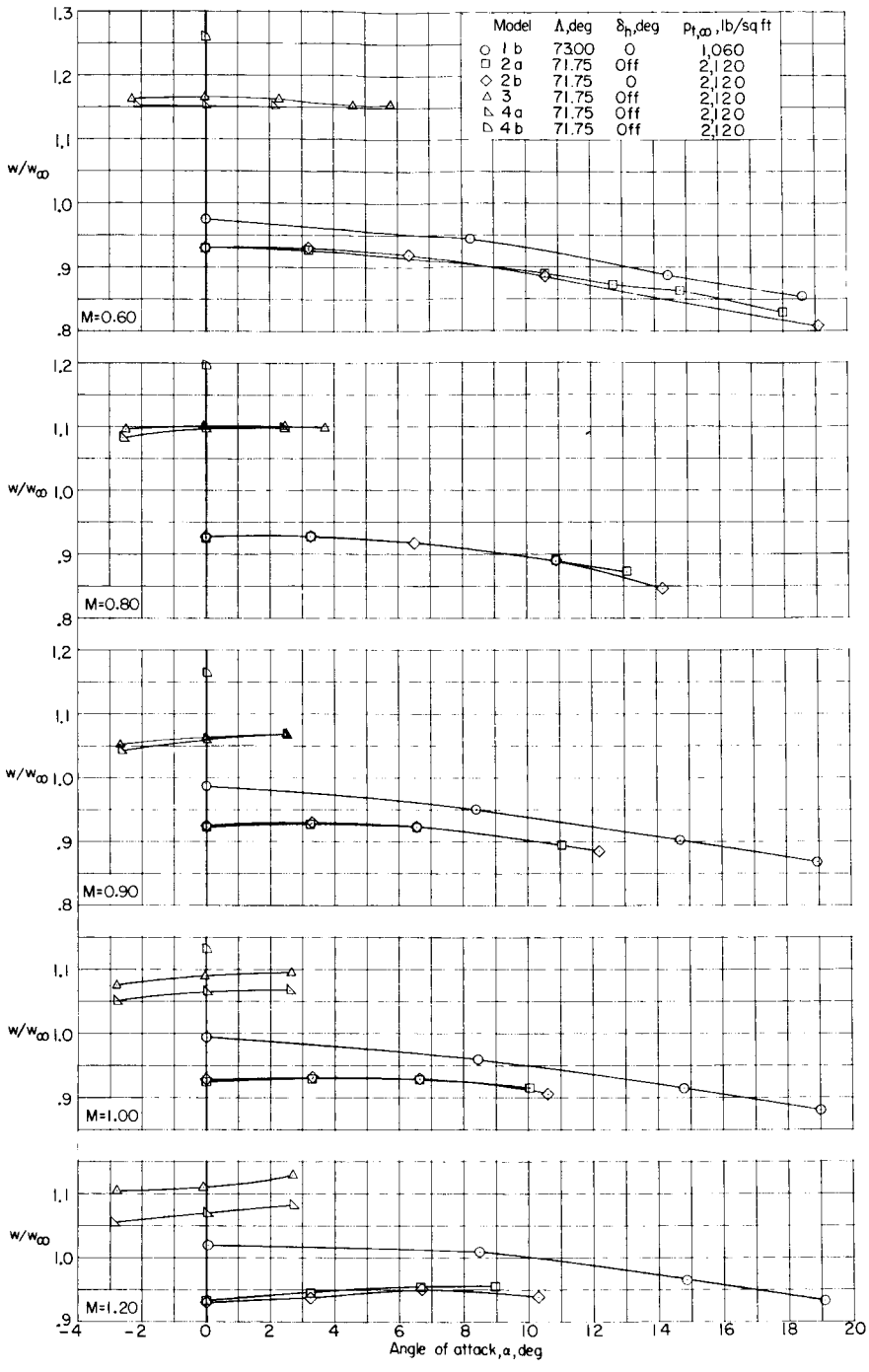

(c) Variation of w/w_∞ with α.

Figure 7.- Continued.

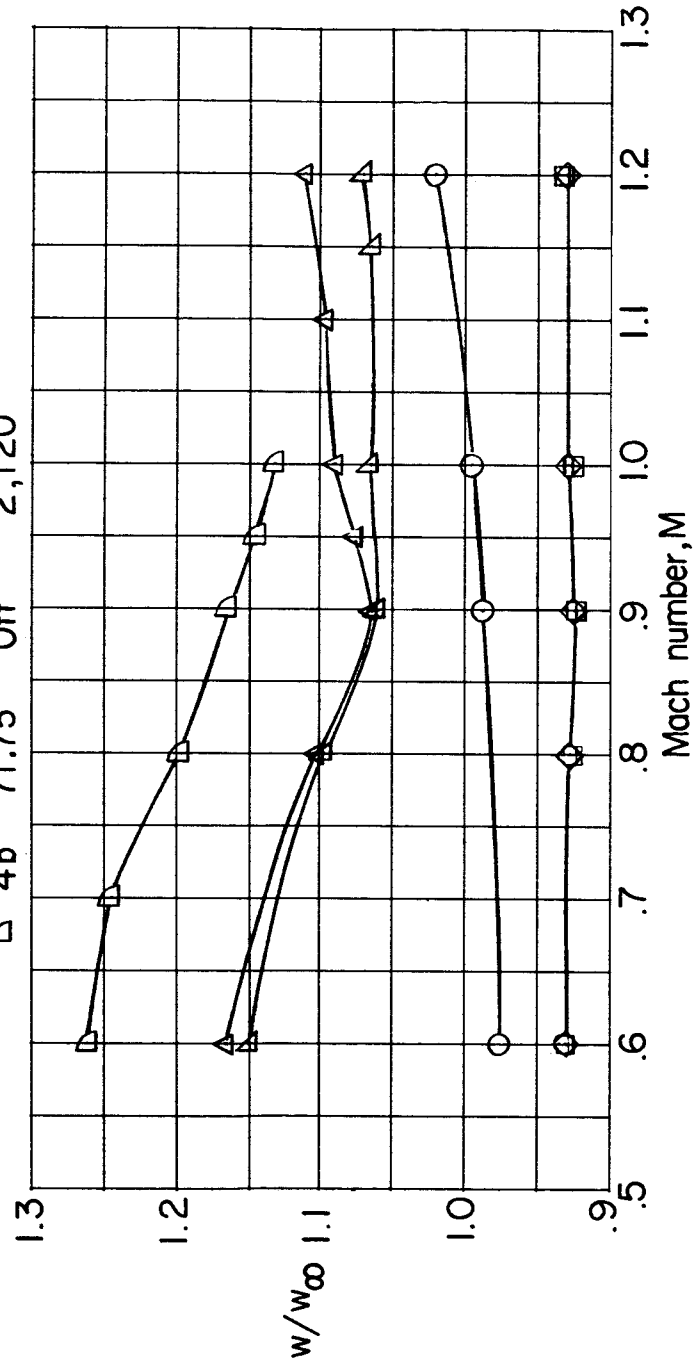

(d) Variation of w/w_∞ with M. $\alpha = 0^\circ$.

Figure 7.- Concluded.

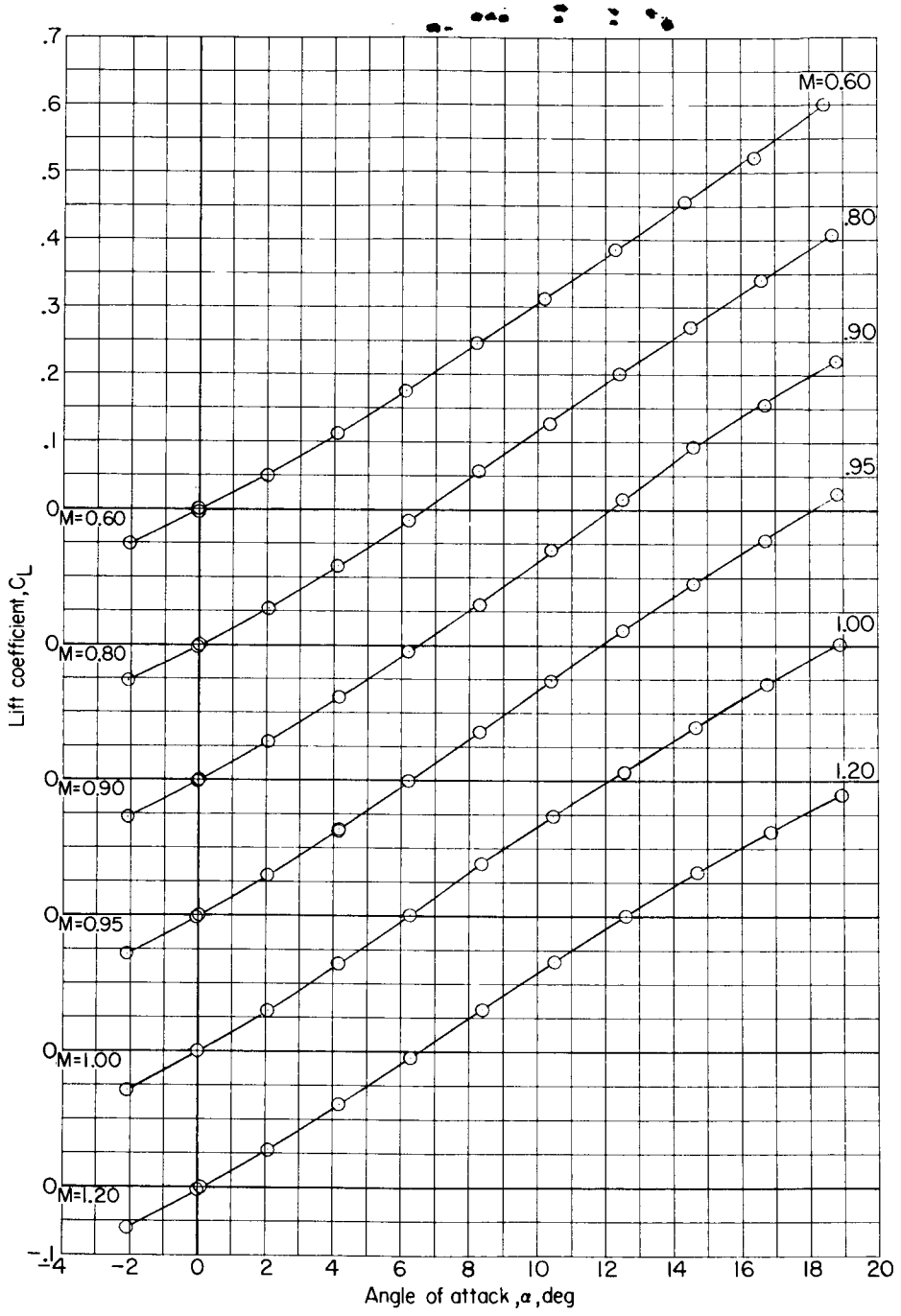

(a) Variation of C_L with α.

Figure 8.- Longitudinal aerodynamic characteristics of model 1a. $\Lambda = 81^\circ$; $\delta_h = 0^\circ$; $p_{t,\infty} = 1{,}060$ lb/sq ft.

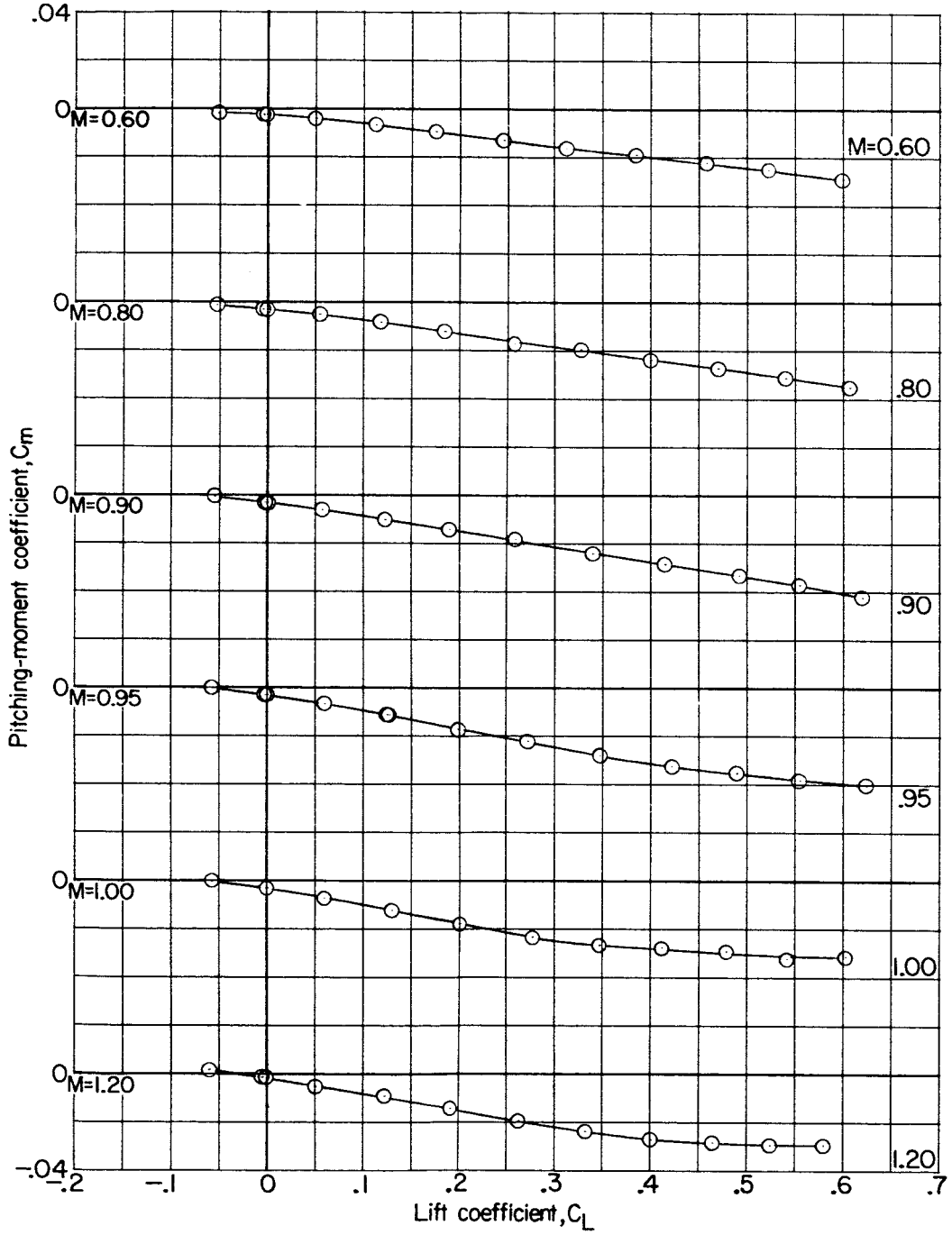

(b) Variation of C_m with C_L.

Figure 8.- Continued.

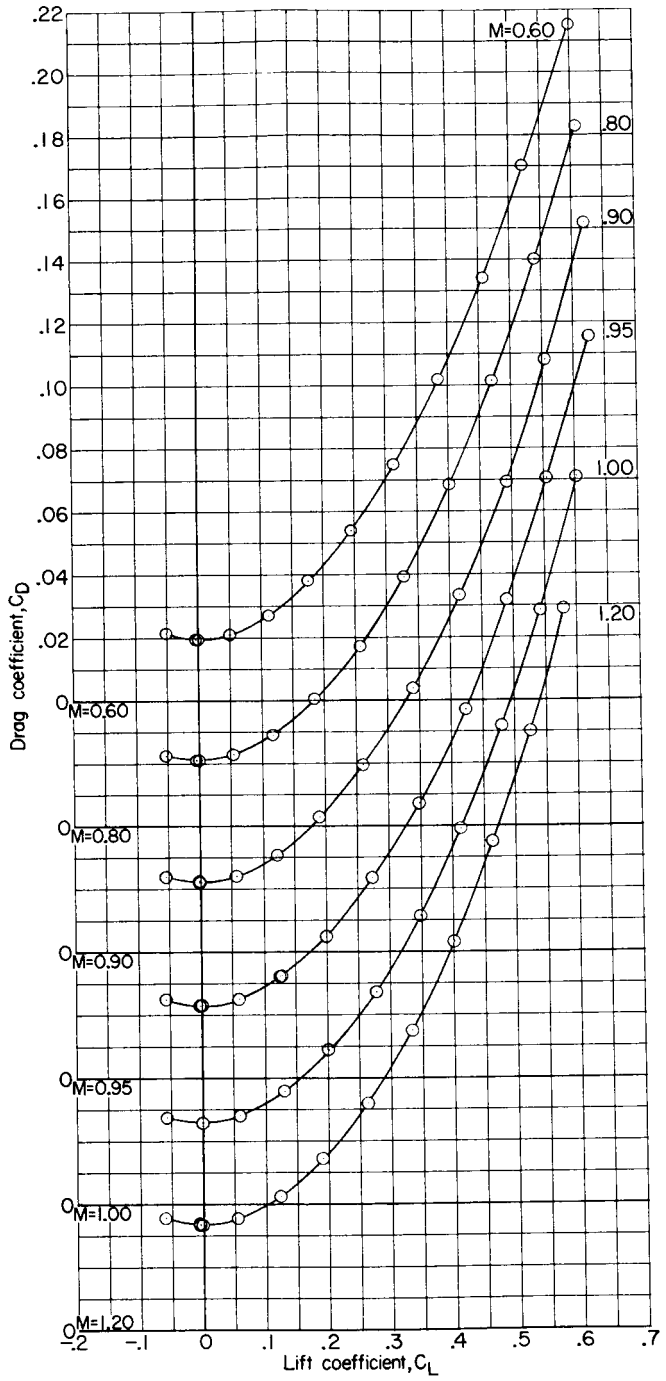

(c) Variation of C_D with C_L.

Figure 8.- Continued.

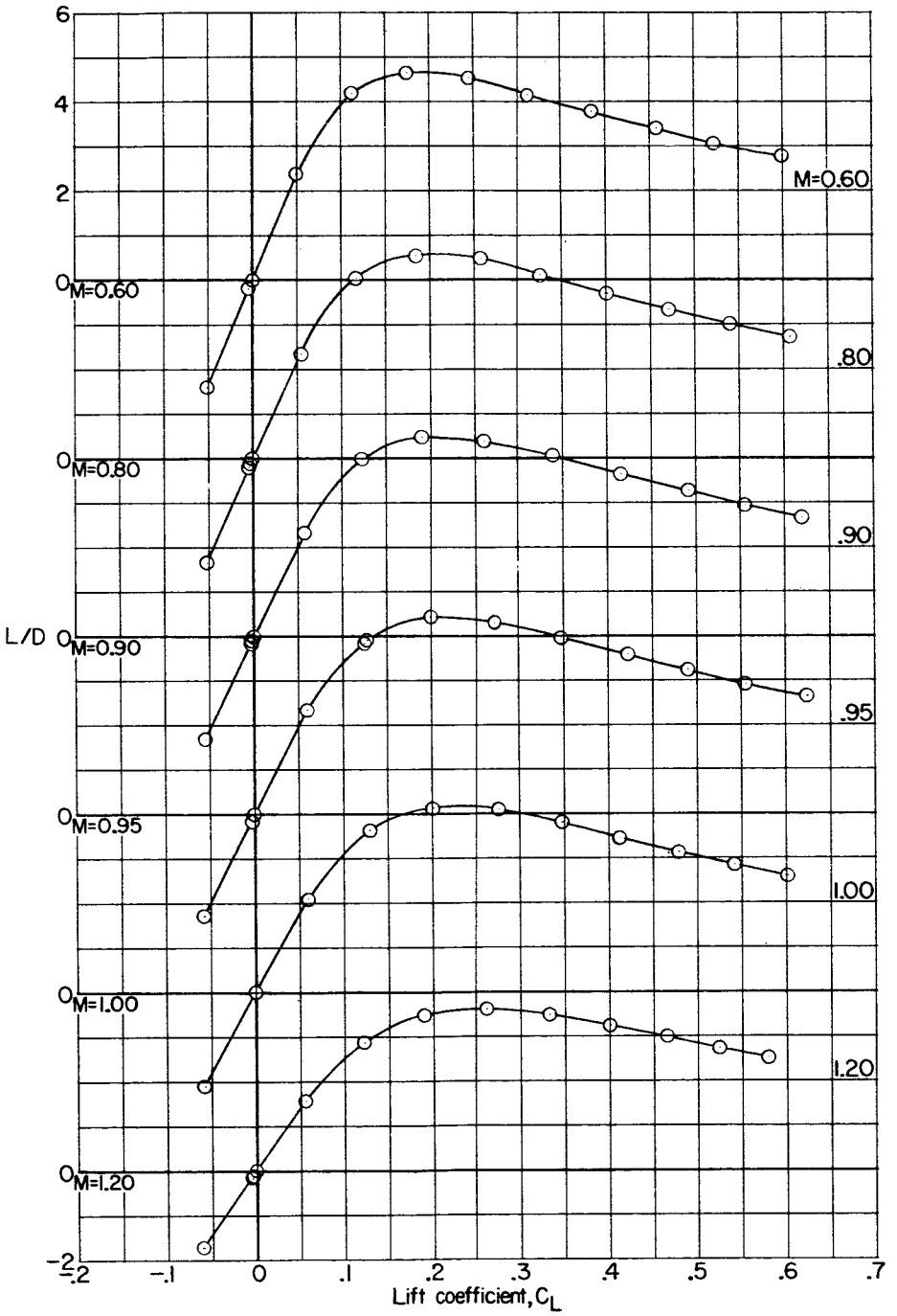

(d) Variation of L/D with C_L.

Figure 8.- Concluded.

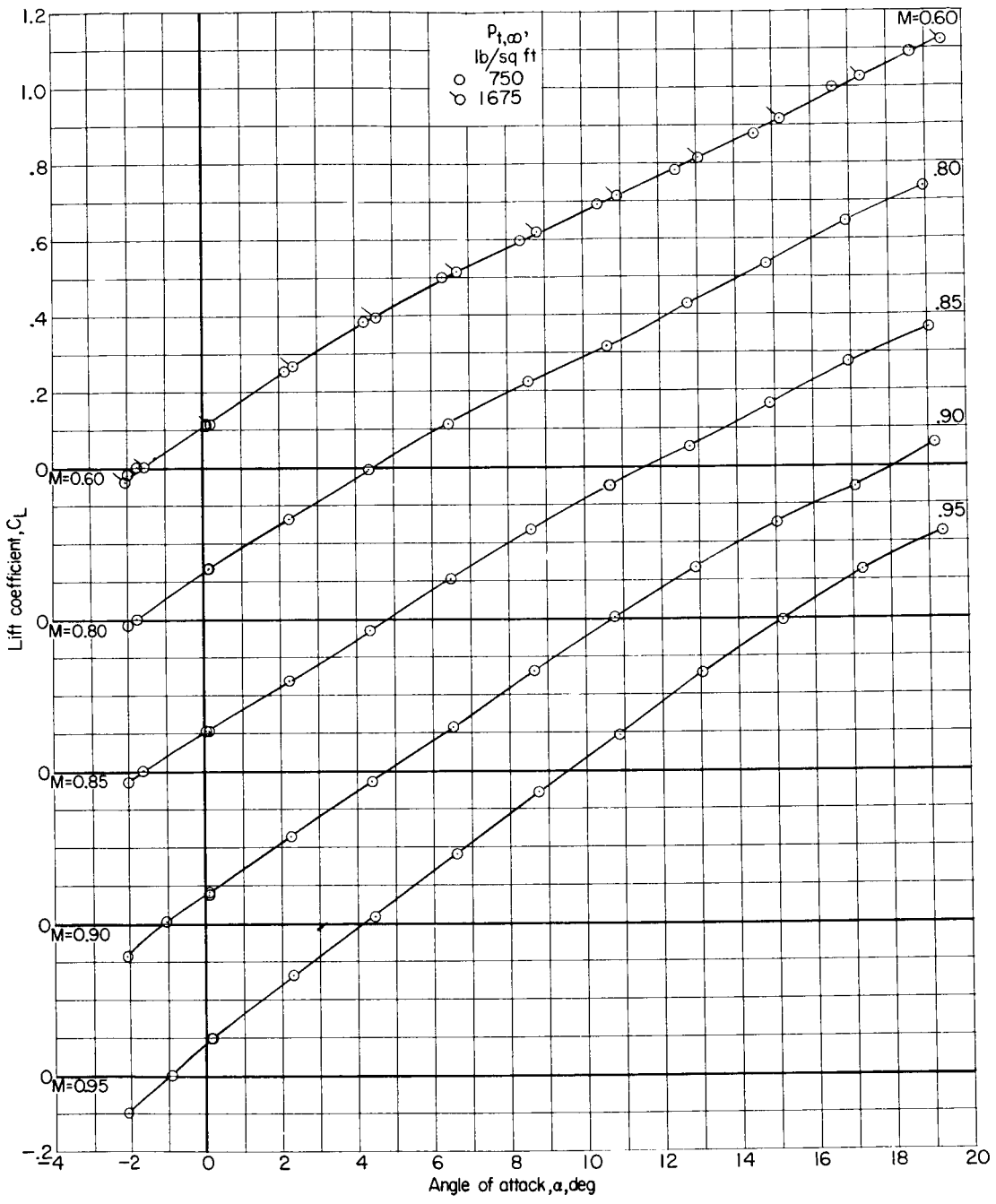

(a) Variation of C_L with α.

Figure 9.- Longitudinal aerodynamic characteristics of model 1b. $\Lambda = 12^\circ$; $\delta_h = 0^\circ$.

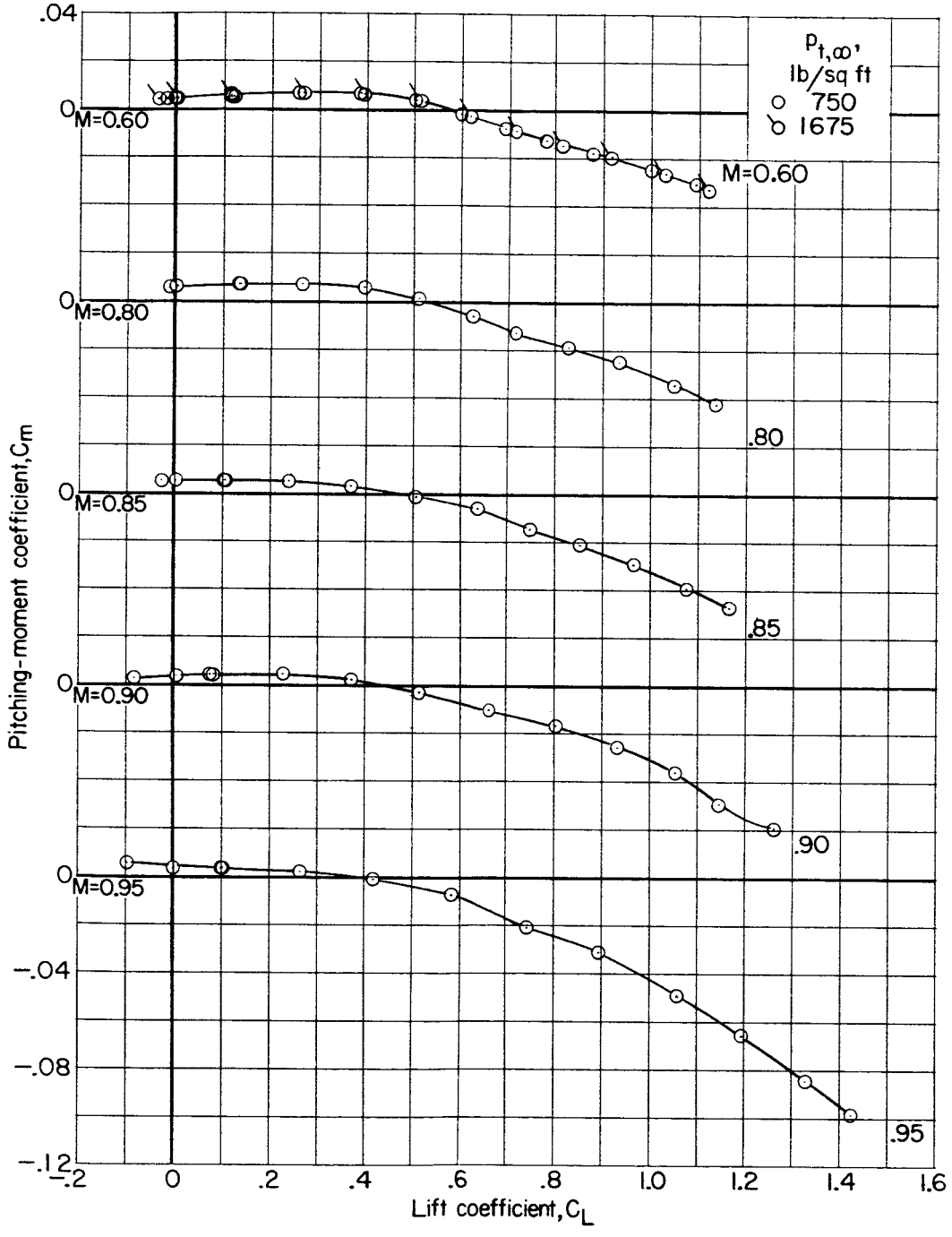

(b) Variation of C_m with C_L.

Figure 9.- Continued.

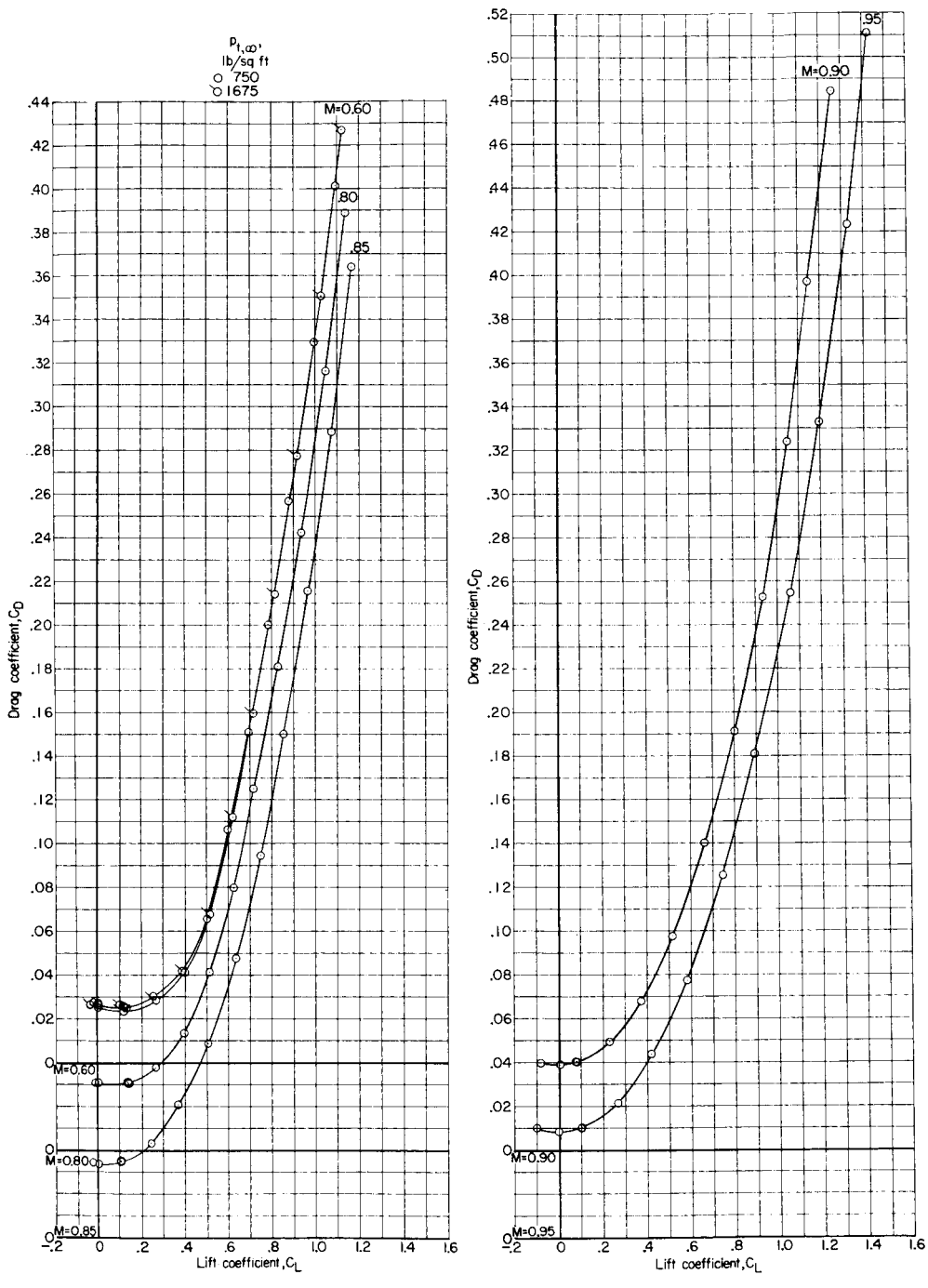

(c) Variation of C_D with C_L.

Figure 9.- Continued.

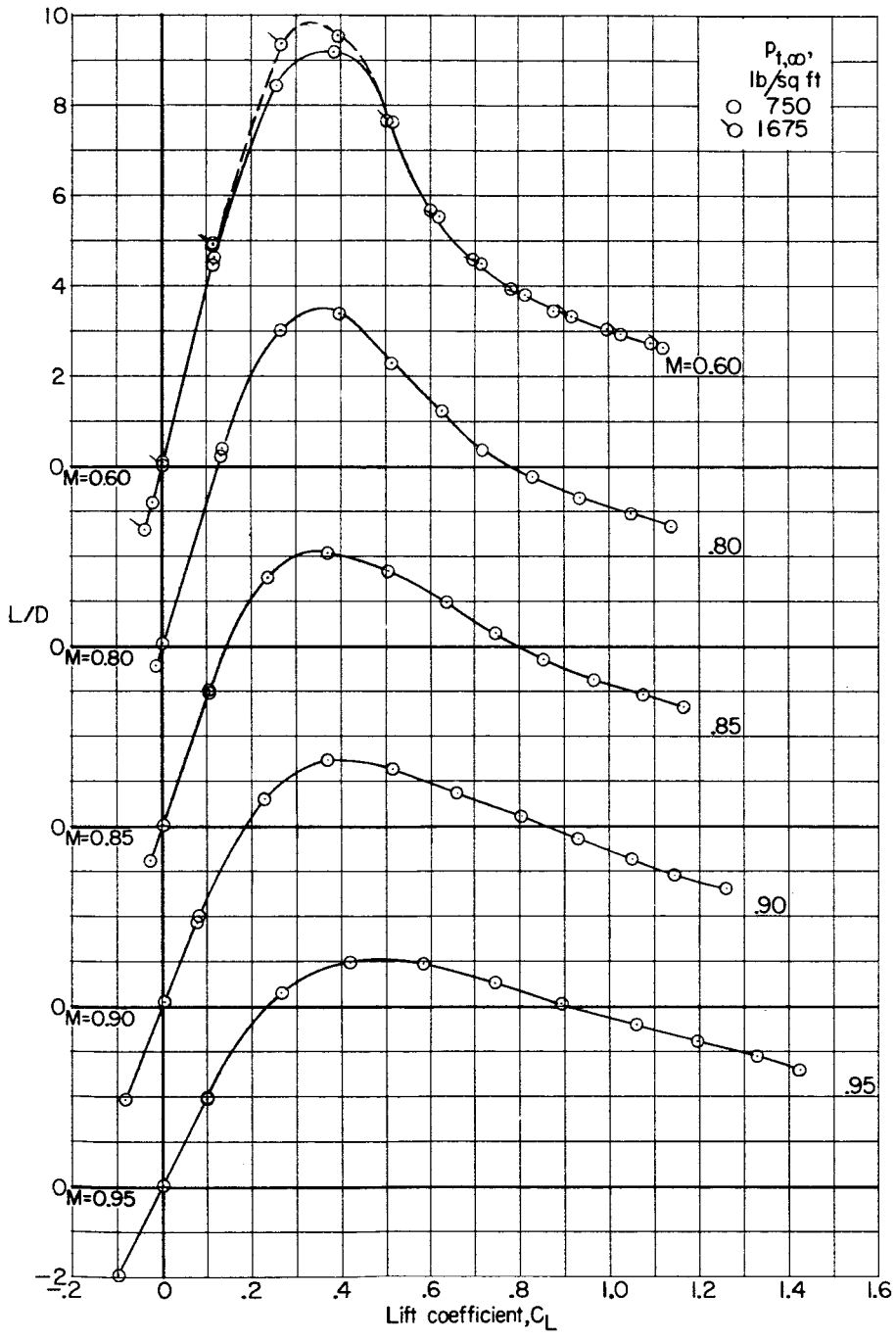

(d) Variation of L/D with C_L.

Figure 9.- Concluded.

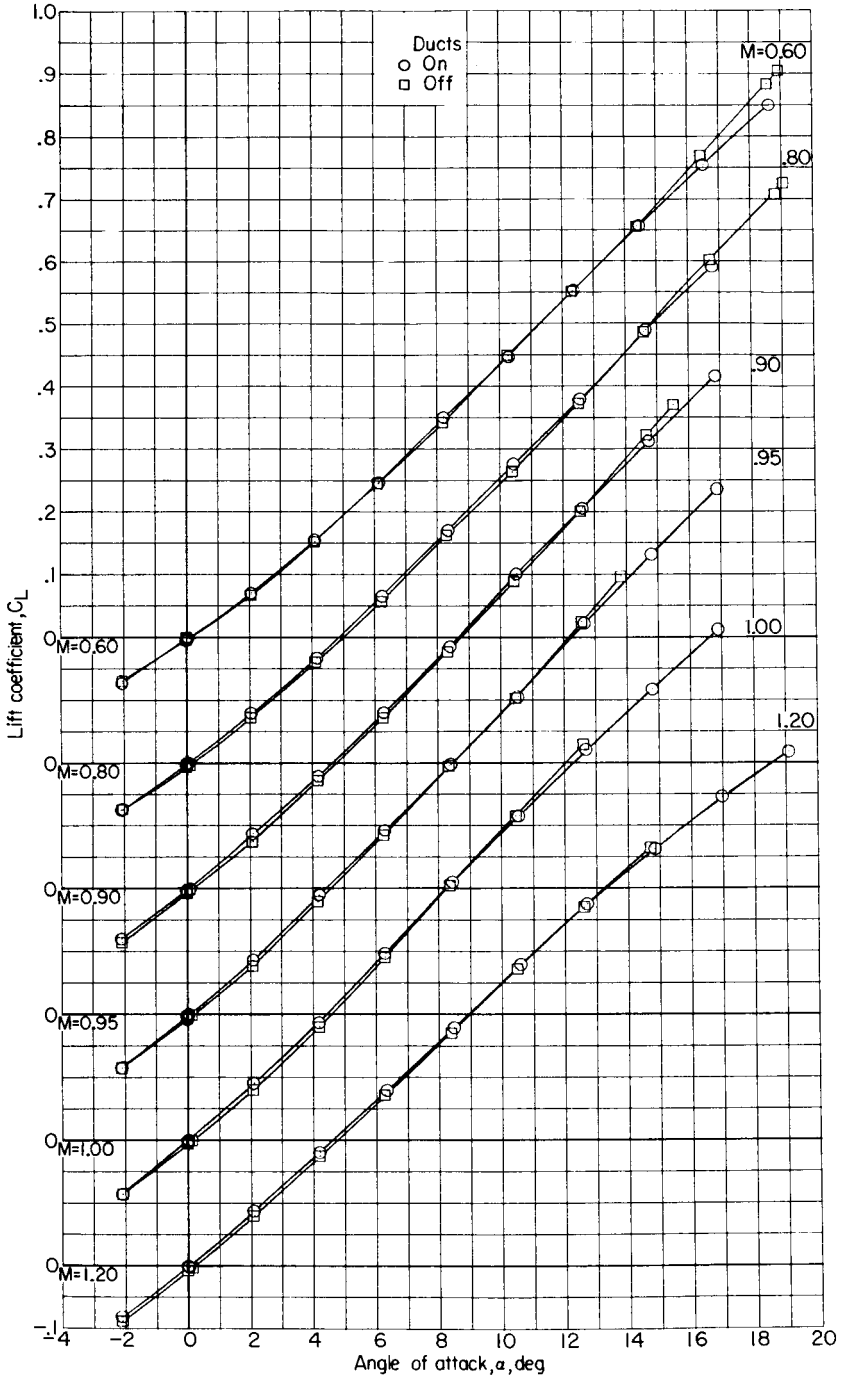

(a) Variation of C_L with α.

Figure 10.- Effect of ducts on longitudinal aerodynamic characteristics of model 1b. $\Lambda = 73^\circ$; $\delta_h = 0^\circ$; $p_{t,\infty} = 1{,}060$ lb/sq ft.

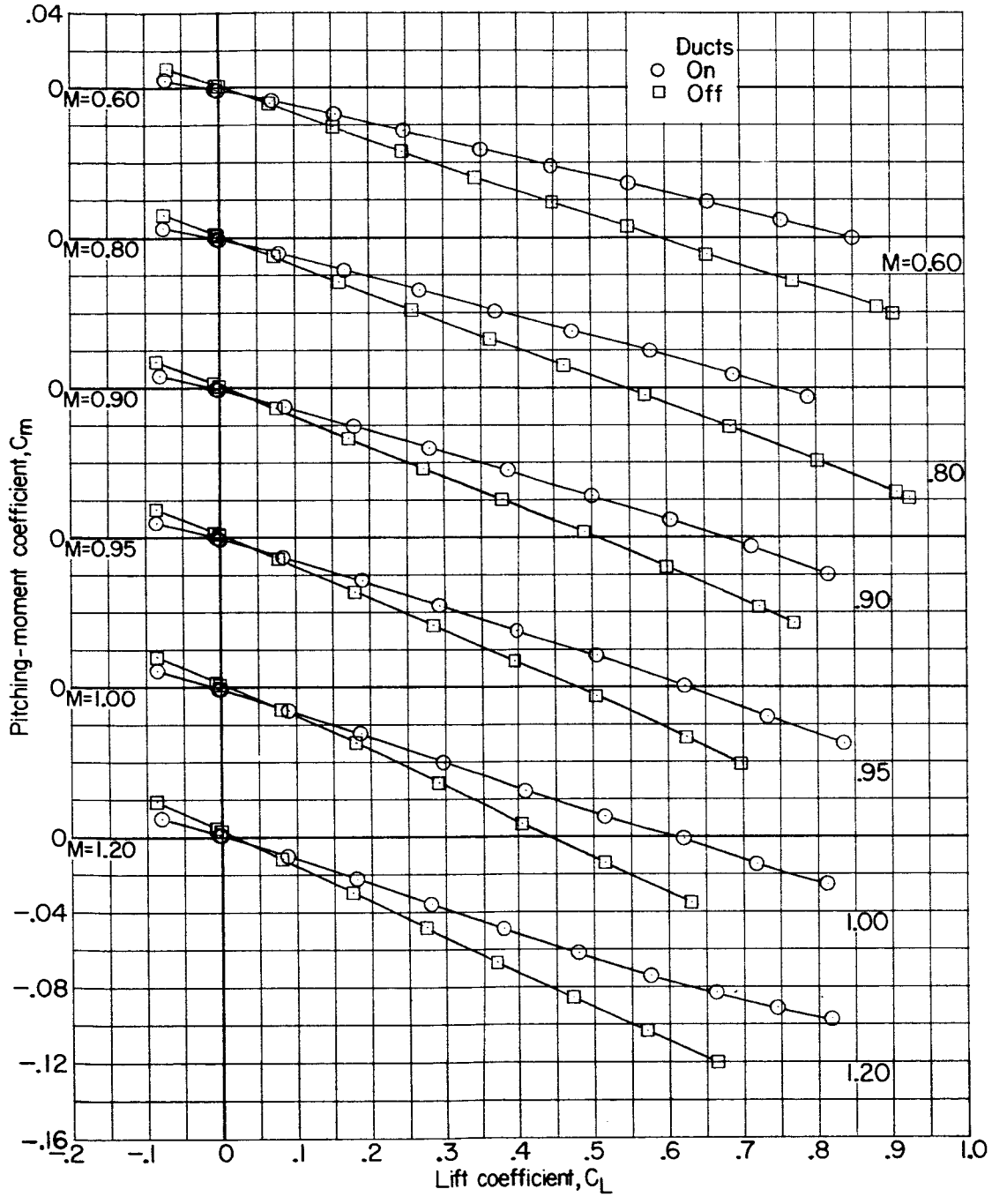

(b) Variation of C_m with C_L.

Figure 10.- Continued.

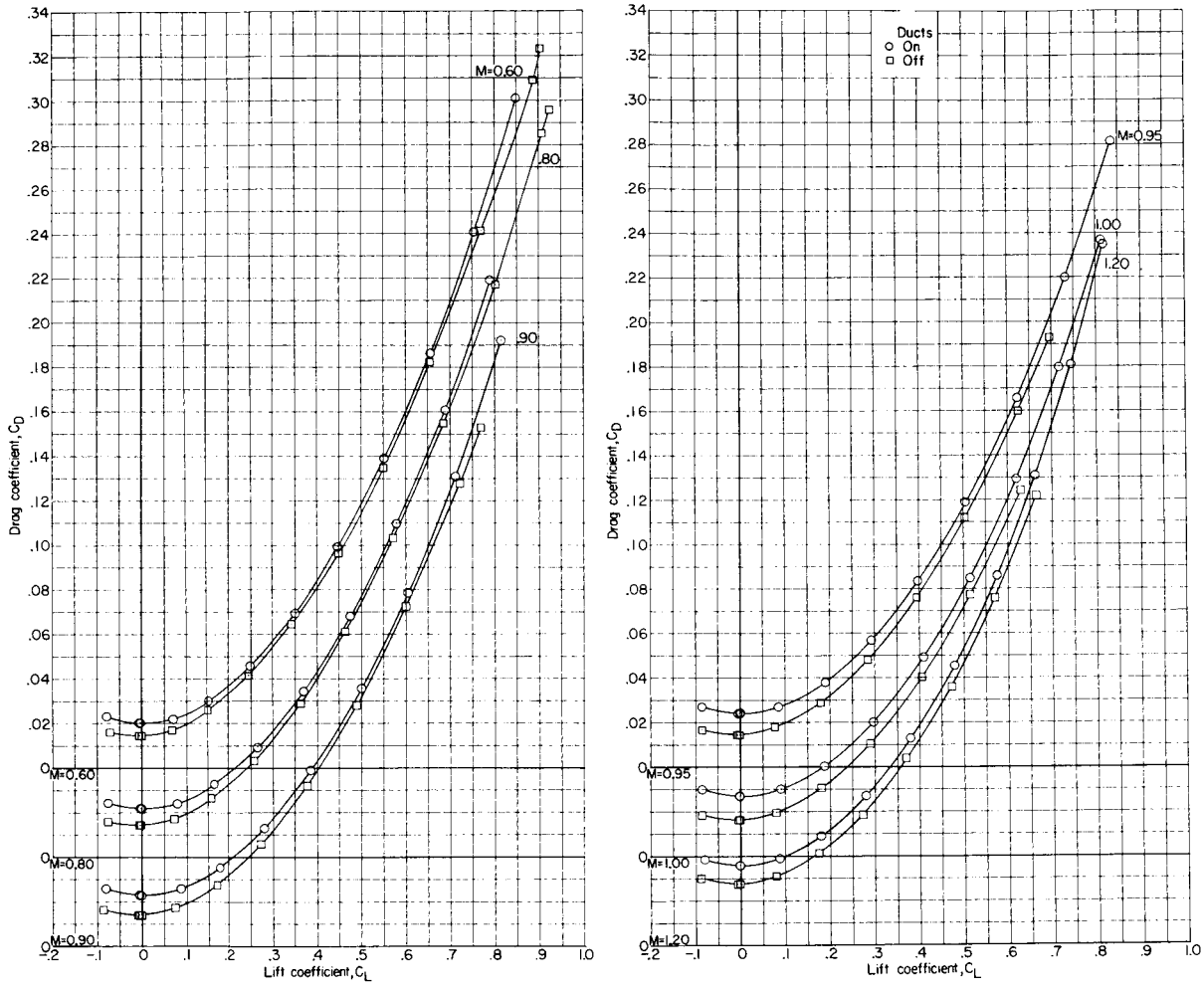

(c) Variation of C_D with C_L.

Figure 10.- Continued.

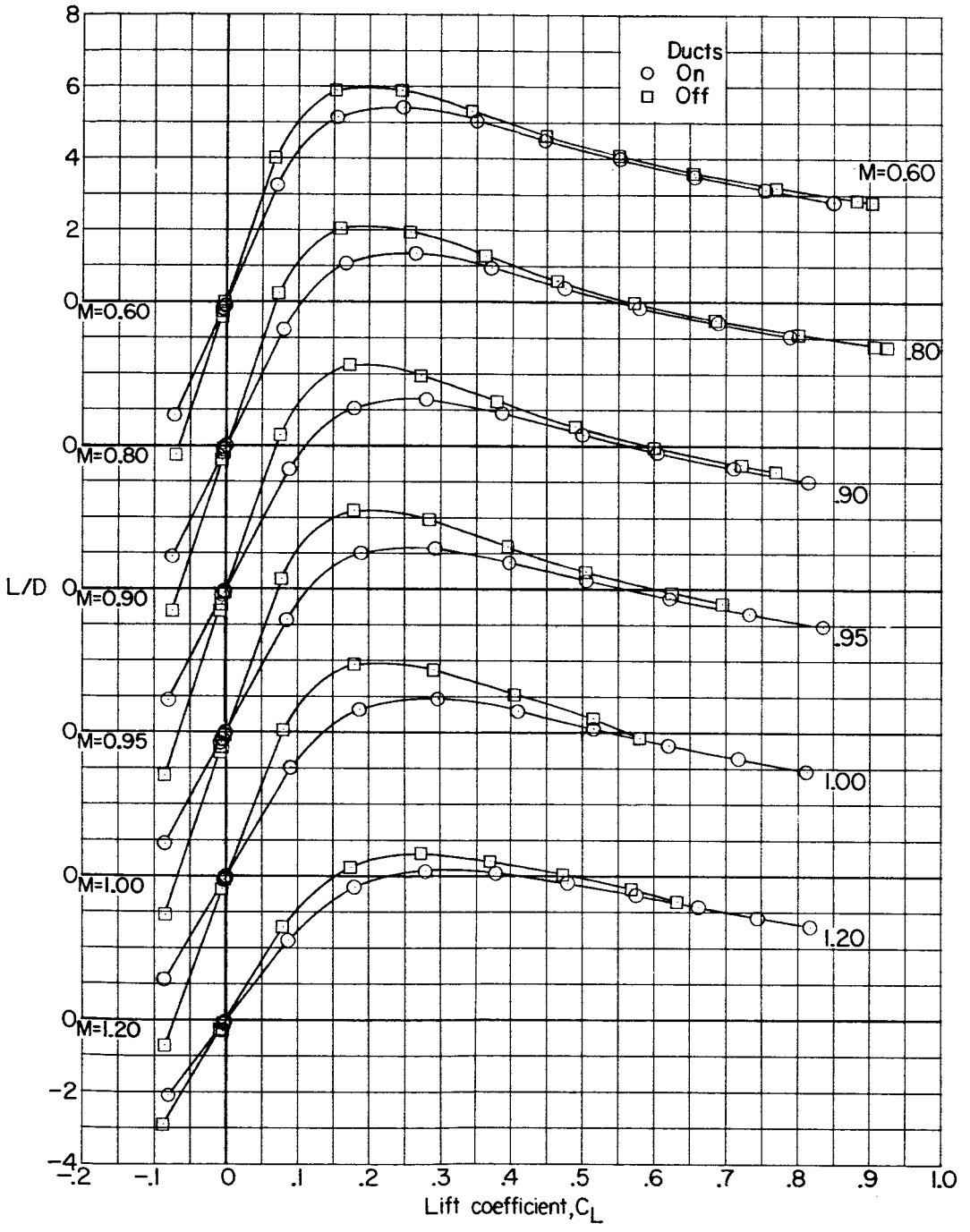

(d) Variation of L/D with C_L.

Figure 10.- Concluded.

L-1977

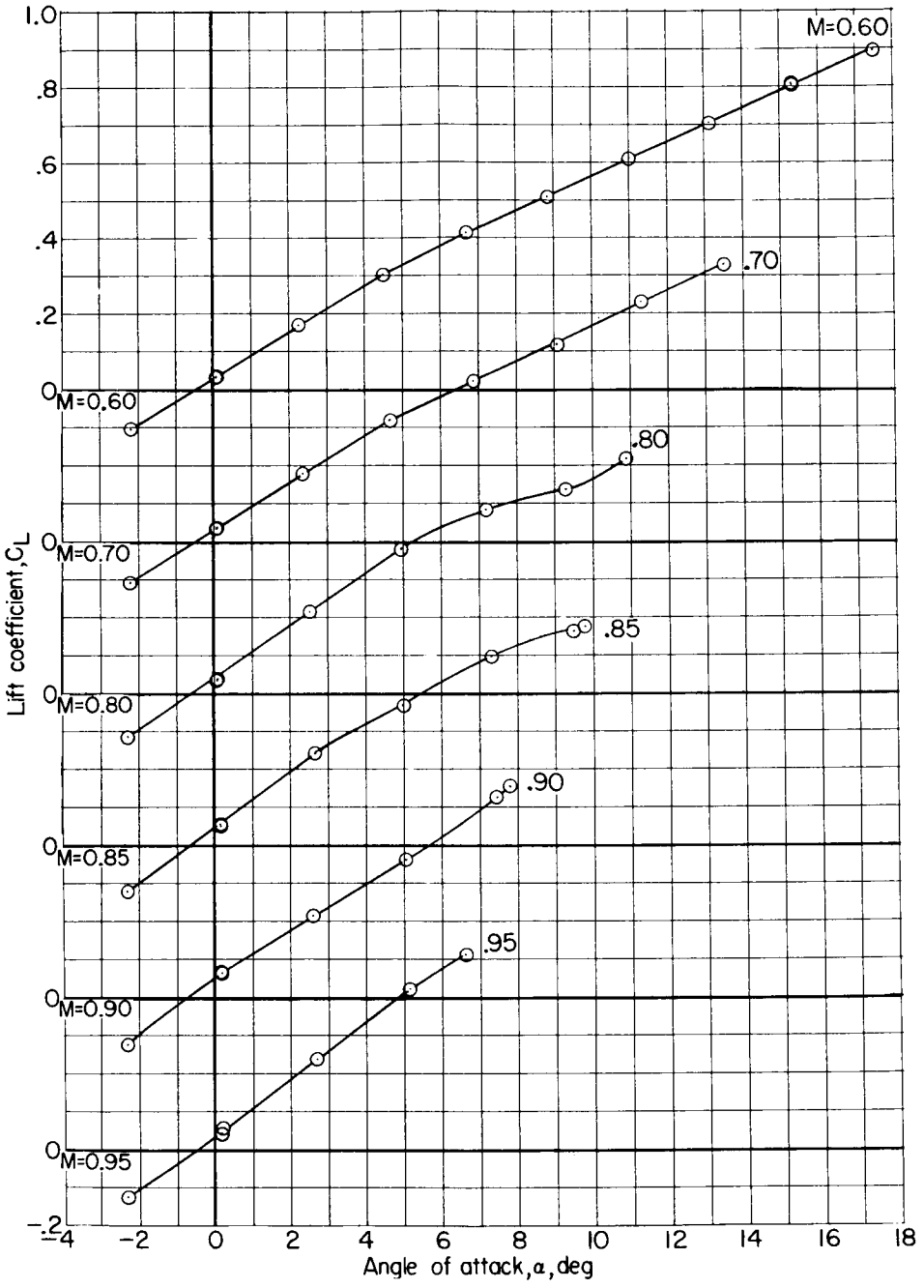

(a) Variation of C_L with α.

Figure 11.- Longitudinal aerodynamic characteristics of model 2a. $\Lambda = 15^\circ$; horizontal tail off; $p_{t,\infty}$ = 2,120 lb/sq ft.

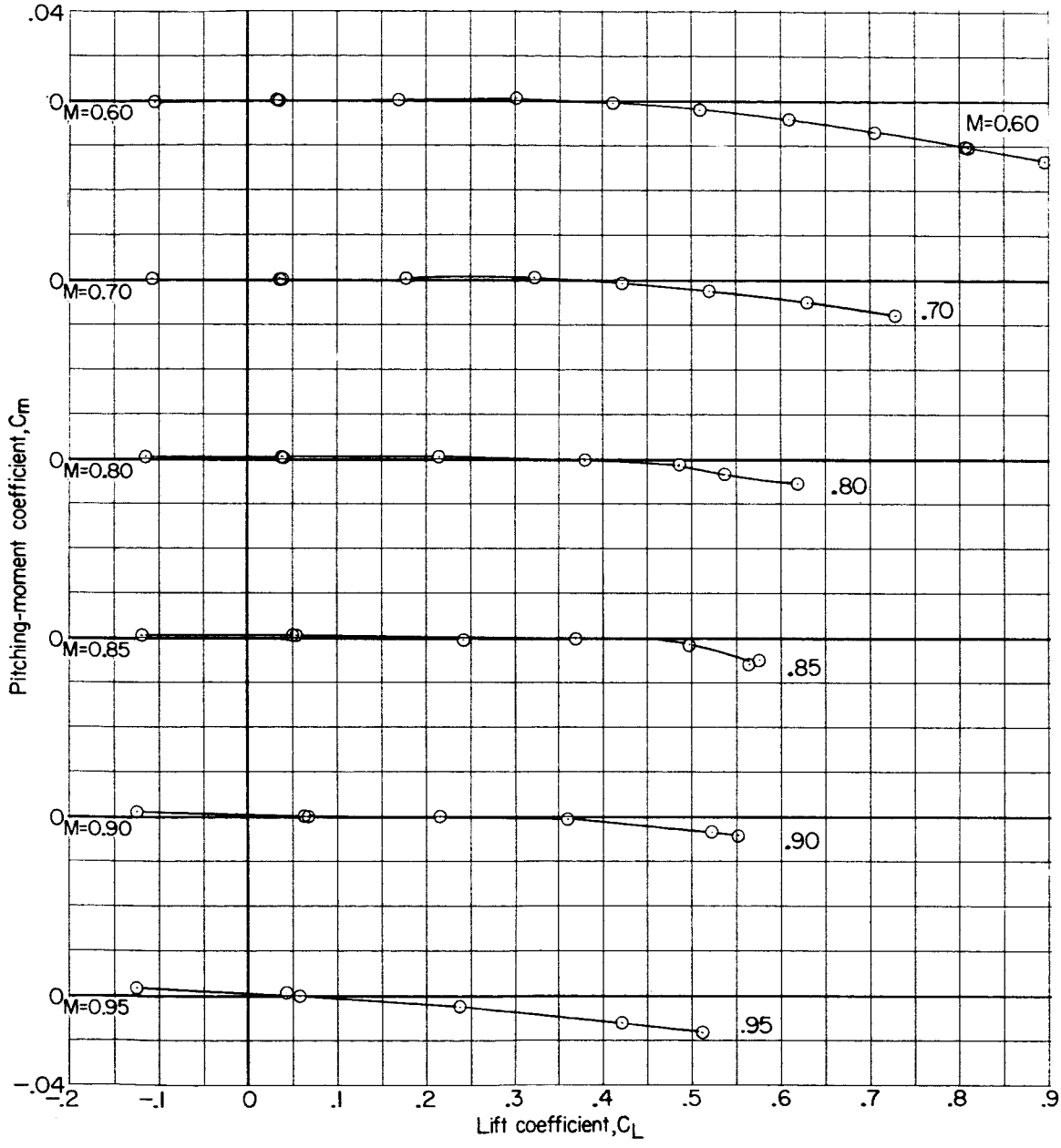

(b) Variation of C_m with C_L.

Figure 11.- Continued.

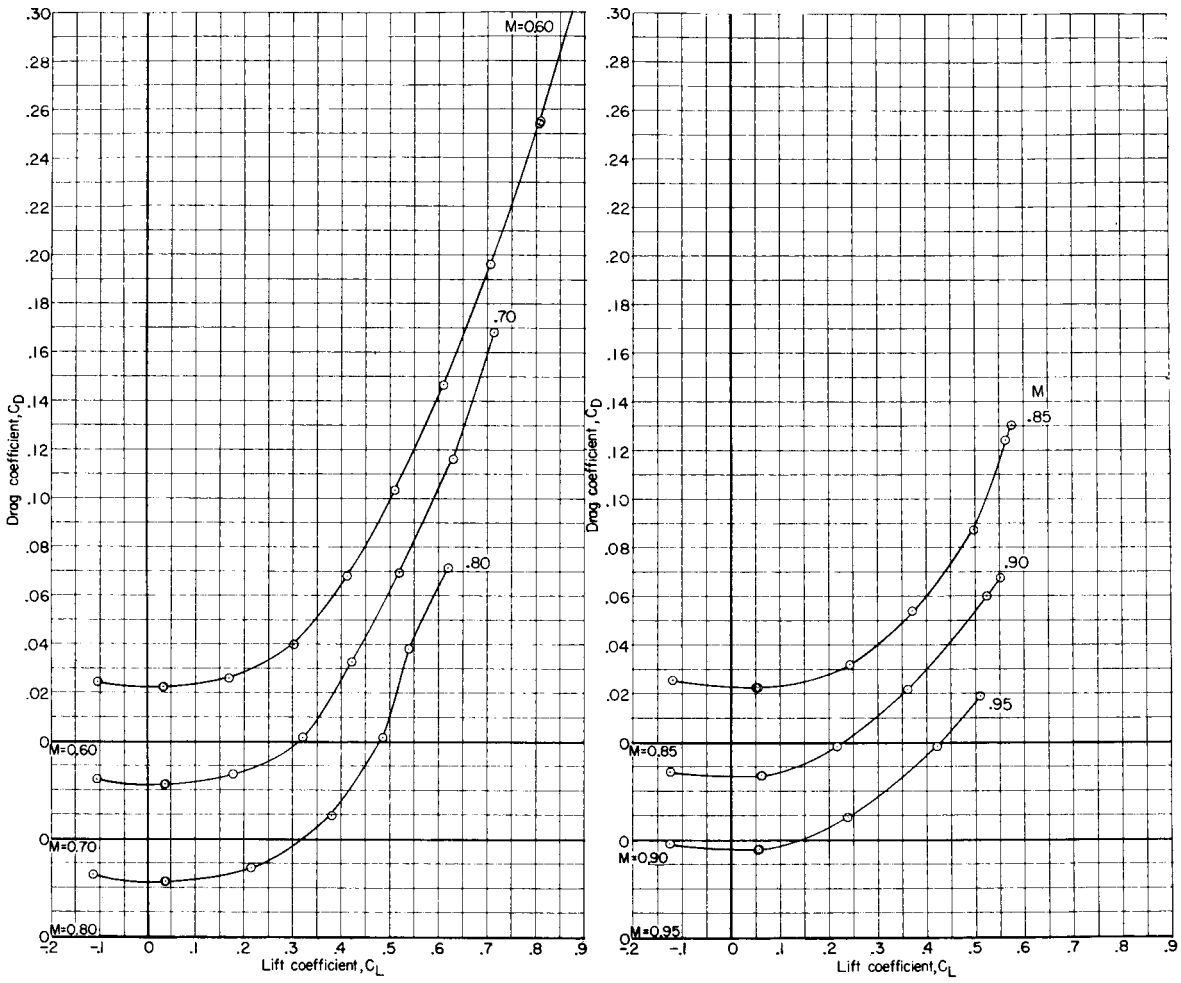

(c) Variation of C_D with C_L.

Figure 11.- Continued.

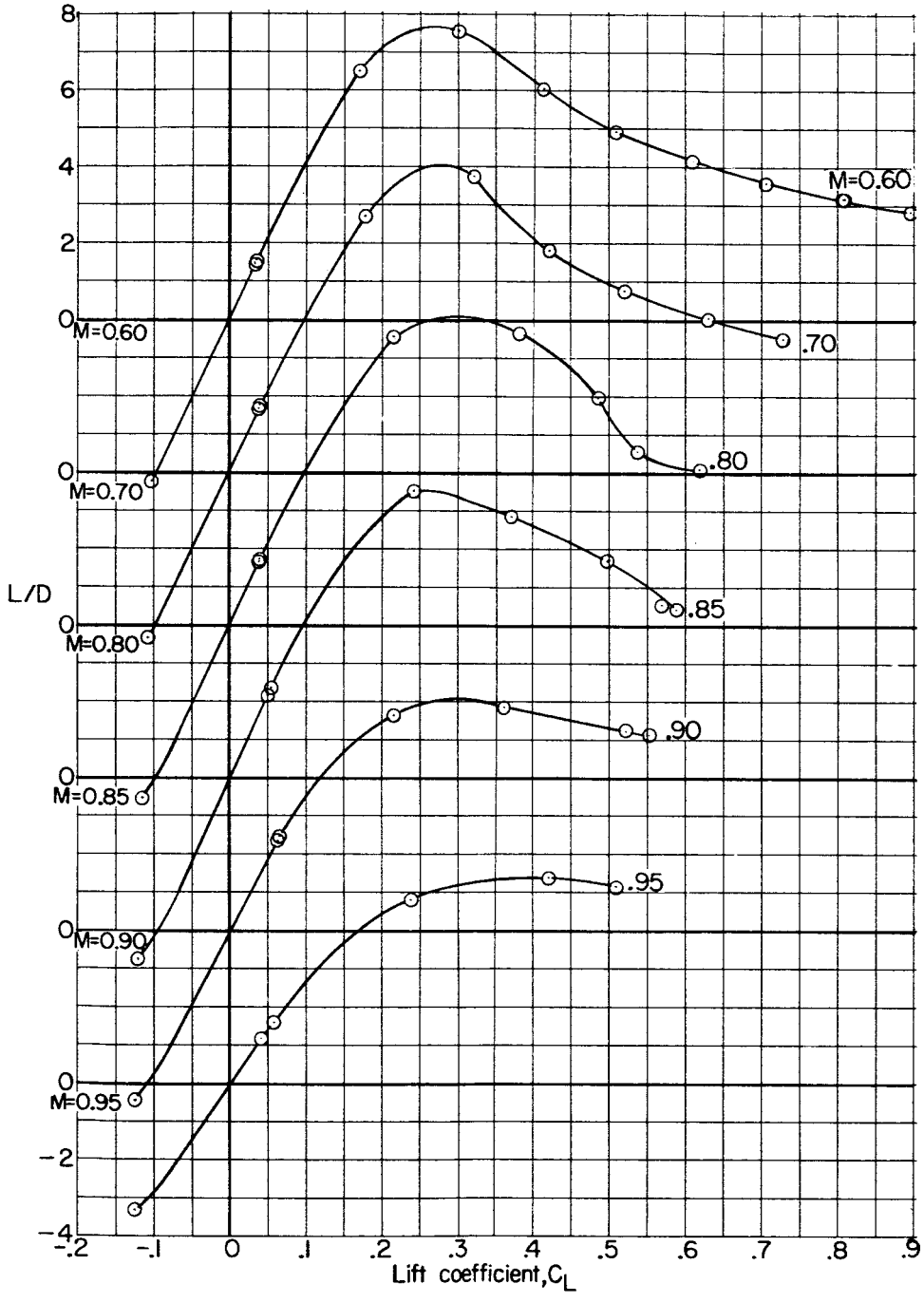

(d) Variation of L/D with C_L.

Figure 11.- Concluded.

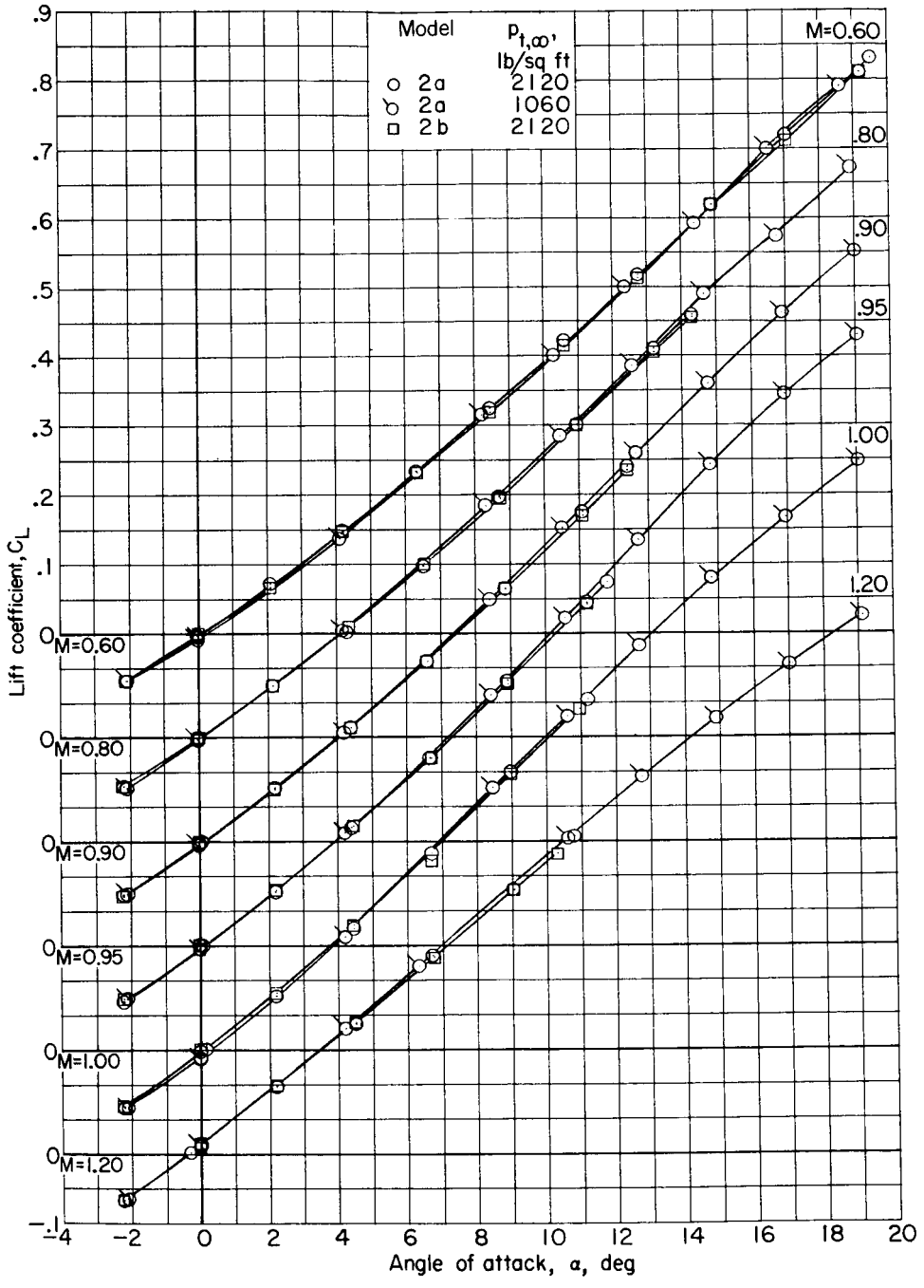

(a) Variation of C_L with α.

Figure 12.- Effect of modification of external shape of duct on characteristics of models 2a and 2b. $\Lambda = 71.75^\circ$; $\delta_h = 0^\circ$.

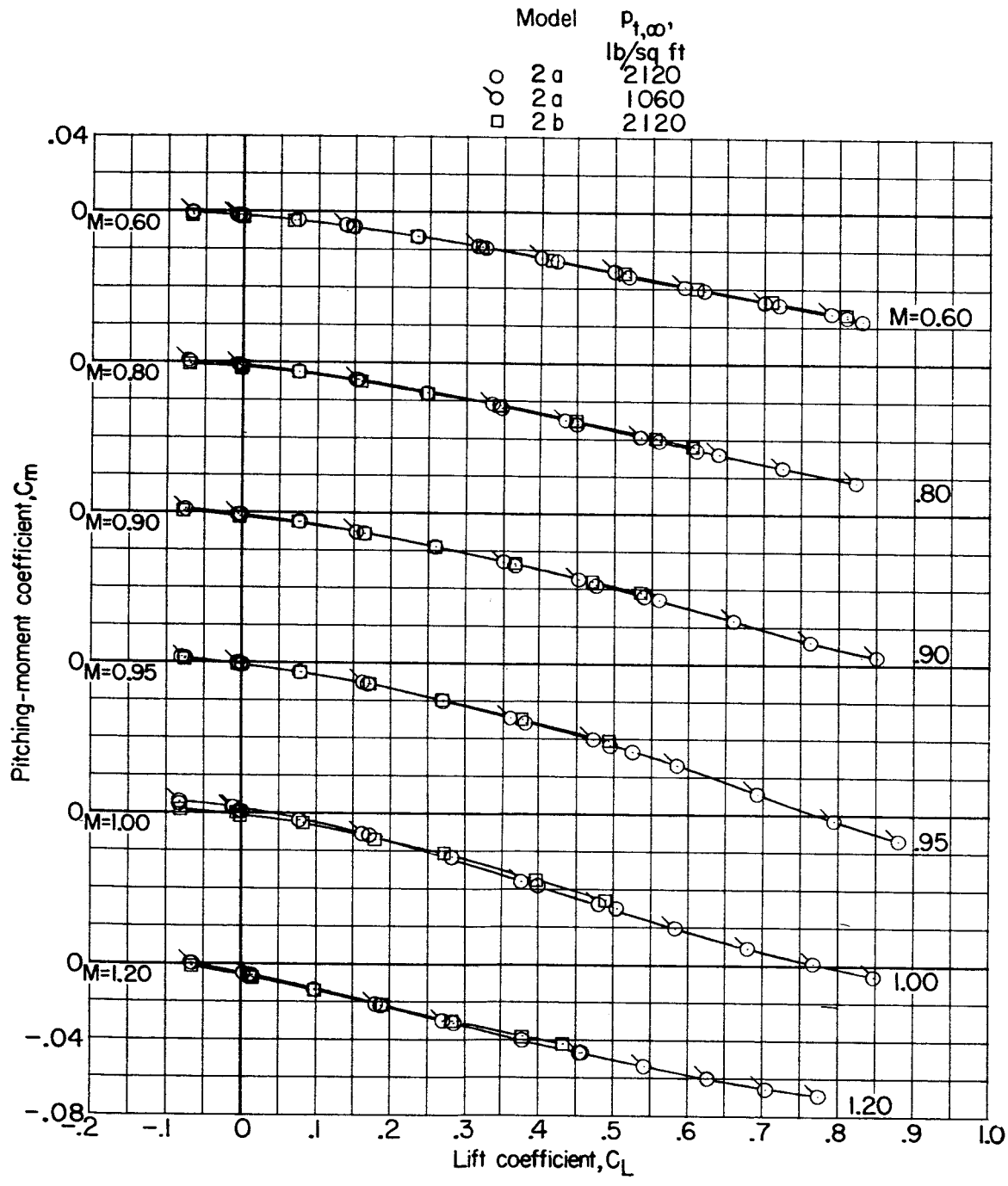

(b) Variation of C_m with C_L.

Figure 12.- Continued.

L-1977

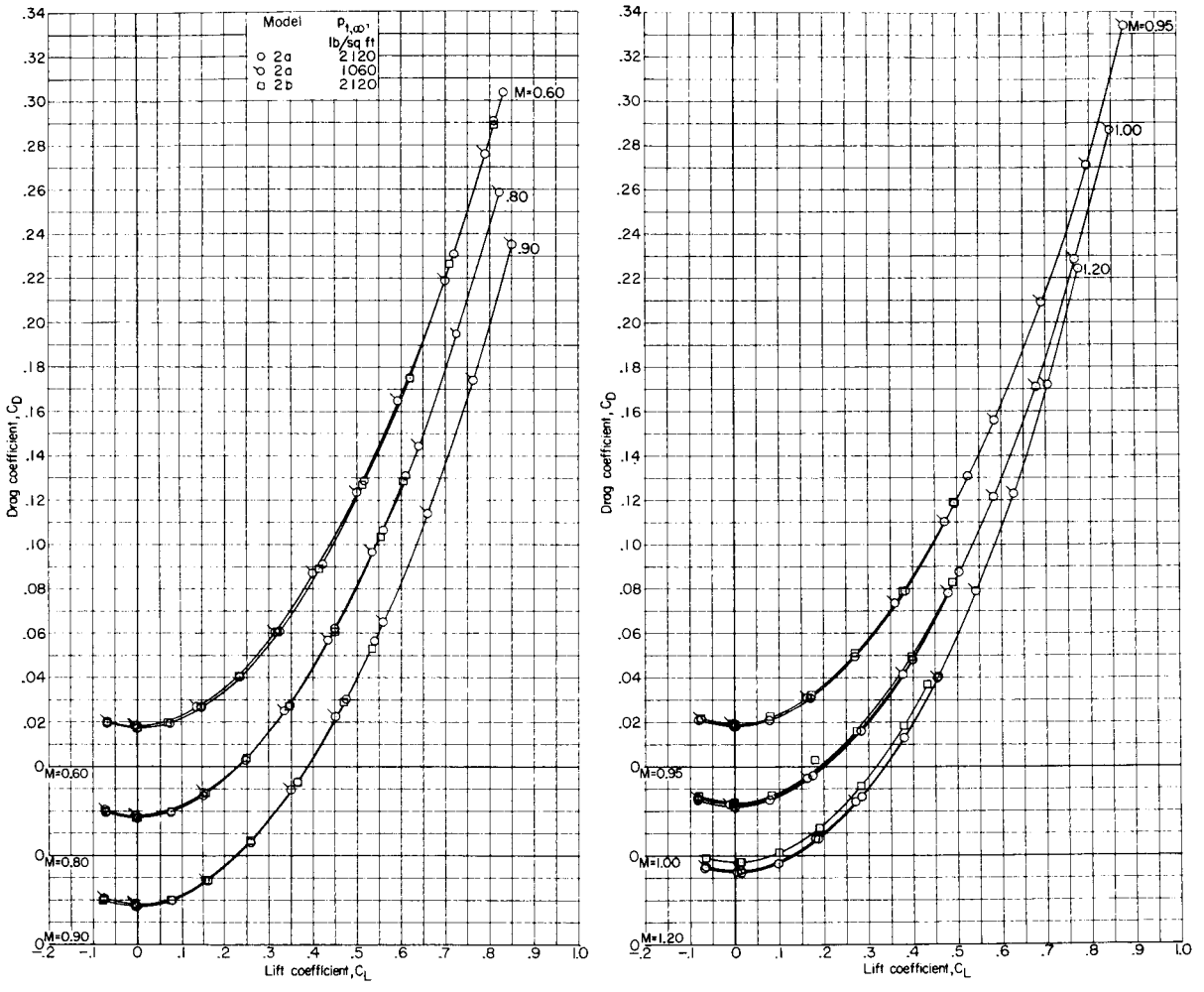

(c) Variation of C_D with C_L.

Figure 12.- Continued.

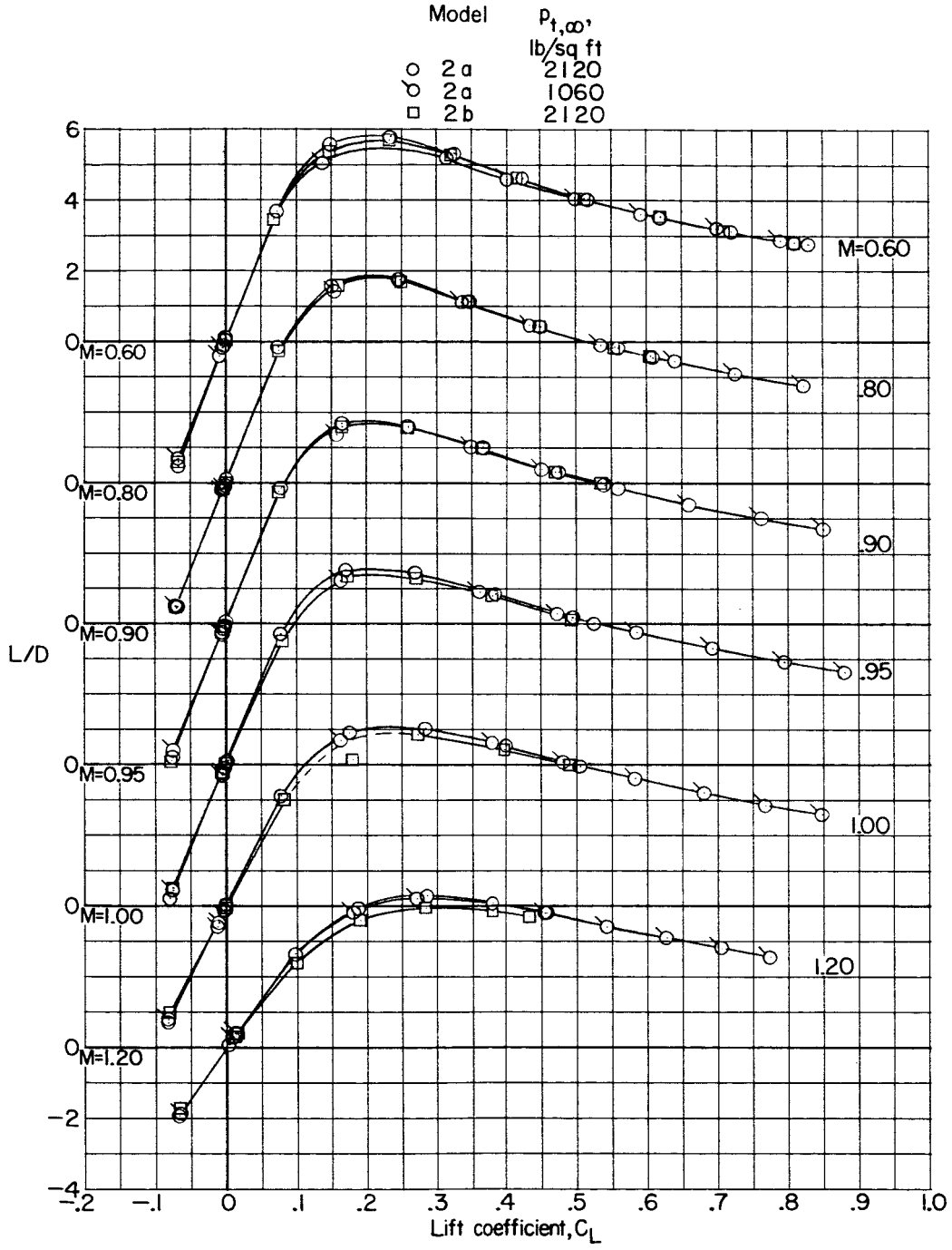

(d) Variation of L/D with C_L.

Figure 12.- Concluded.

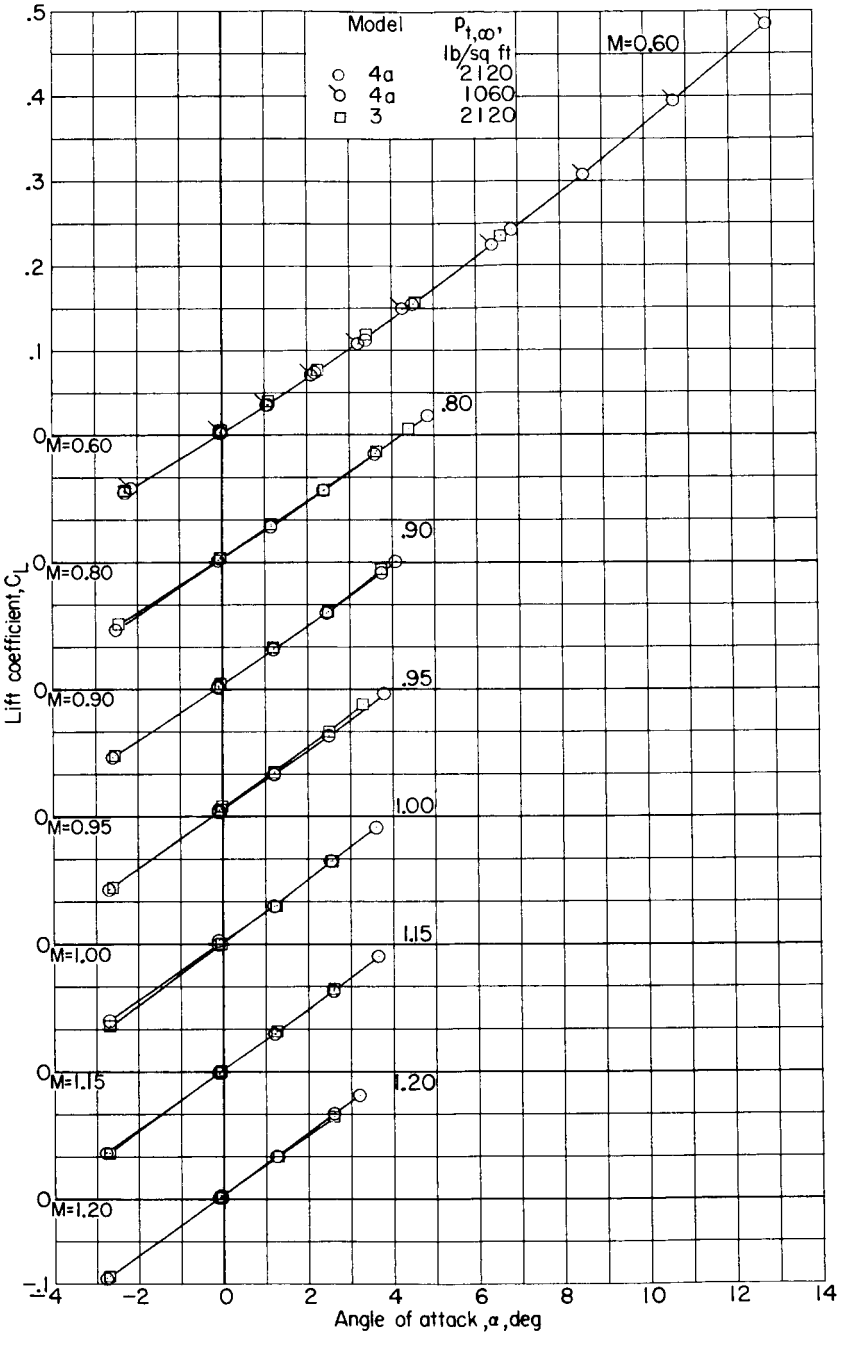

(a) Variation of C_L with α.

Figure 13.- Longitudinal aerodynamic characteristics of models 3 and 4a. $\Lambda = 71.75^\circ$; vertical and horizontal tails off.

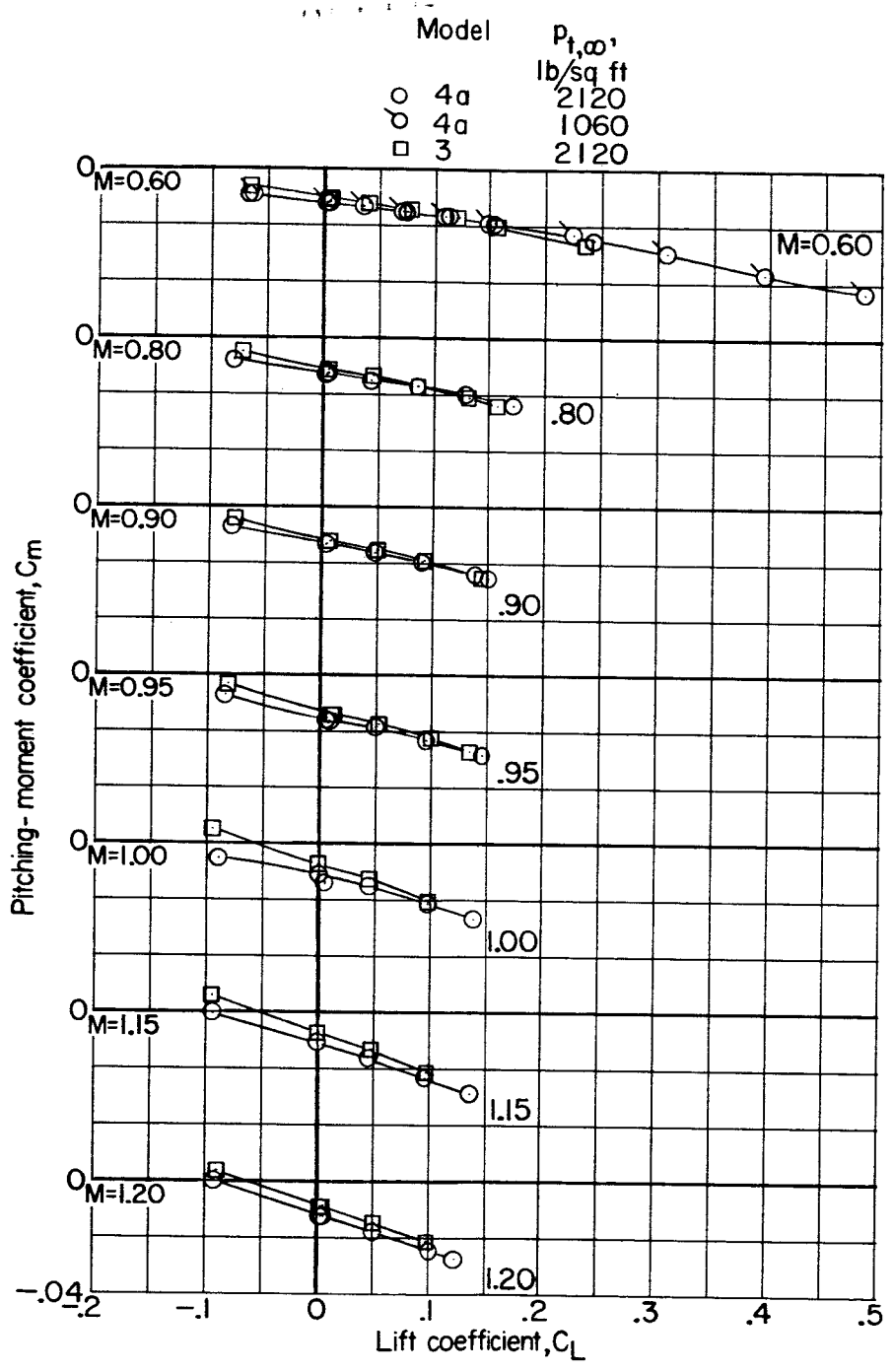

(b) Variation of C_m with C_L.

Figure 13.- Continued.

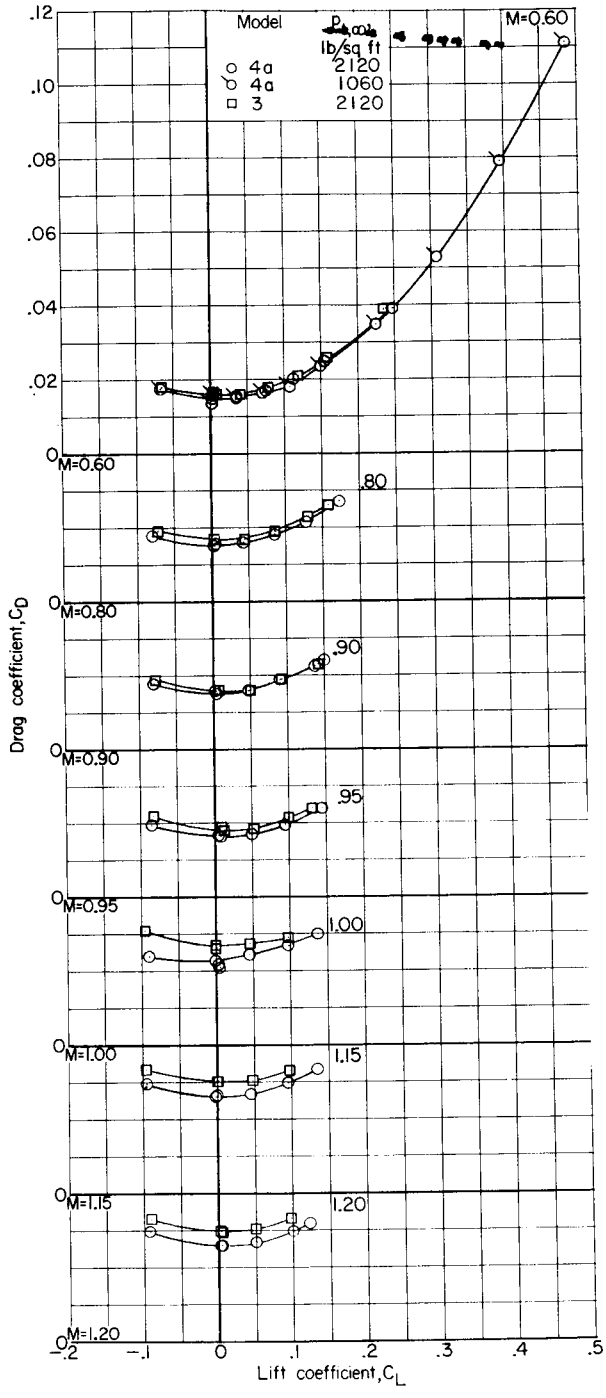

(c) Variation of C_D with C_L.

Figure 13.- Continued.

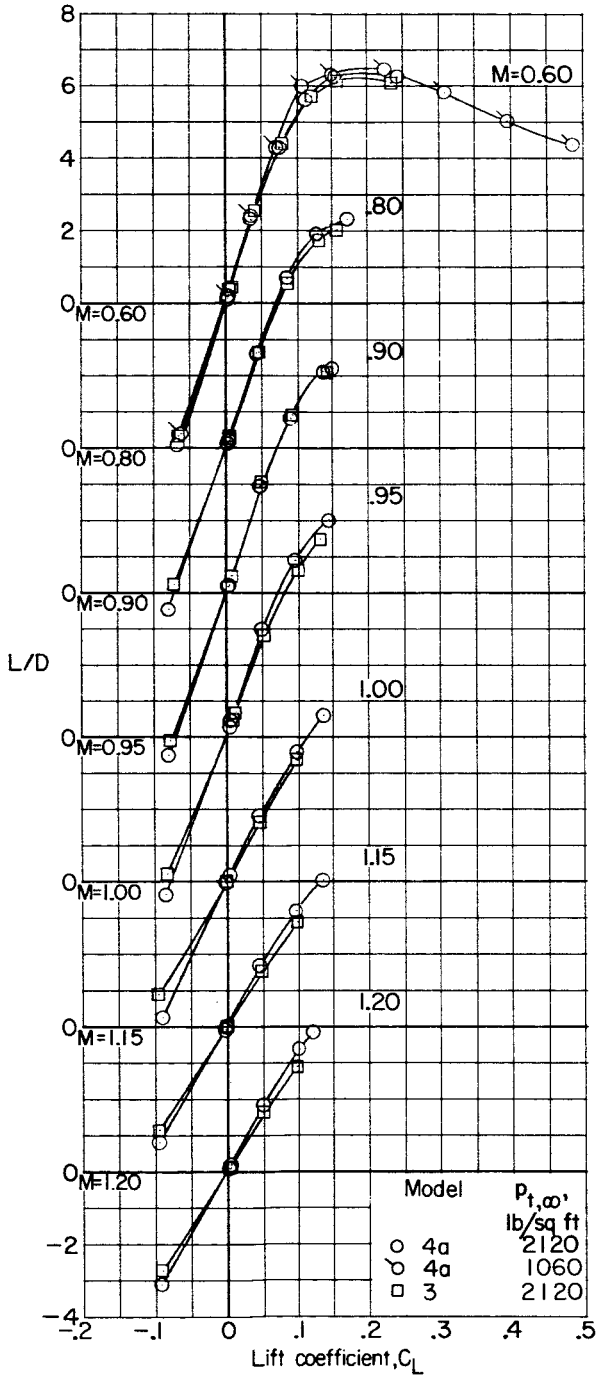

(d) Variation of L/D with C_L.

Figure 13.- Concluded.

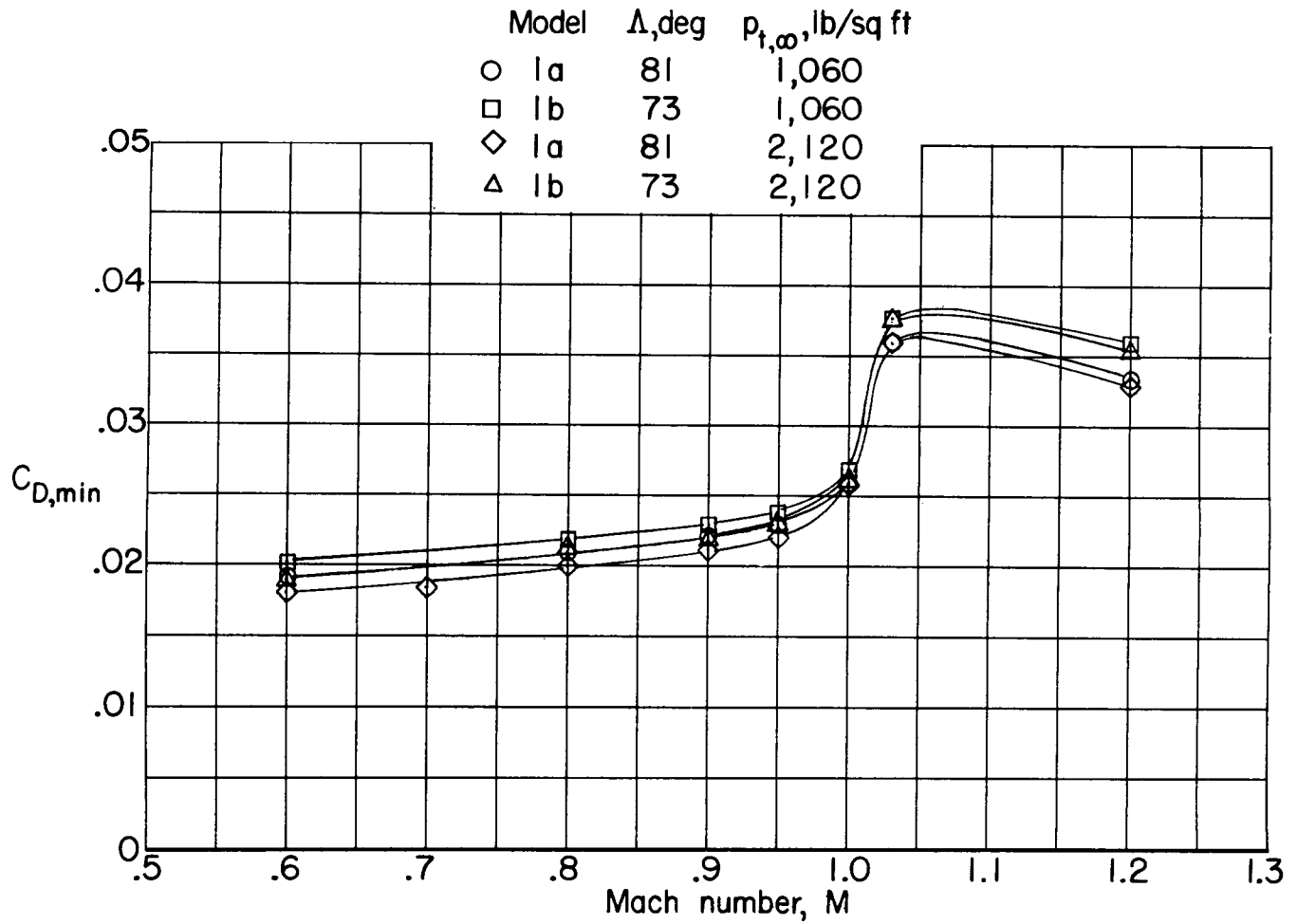

(a) Variation of $C_{D,min}$ with M.

Figure 14.- Effect of leading-edge sweep of fixed delta wing on performance and longitudinal-stability derivatives of models 1a and 1b. $\delta_h = 0^\circ$.

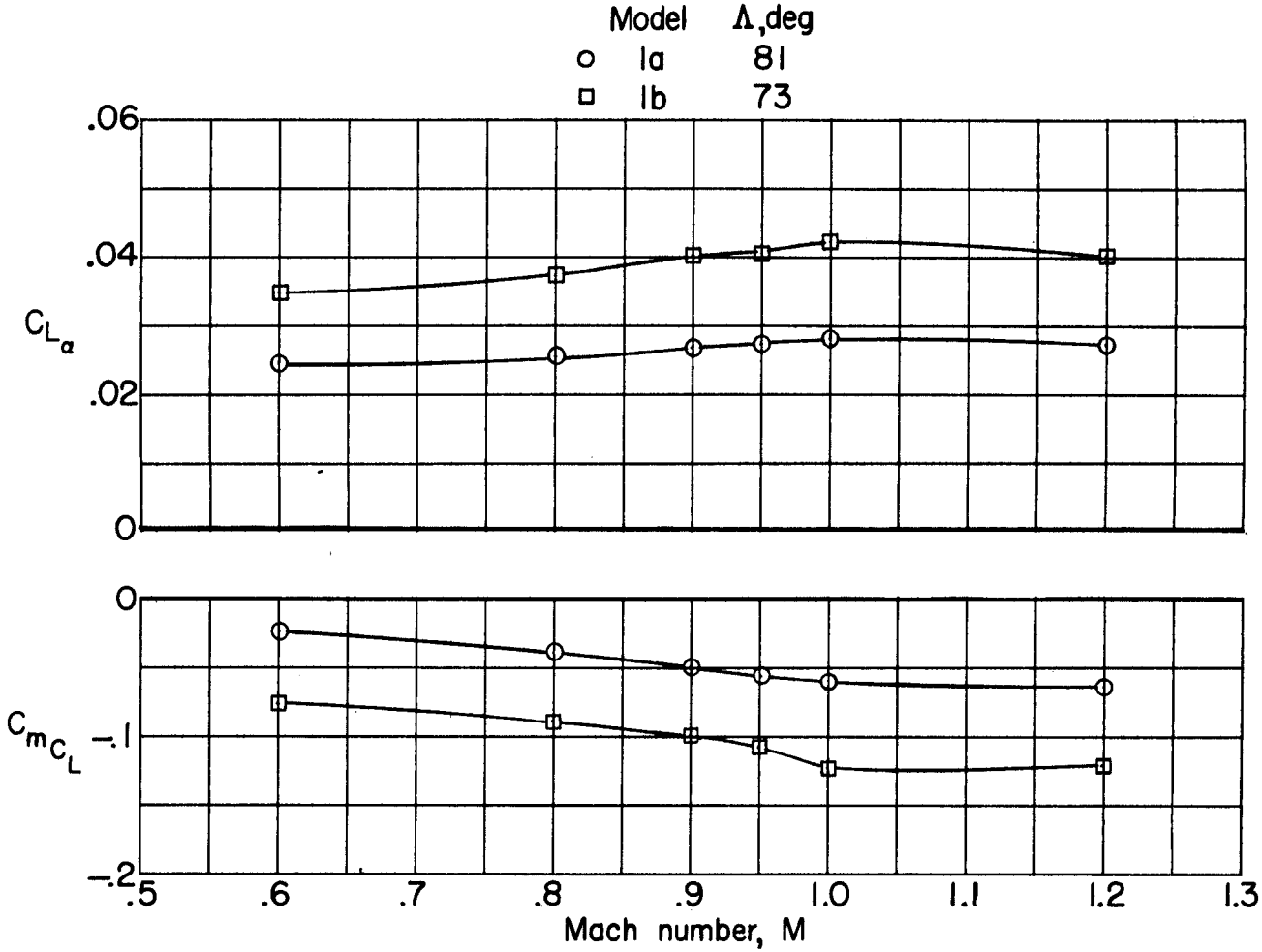

(b) Variation of C_{L_α} and $C_{m_{C_L}}$ with M. $p_{t,\infty}$ = 1,060 lb/sq ft.

Figure 14.- Continued.

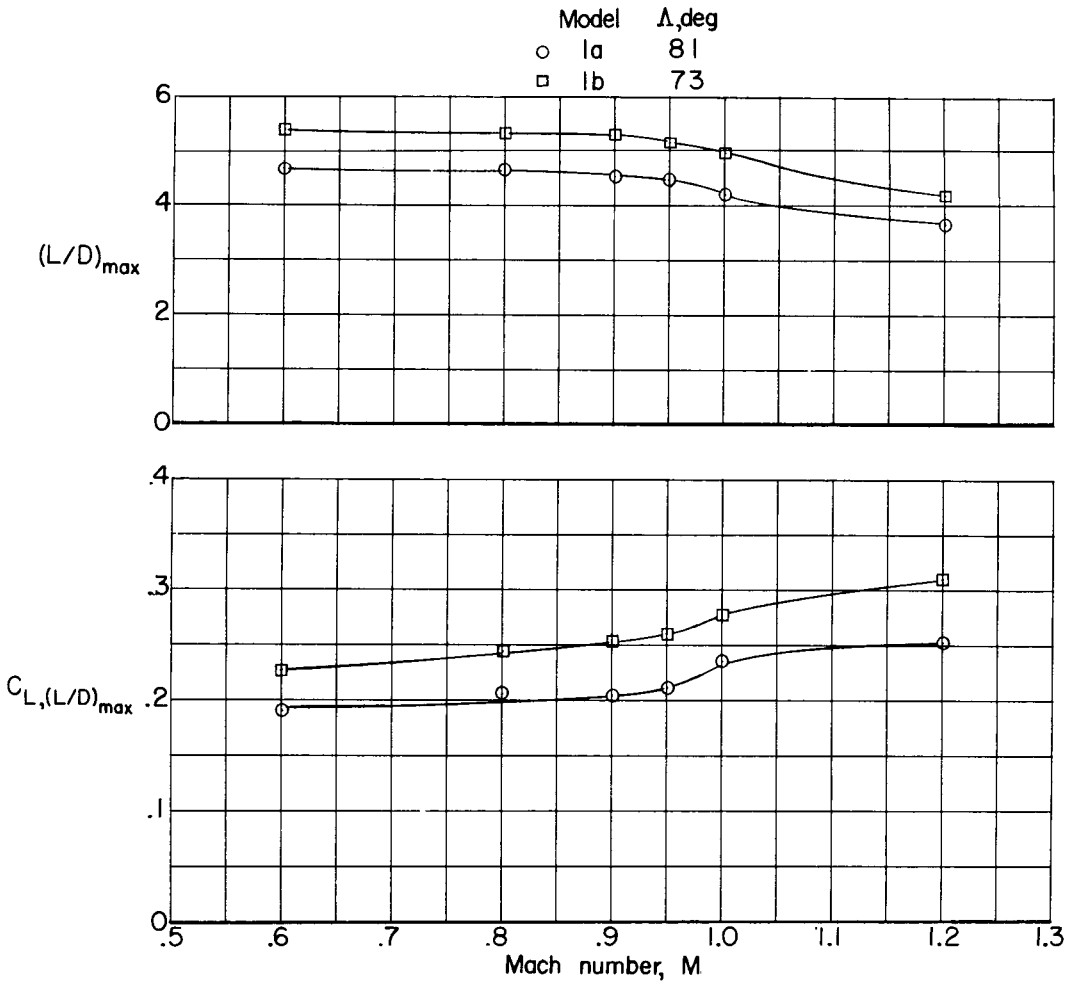

(c) Variation of $(L/D)_{max}$ and $C_{L,(L/D)_{max}}$ with M. $p_{t,\infty}$ = 1,060 lb/sq ft.

Figure 14.- Concluded.

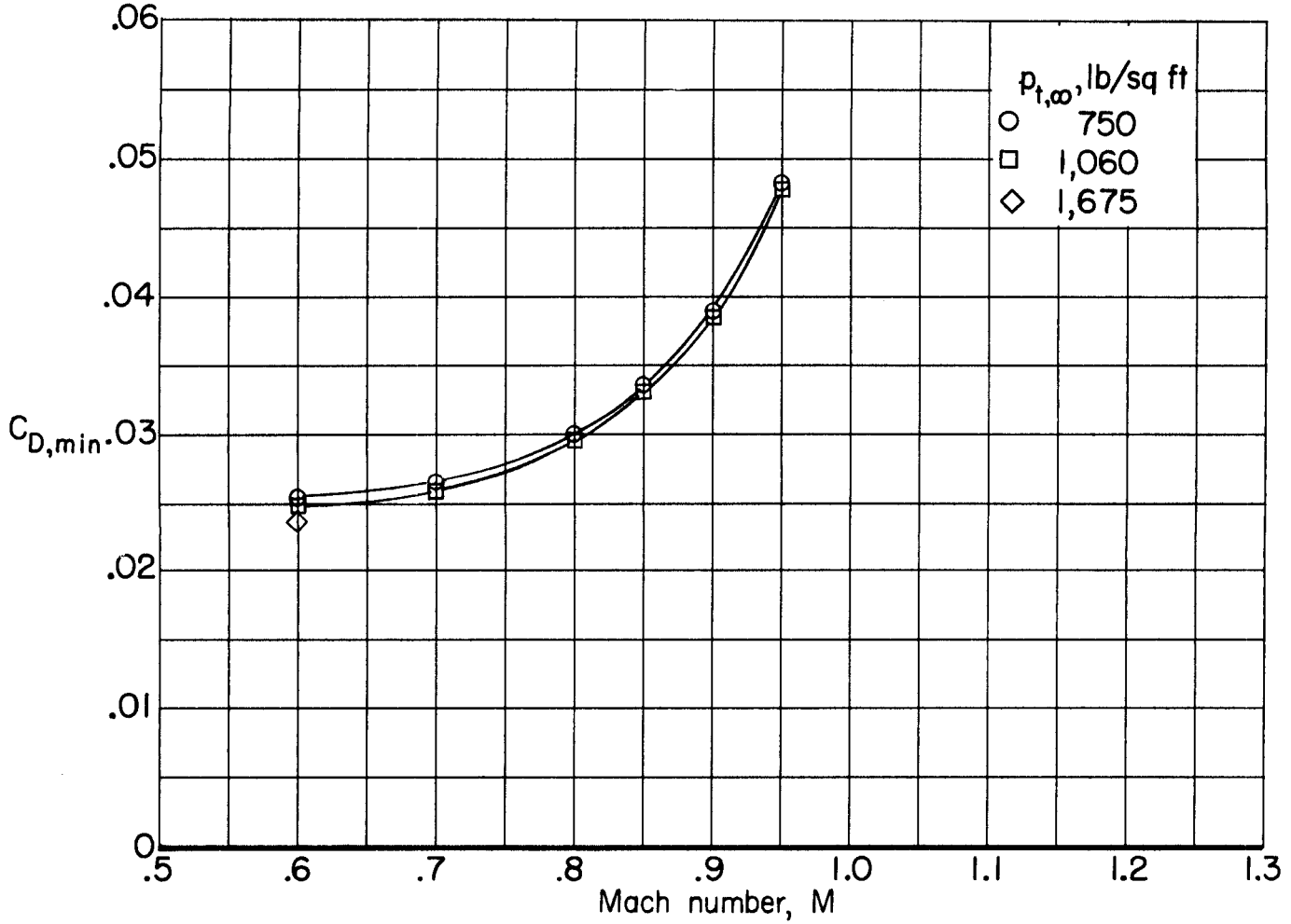

(a) Variation of $C_{D,min}$ with M.

Figure 15.- Performance and longitudinal-stability derivatives of model 1b. $\Lambda = 12^{\circ}$; $\delta_h = 0^{\circ}$.

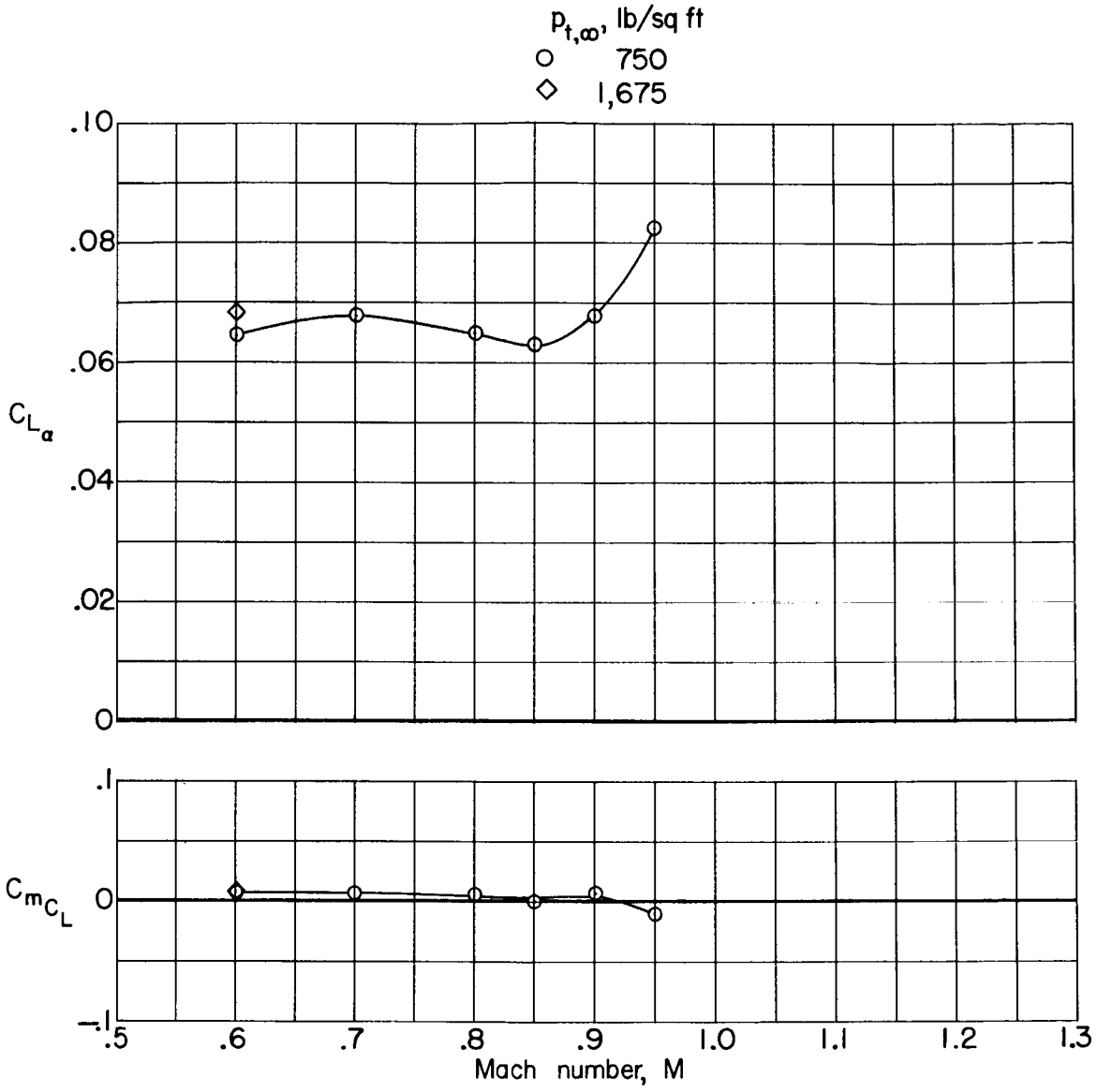

(b) Variation of C_{L_α} and $C_{m_{C_L}}$ with M.

Figure 15.- Continued.

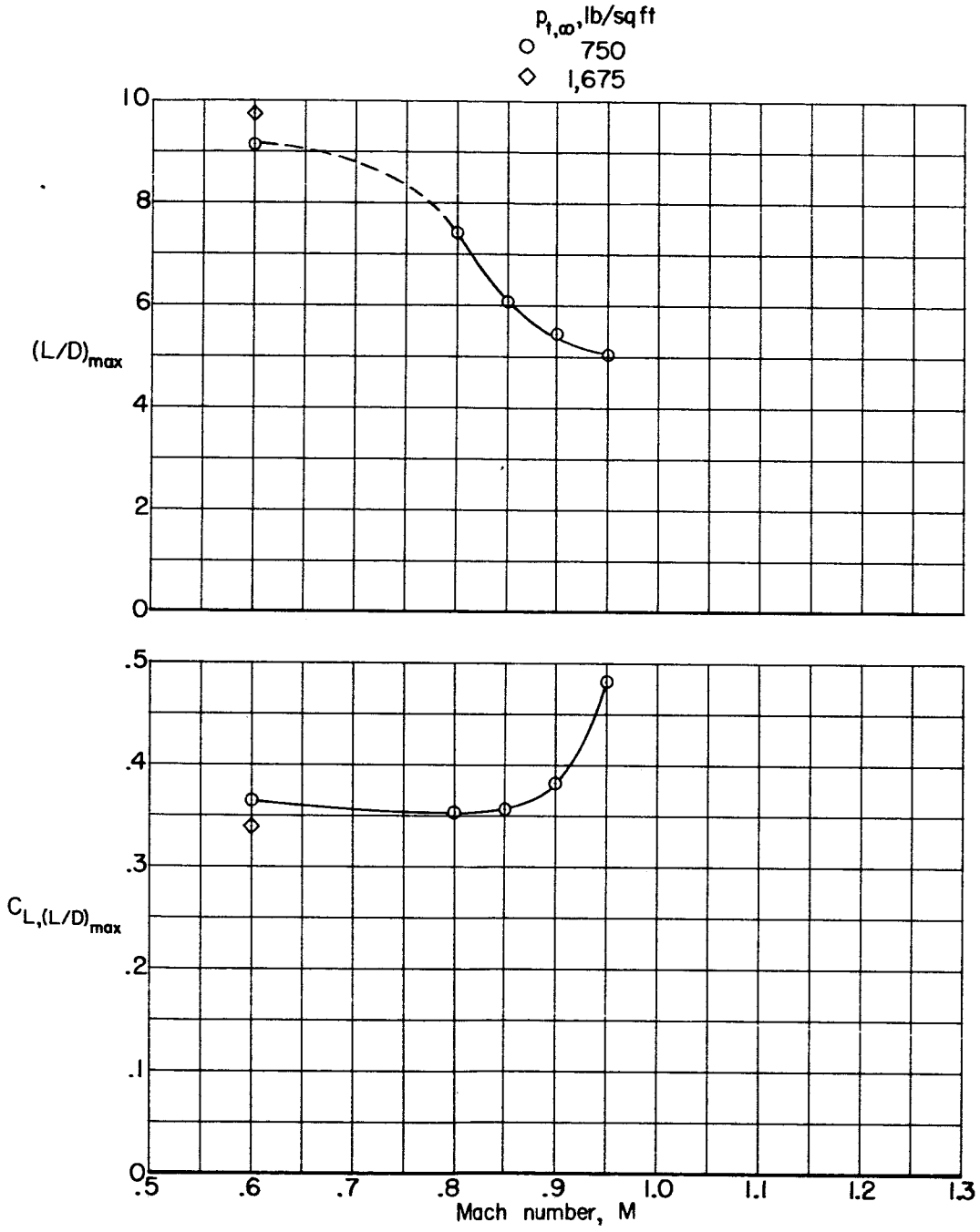

(c) Variation of $(L/D)_{max}$ and $C_{L,(L/D)_{max}}$ with M.

Figure 15.- Concluded.

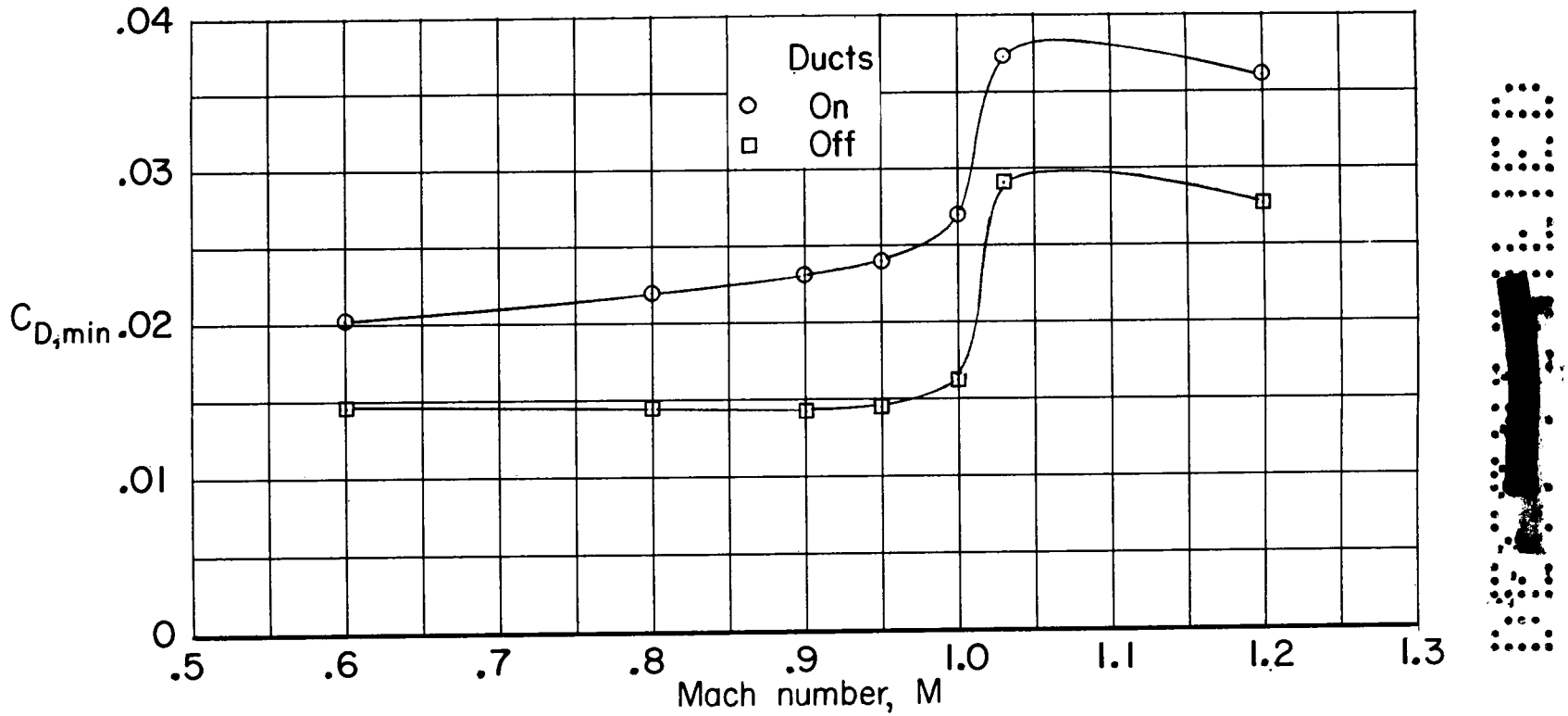

(a) Variation of $C_{D,min}$ with M.

Figure 16.- Effect of ducts on performance and longitudinal-stability derivatives of model 1b. $\Lambda = 73^{\circ}$; $\delta_h = 0^{\circ}$; $p_{t,\infty} = 1{,}060$ lb/sq ft.

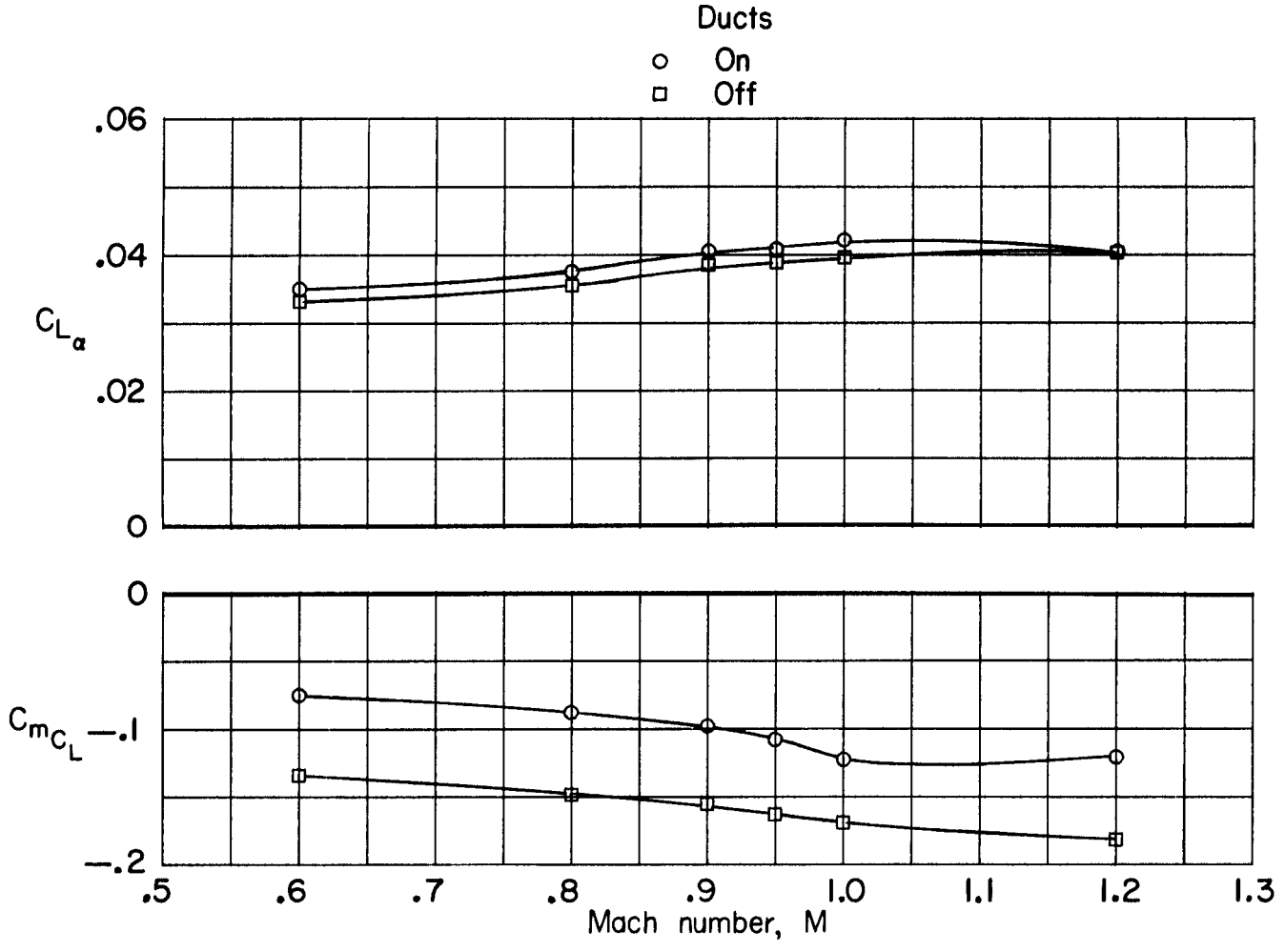

(b) Variation of C_{L_α} and $C_{m_{C_L}}$ with M.

Figure 16.- Continued.

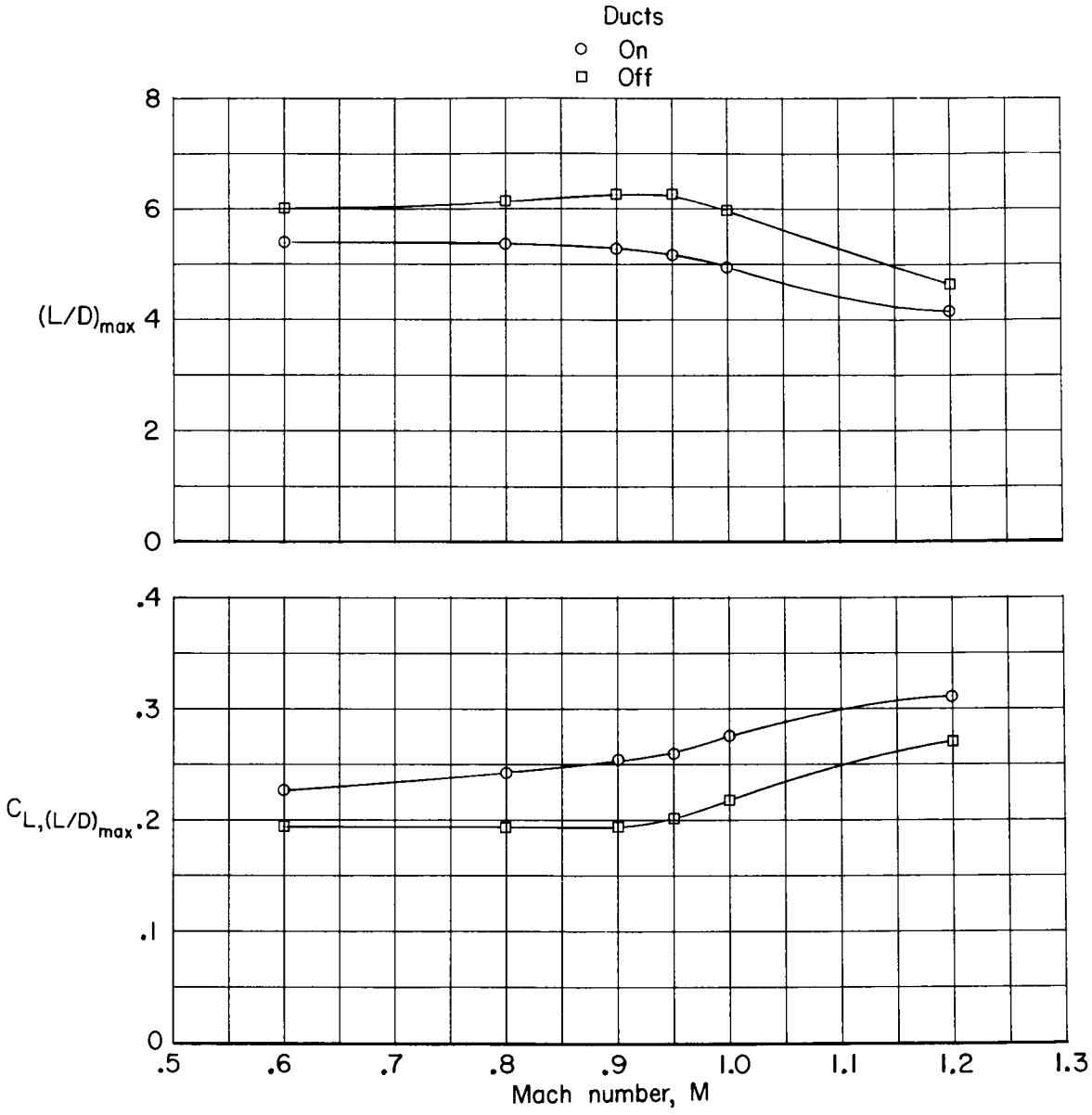

(c) Variation of $(L/D)_{max}$ and $C_{L,(L/D)_{max}}$ with M.

Figure 16.- Concluded.

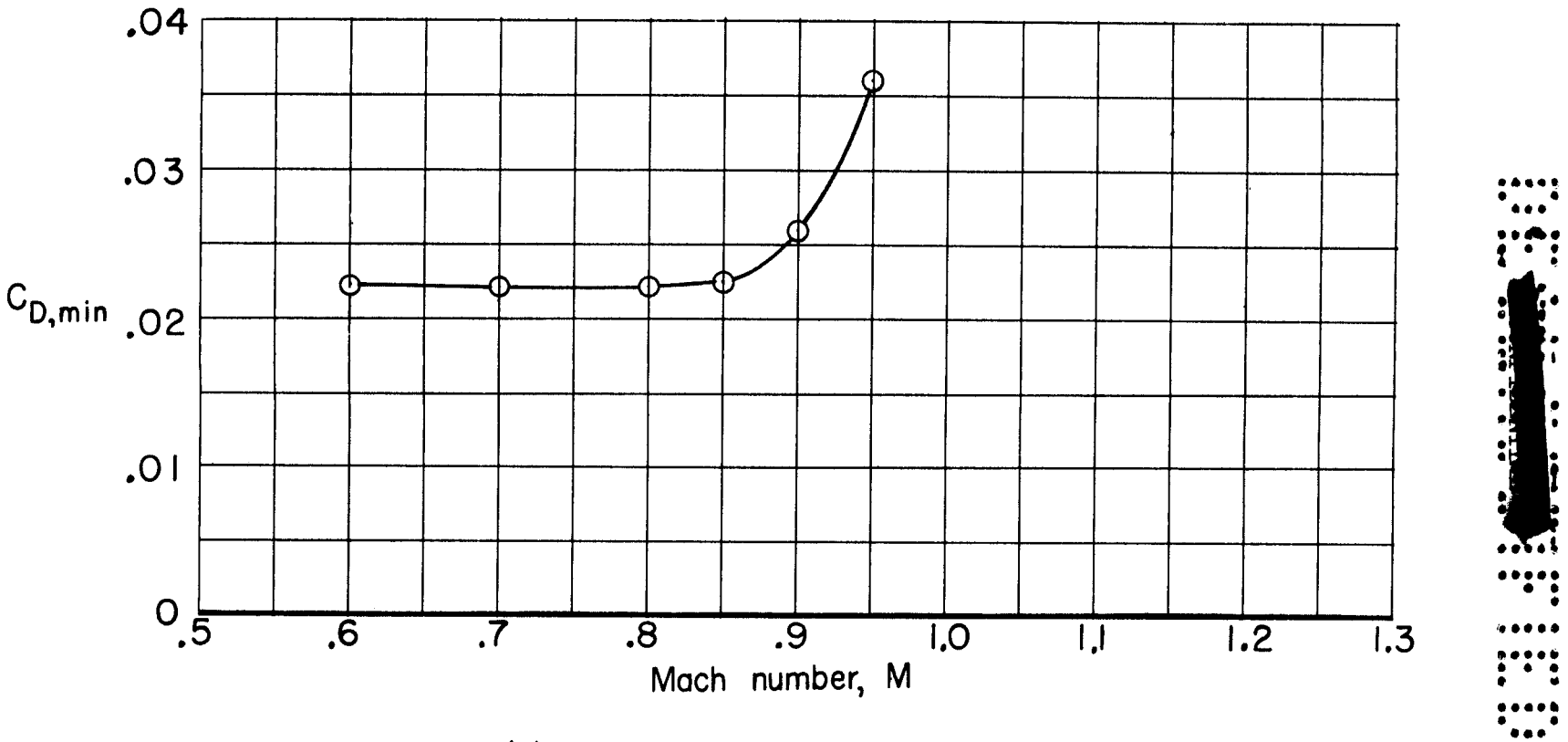

(a) Variation of $C_{D,min}$ with M.

Figure 17.- Performance and longitudinal-stability derivatives of model 2a. $\Lambda = 15^{\circ}$; horizontal tail off; $p_{t,\infty}$ = 2,120 lb/sq ft.

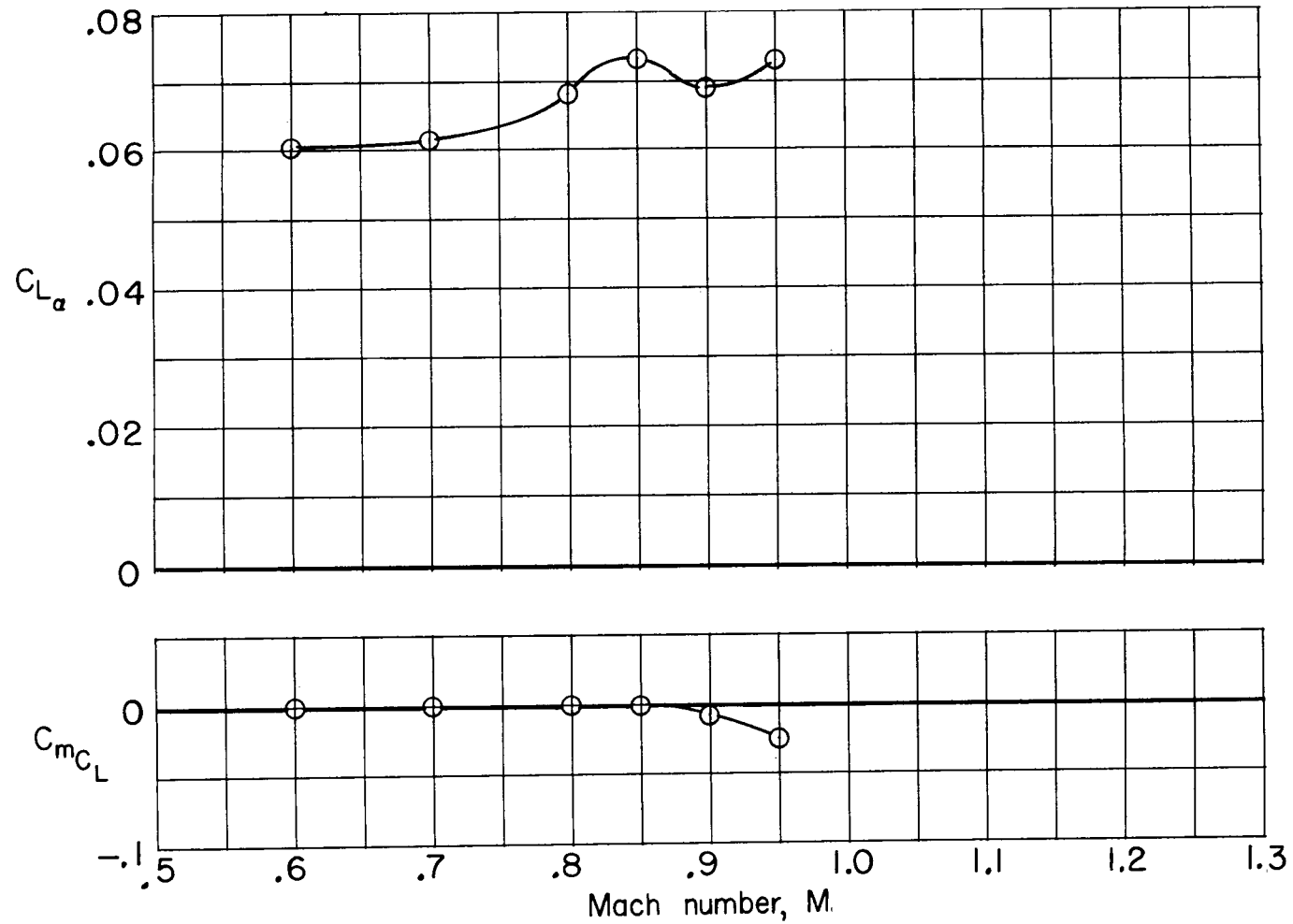

(b) Variation of C_{L_α} and $C_{m_{C_L}}$ with M.

Figure 17.- Continued.

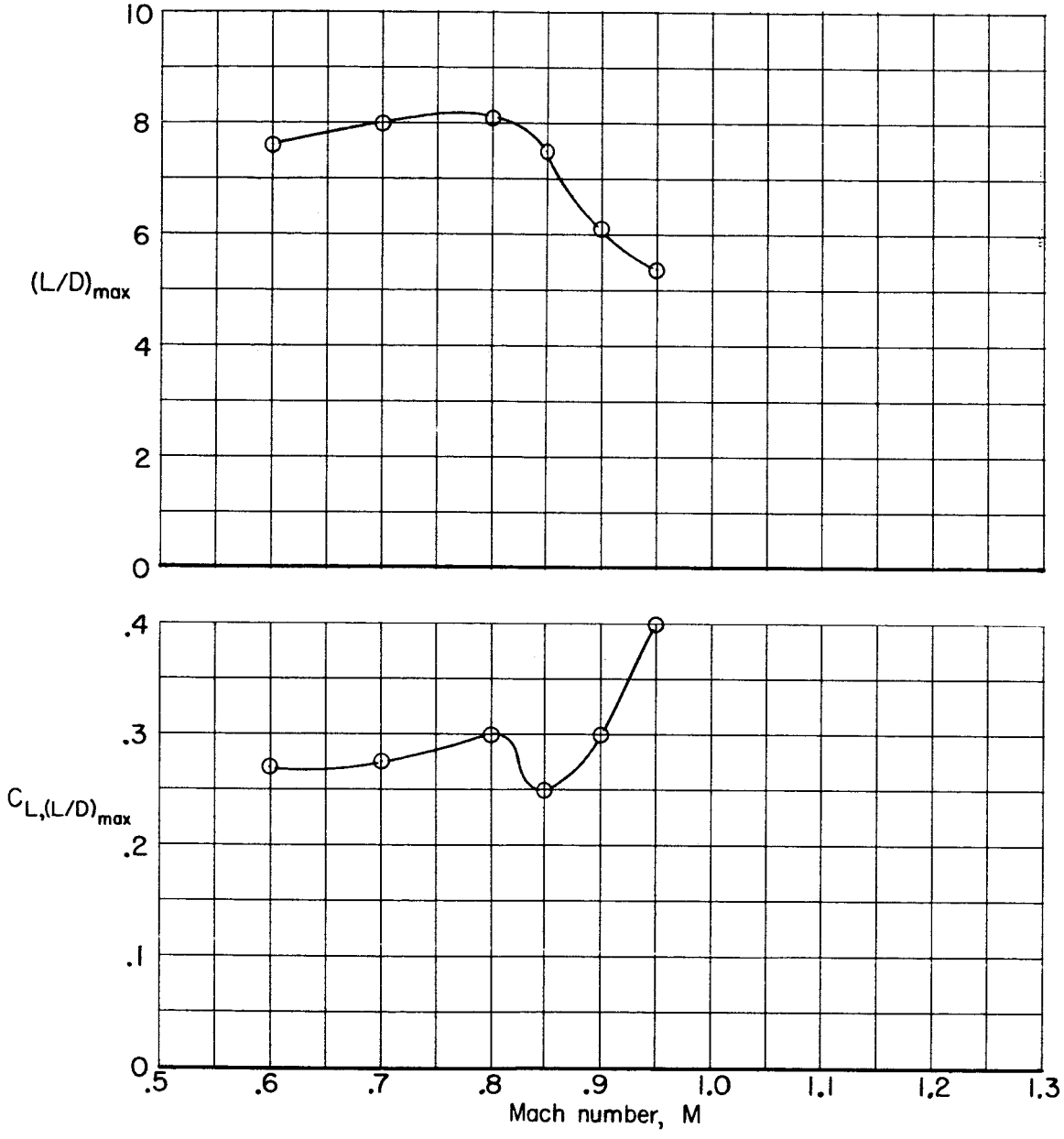

(c) Variation of $(L/D)_{max}$ and $C_{L,(L/D)_{max}}$ with M.

Figure 17.- Concluded.

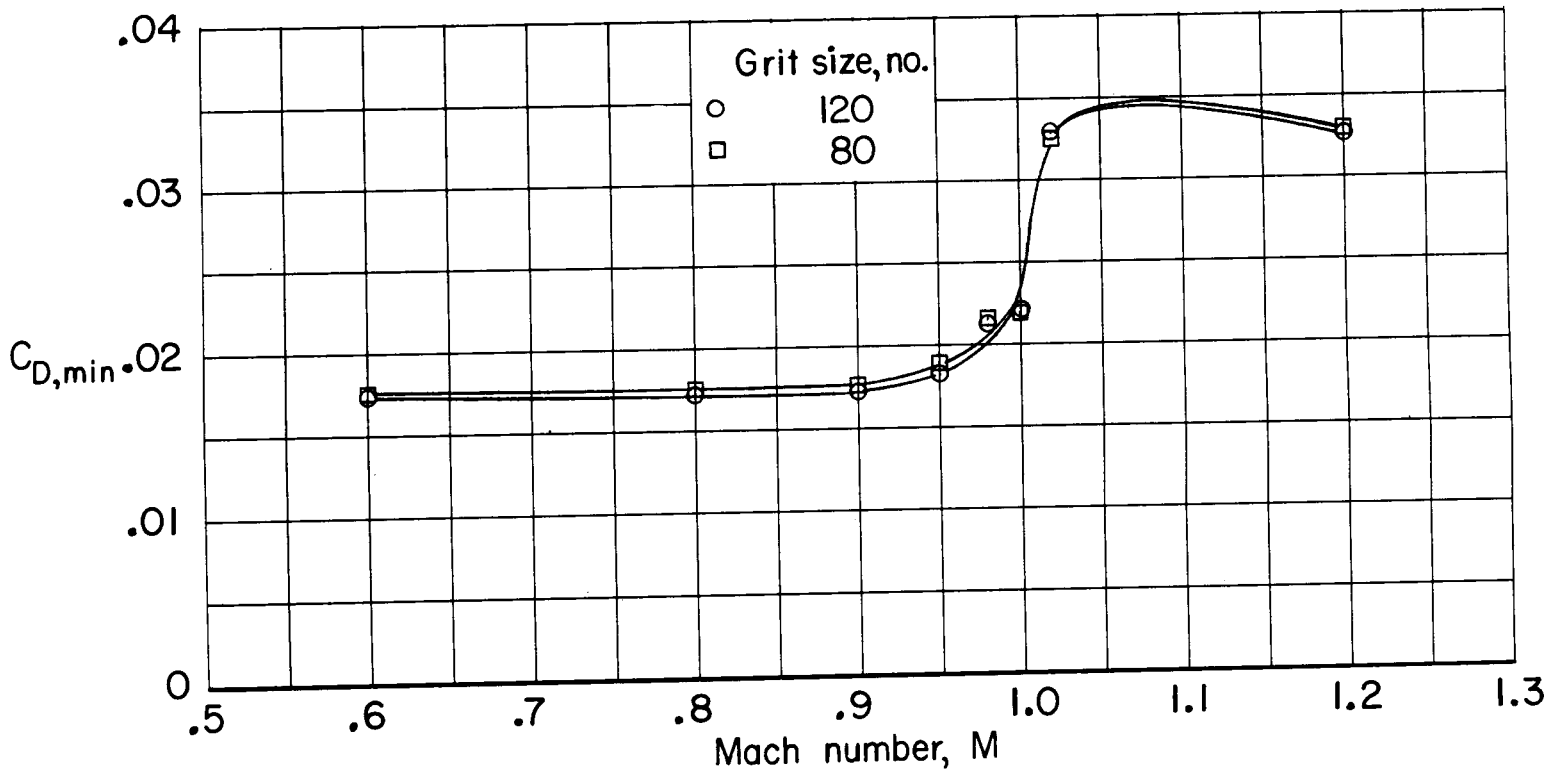

Figure 18.- Effect of transition grit size on minimum drag of model 2a. $\Lambda = 71.75^{\circ}$; $\delta_h = 0^{\circ}$; $p_{t,\infty} = 2{,}120$ lb/sq ft.

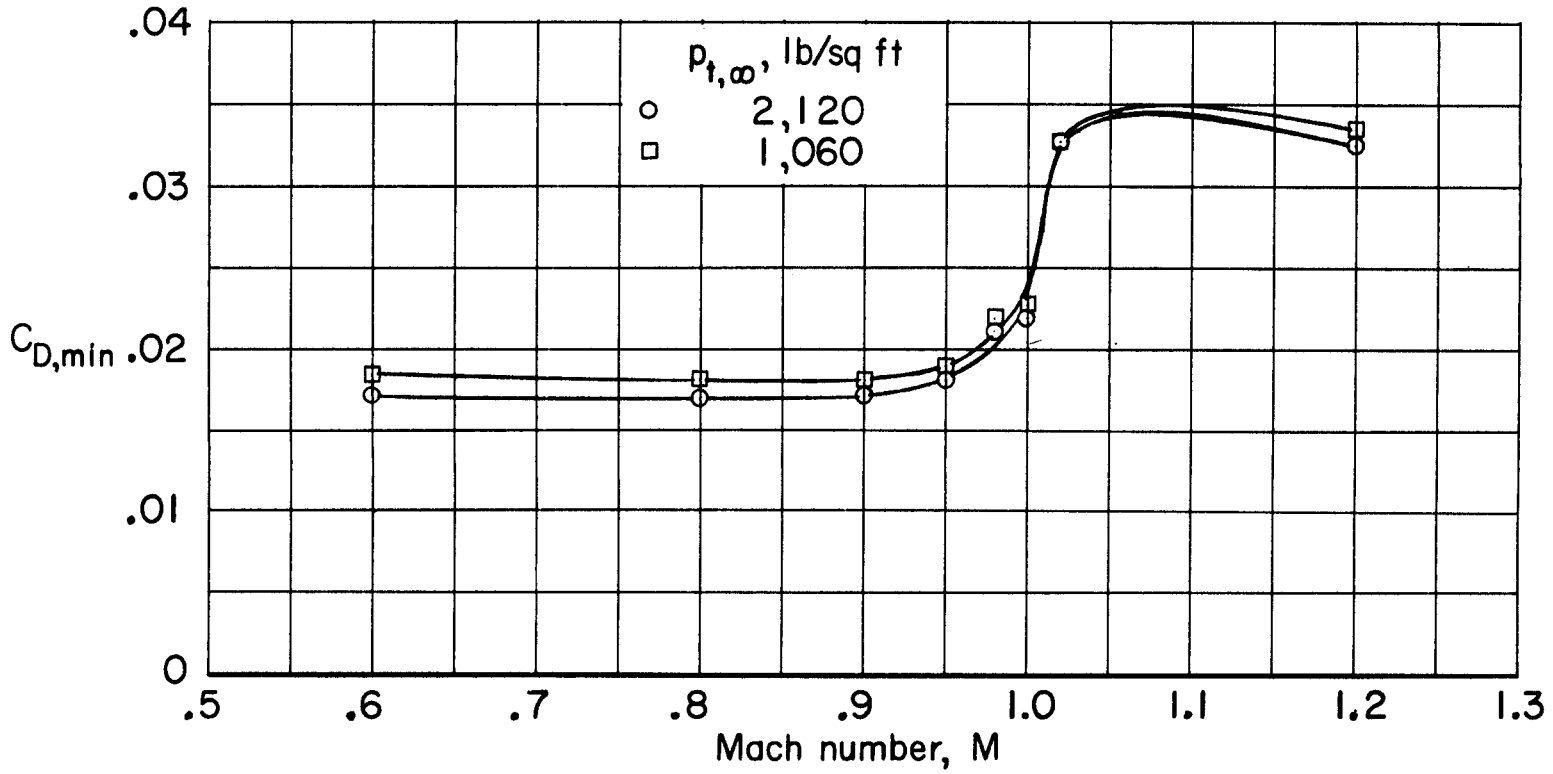

(a) Variation of $C_{D,min}$ with M.

Figure 19.- Effect of total pressure on performance and longitudinal-stability derivatives of model 2a. $\Lambda = 71.75^{\circ}$; $\delta_h = 0^{\circ}$.

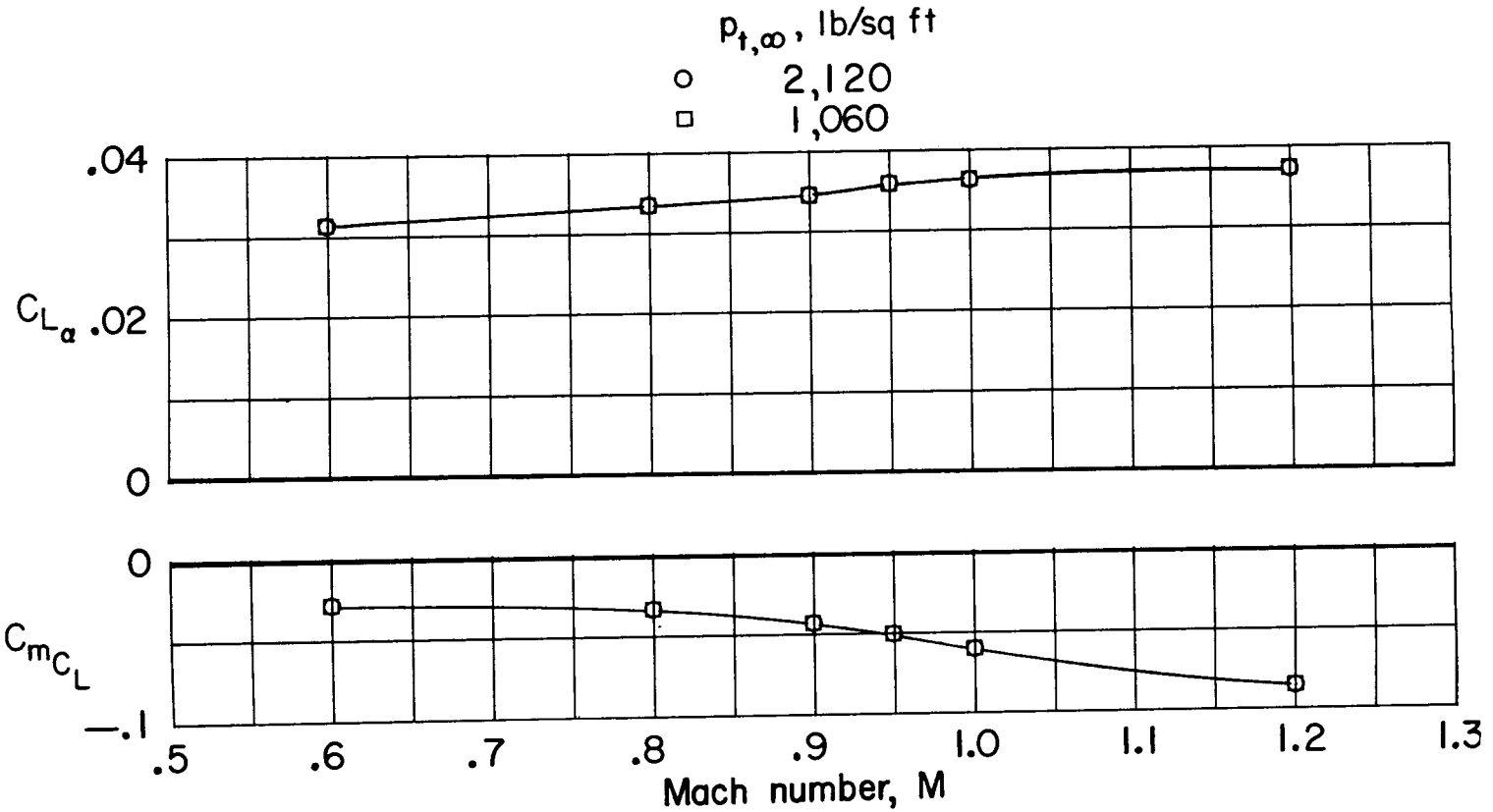

(b) Variation of C_{L_α} and $C_{m_{C_L}}$ with M.

Figure 19.- Continued.

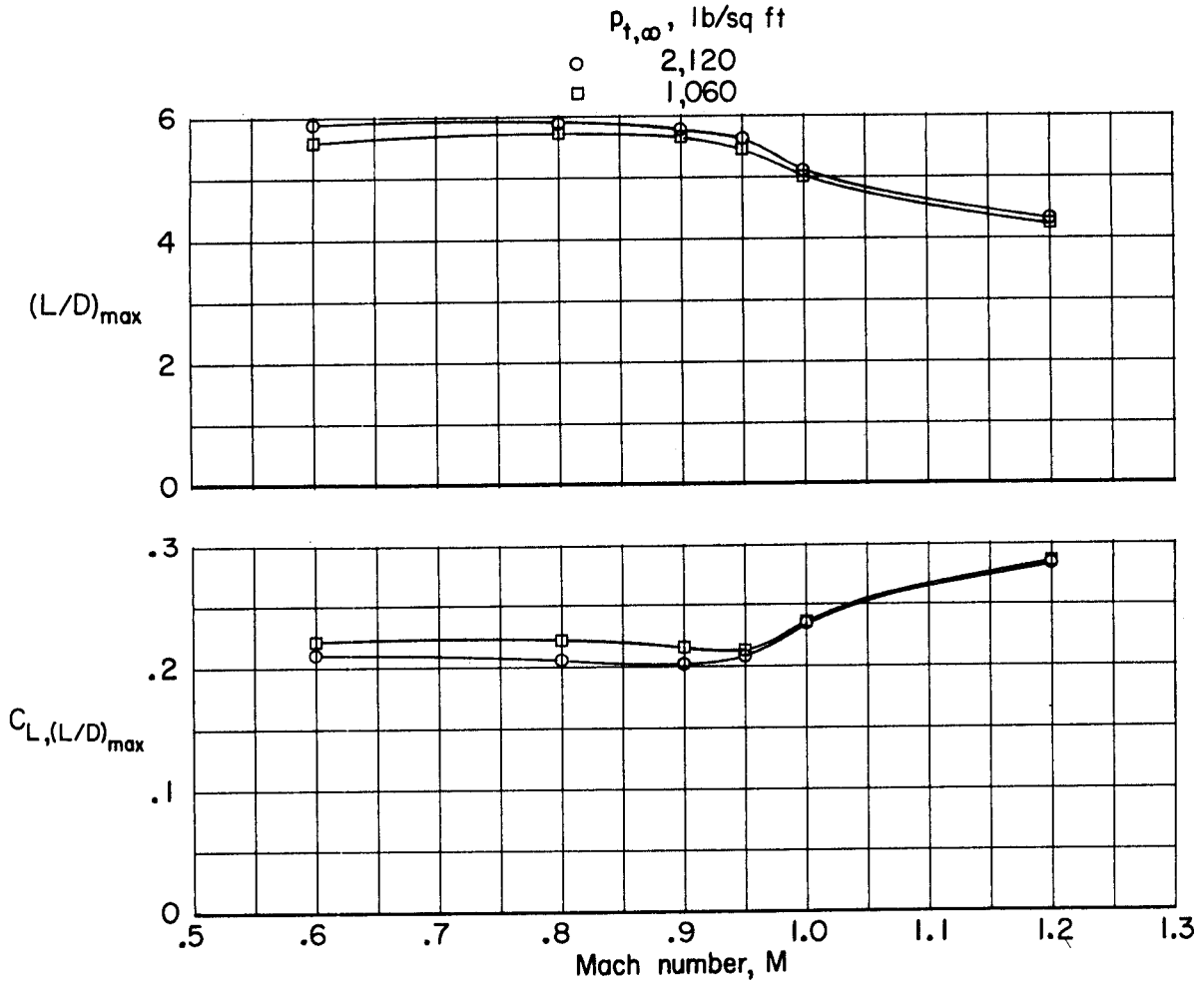

(c) Variation of $(L/D)_{max}$ and $C_{L,(L/D)_{max}}$ with M.

Figure 19.- Concluded.

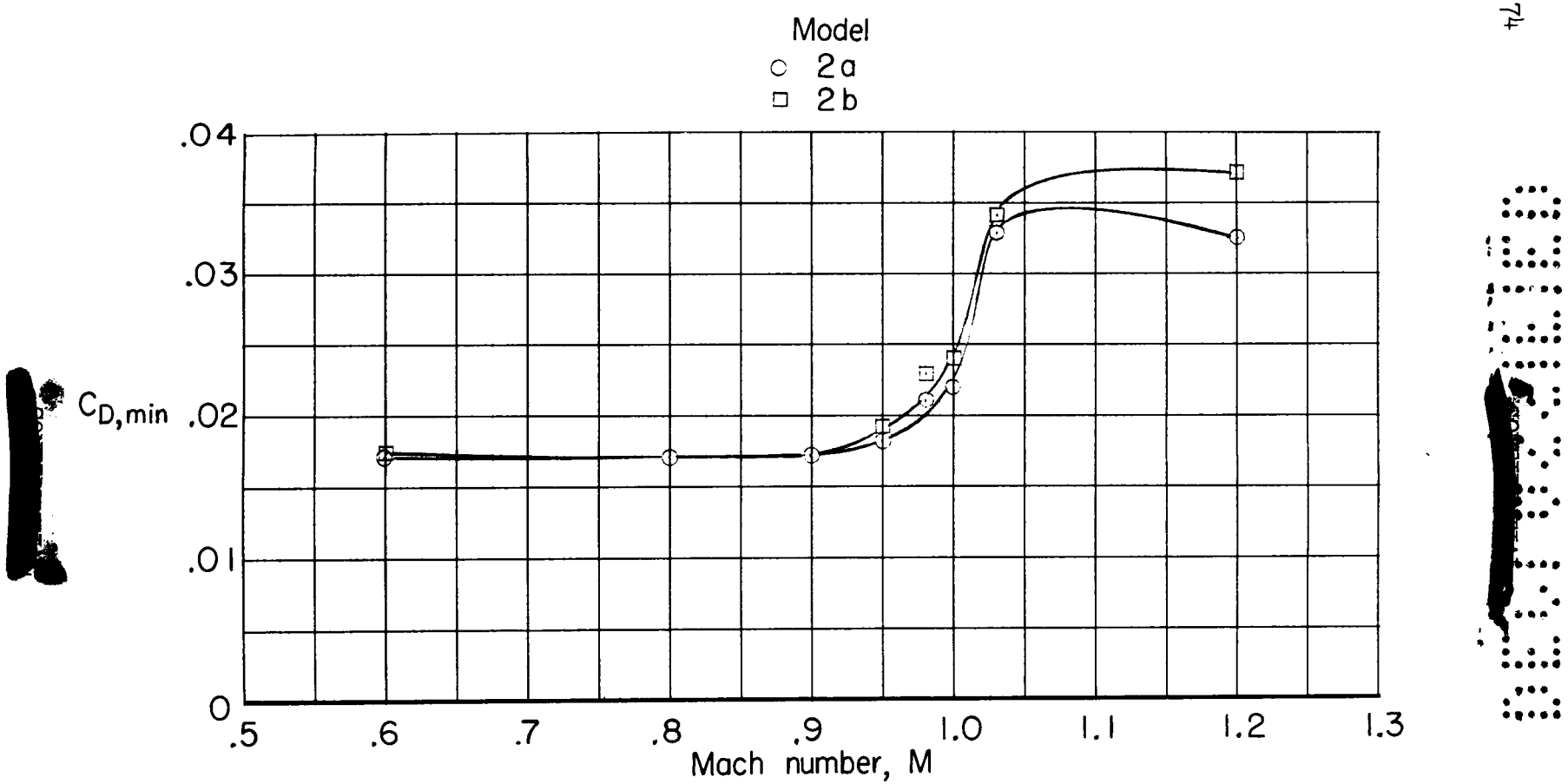

(a) Variation of $C_{D,min}$ with M.

Figure 20.- Effect of modification of external shape of duct on performance and longitudinal-stability derivatives of models 2a and 2b. $\Lambda = 71.75^{\circ}$; $\delta_h = 0^{\circ}$; $p_{t,\infty} = 2,120$ lb/sq ft.

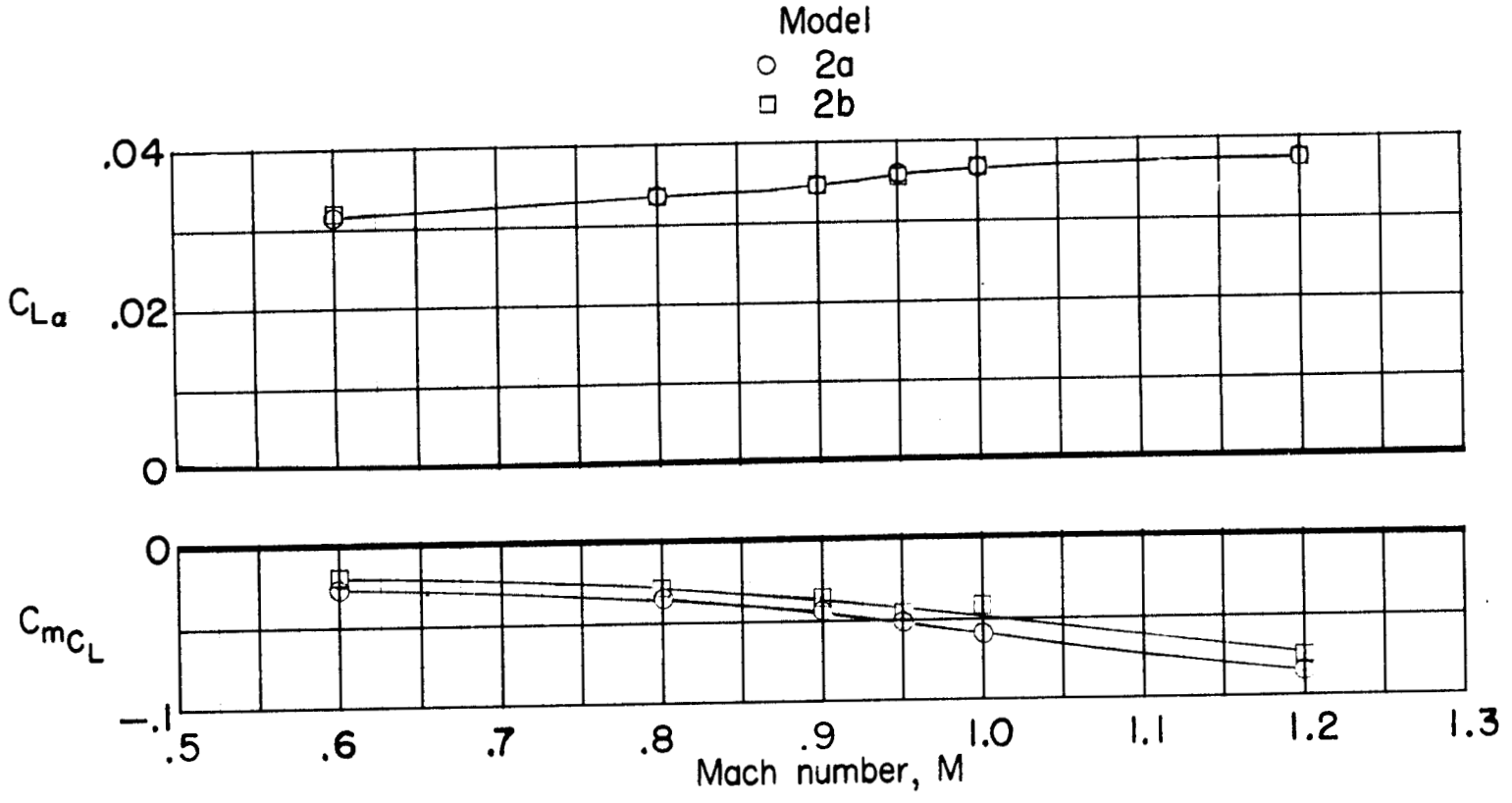

(b) Variation of C_{L_α} and $C_{m_{C_L}}$ with M.

Figure 20.- Continued.

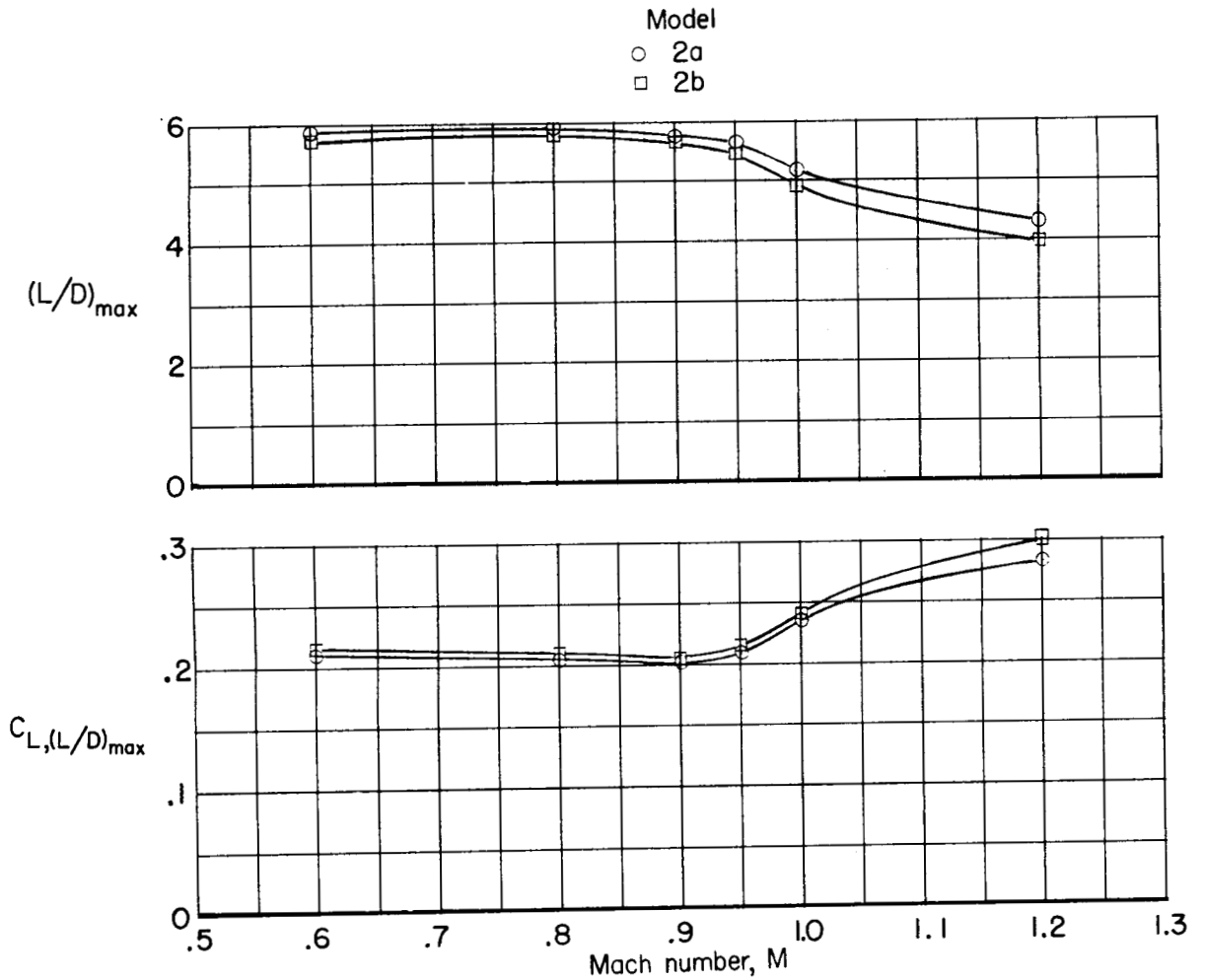

(c) Variation of $(L/D)_{max}$ and $C_{L,(L/D)_{max}}$ with M.

Figure 20.- Concluded.

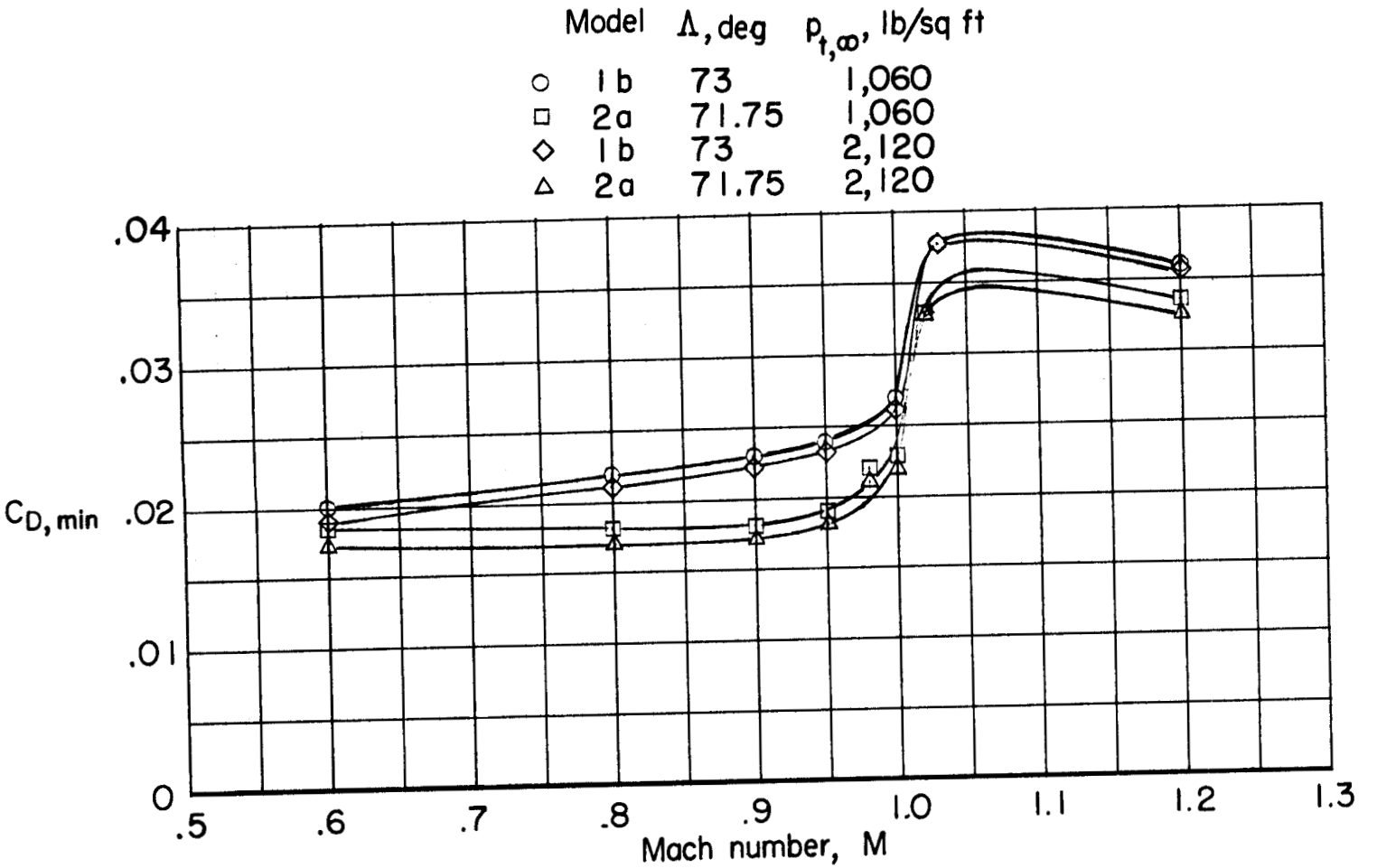

(a) Variation of $C_{D,min}$ with M.

Figure 21.- Comparison of performance and longitudinal-stability derivatives of models 1b and 2a. $\delta_h = 0^\circ$.

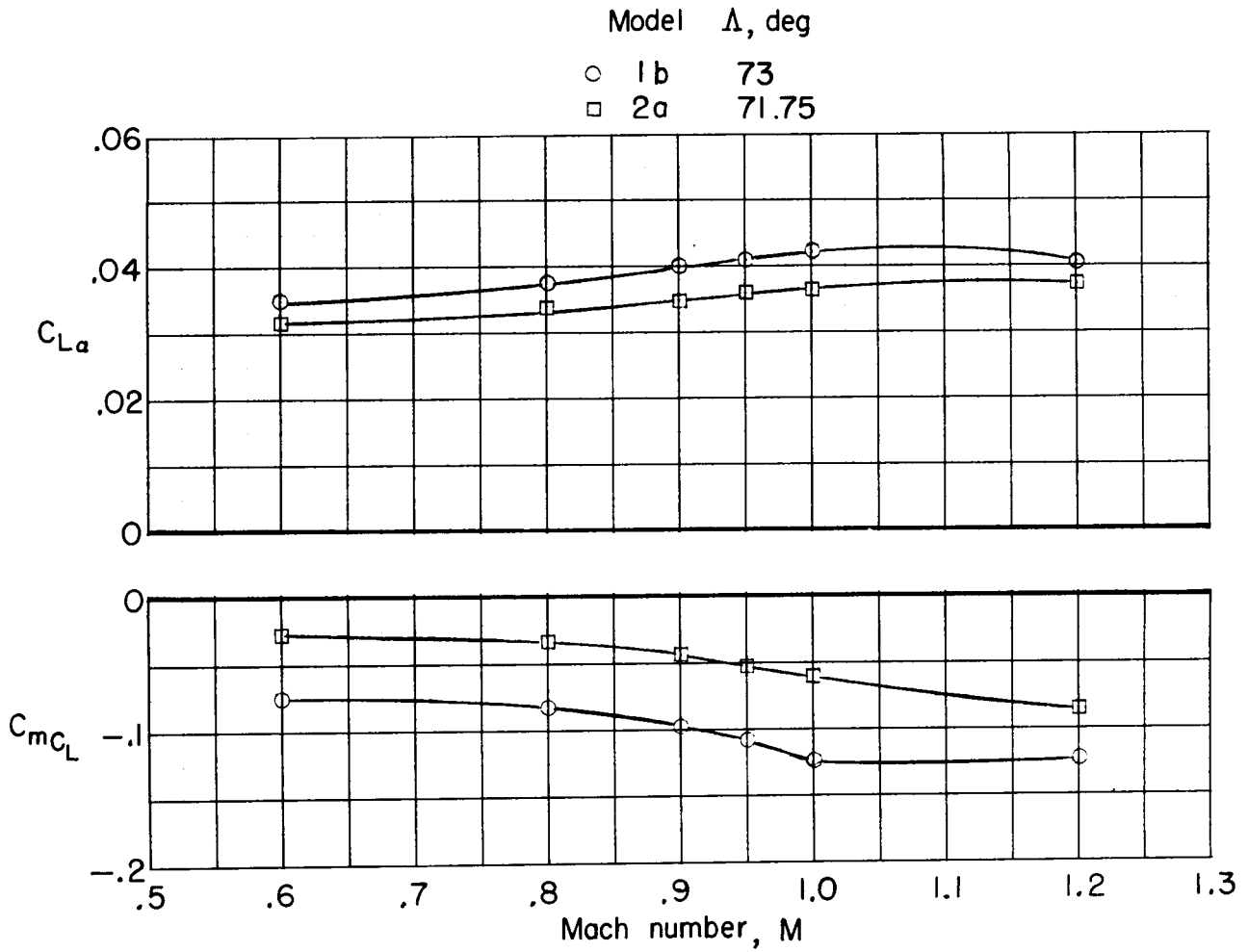

(b) Variation of C_{L_α} and $C_{m_{C_L}}$ with M. $p_{t,\infty}$ = 1,060 lb/sq ft.

Figure 21.- Continued.

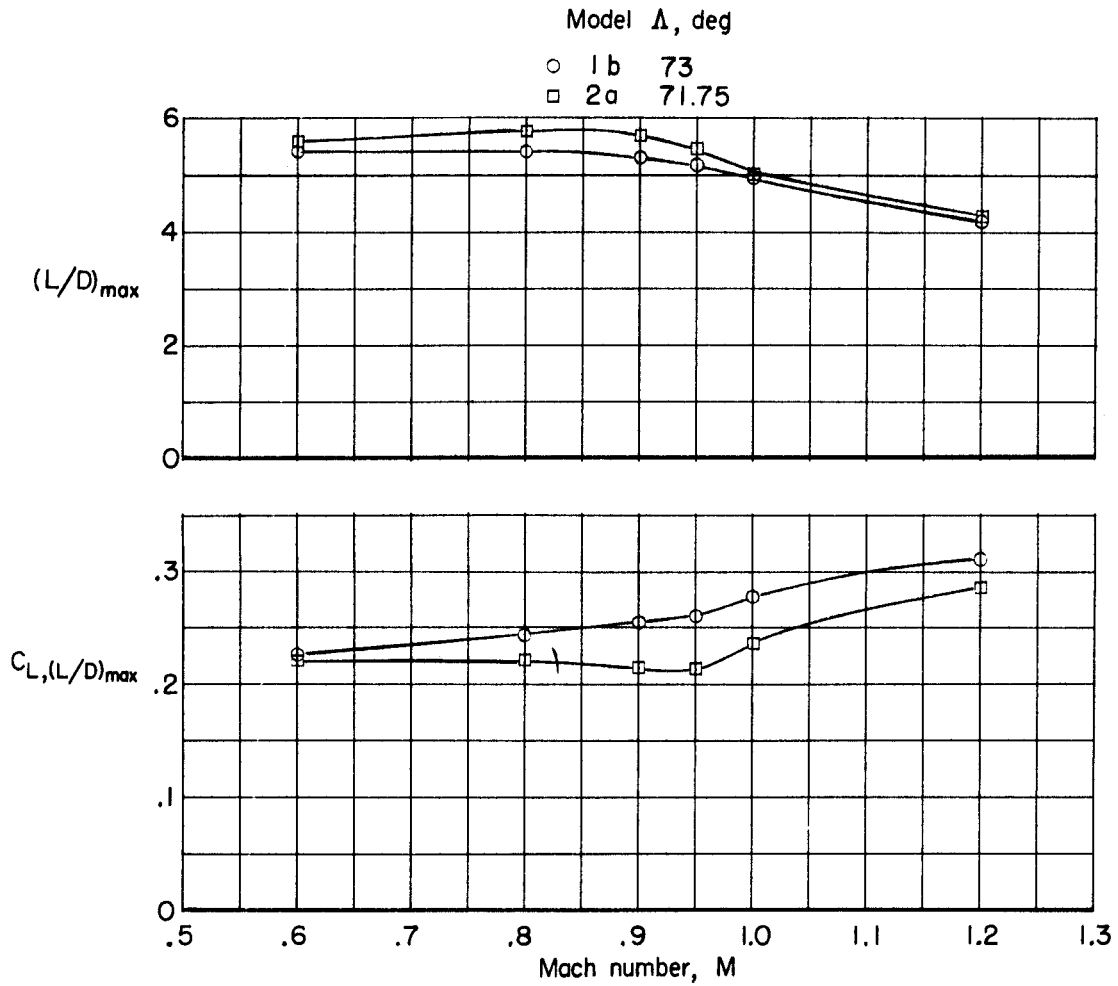

(c) Variation of $(L/D)_{max}$ and $C_{L,(L/D)_{max}}$ with M. $p_{t,\infty}$ = 1,060 lb/sq ft.

Figure 21.- Concluded.

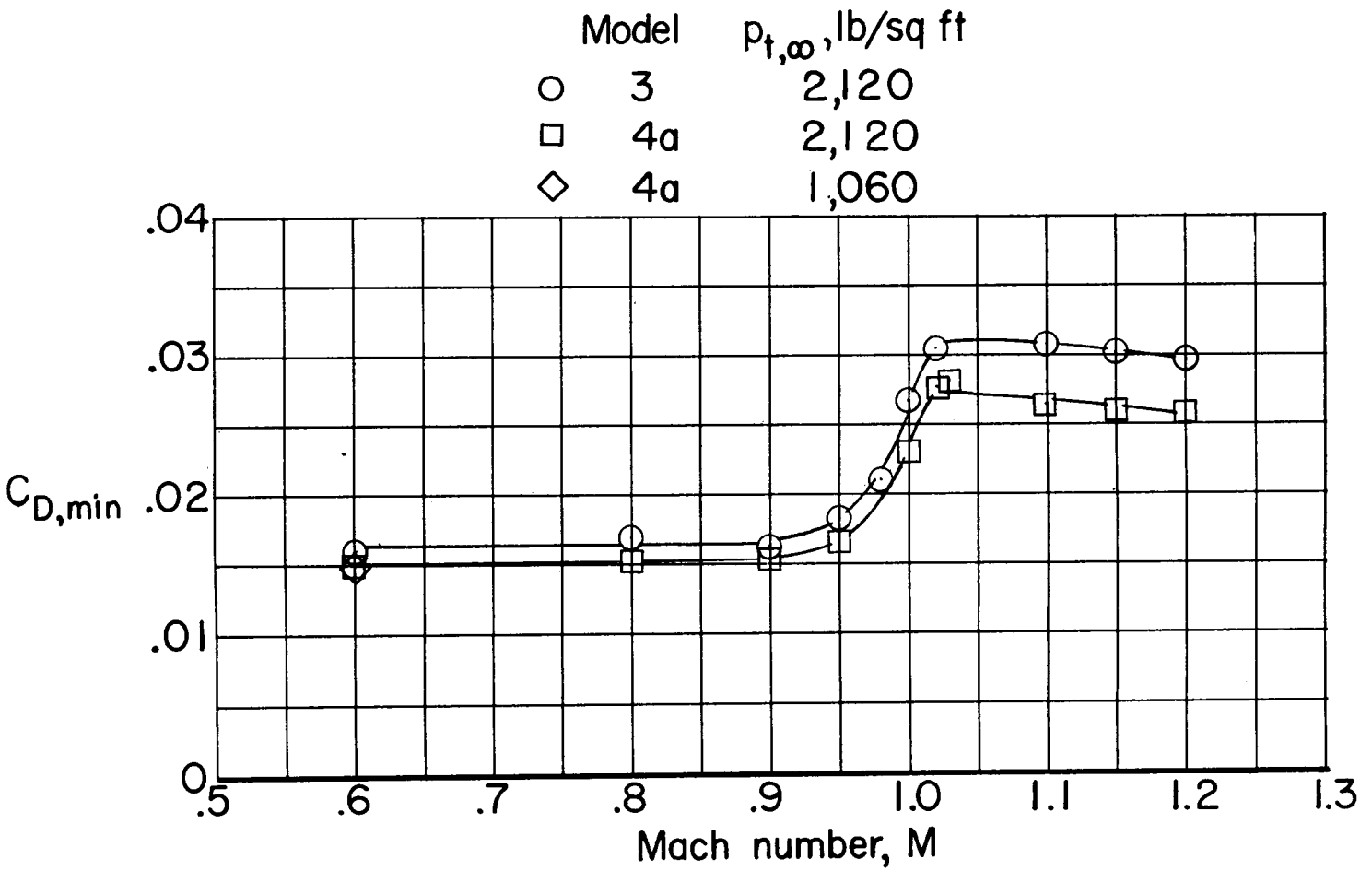

(a) Variation of $C_{D,min}$ with M.

Figure 22.- Comparison of performance and longitudinal-stability derivatives of models 3 and 4a. $\Lambda = 71.75°$; horizontal and vertical tails off.

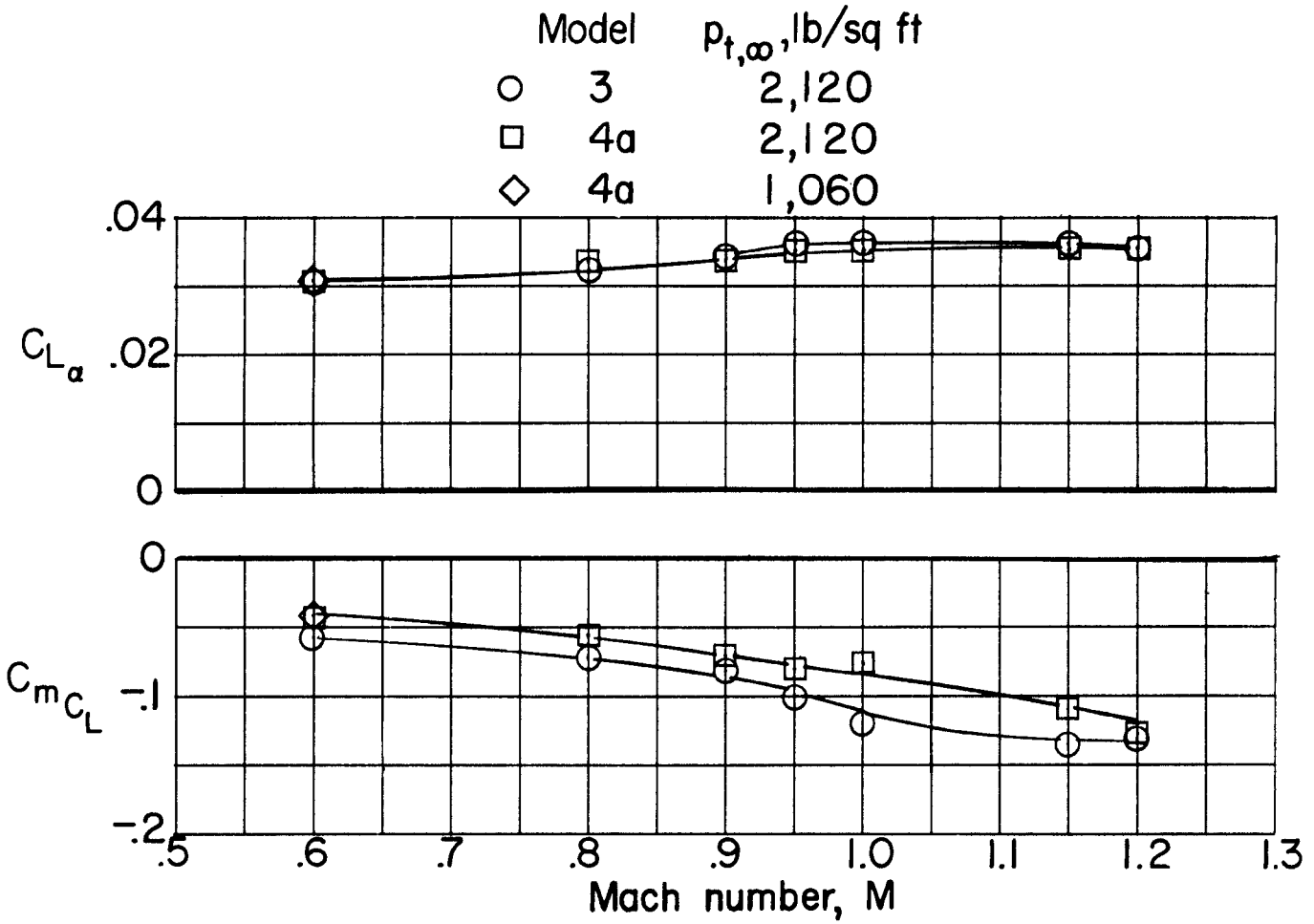

(b) Variation of C_{L_α} and $C_{m_{C_L}}$ with M.

Figure 22.- Concluded.

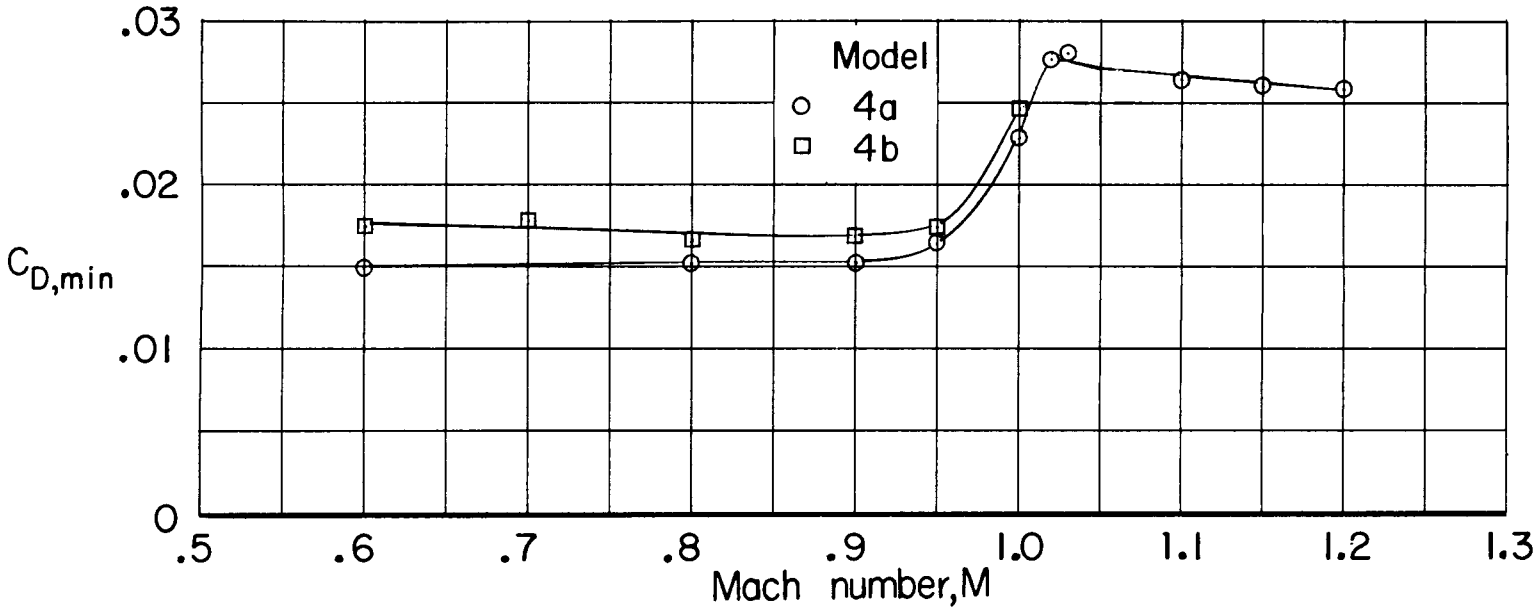

Figure 23.- Effect of duct-exit arrangement on minimum drag of models 4a and 4b. $\Lambda = 71.75^{\circ}$; horizontal and vertical tails off; $p_{t,\infty}$ = 2,120 lb/sq ft.